UC Irvine
UC Irvine Electronic Theses and Dissertations

Title

Assessment of Post-Fire Performance of FRP-Confined RC Columns

Permalink

https://escholarship.org/uc/item/9kc2j8nm

Author

WAFA, LOUAI FAISAL F F

Publication Date

2022

Peer reviewed|Thesis/dissertation

University of California

Irvine

Department of Civil and Environmental Engineering

Assessment of Post-Fire Performance of FRP-Confined RC Columns

Submitted in partial satisfaction of the requirements

For the degree of

DOCTOR OF PHILOSOPHY

IN Civil Engineering and Environmental Engineering

By

Louai Faisal F. Wafa

Dissertation Committee:

Prof. Ayman Mosallam (CEE Department), Chair

Prof. Mo Li (CEE Department), Member

Prof. Joel Lanning (CEE Department), Member

2022

Dedication

This dissertation is dedicated to my wife, my soulmate and love of my life. Thank you for supporting me and believing in me. I would also like to dedicate this work to my father who is my first Professor and advisor. Thank you for pushing me to achieve greatness. I would like to dedicate this dissertation to my loving mother. Thank you for your loving me and support me through tough times ever since I was a little baby.

I would also like to dedicate this work to my advisor, Professor Ayman Mosallam. It has been an honor and a privilege to learn under guidance for the past five years.

TABLE OF CONTENTS

LIST OF FIGURES

LIST OF TABLES

ACKNOWLEDGMENTS

Finally, I would like to thank my wife, my father and mother, and my family for their patience

and understanding. Your faith gave me the courage to reach my goal.

CURRICULUM VITAE

EDUCATION

August 2017 – present.

   Ph.D. Candidate in Structural Engineering at University of California Irvine,

May 2017

   Master of Science in Structural Engineering, San Jose State University, San Jose, CA

May 2015

   Bachelor of Science in Civil Engineering, San Jose State University, San Jose, CA

PUBLICATIONS

- Akbulut, Y. E., Altunisik, A. C., Basaga, H. B., Mostofi, S., Mosallam, A., & **Wafa, L. F**. (2021). *Numerical investigation on dynamic characteristics changes of RC columns and frames under elevated temperature*. Computers and Concrete, 28(2), 149-187.

- Altunişik, A. C., Akbulut, Y. E., Başağa, H. B., Mostofi, S., Mosallam, A., & **Wafa, L. F.** (2021*). Experimental Investigation on Dynamic Characteristics Changes of Fire Exposed Reinforced Concrete and Steel Members.* Fire Technology, 1-40.

- Akbulut, Y. E., Altunişik, A. C., Başağa, H. B., Mostofi, S., Mosallam, A., & **Wafa, L. F.** (2021). *Elevated Temperature Effect on the Dynamic Characteristics of Steel Columns and Frames*. International Journal of Steel Structures, 21(3), 861-882.

EDUCATIONAL & RESEARCH EXPERIENCES

   2017 – 2022

   Primary Teaching Assistant (TA) for CEE151C. This includes preparing and delivering theoretical problem sessions as well as design and operate small- and large-scale lab experiments for the course.

   2017 – 2022

   Research Assistant (RA): Research work included conducting experimental and theoretical research in the area of RC column confinement, analytical and numerical simulation of seismic behavior or RC and steel structures. Designing and conducting fire experiments. During the research work period, numerical software packages such as Opensees, ANSYS and ABAQUS were utilized.

PROFESSIONAL TRAINING / CERTIFICATES

      ACI – Certified Concrete Field-Testing Technician—Grade I *June 2015*

      ACI – 311 Manual of Concrete Inspection Course *June 2015*

PROFESSIONAL MEMBERSHIPS

➢ American Society of Civil Engineers (ASCE)

➢ American Concrete Institute (ACI)

➢ Concrete Reinforcing Steel Institute (CRSI)

COMPUTER SKILLS

      ANSYS, OPENSEES, Python, Solidworks, ABAQUS, AutoCAD, SAP 2000, MATLAB.

ABSTRACT

Assessment of Post-Fire Performance of

FRP-Confined RC Columns

By

Louai Faisal F Wafa

Doctor of Philosophy in Civil Engineering, 2022

Professor Ayman S. Mosallam, Chair

This study focuses on assessing the post-fire performance of reinforced concrete (RC) columns confined with fiber-reinforced polymer (FRP) composites. The main goal of this research is to reduce uncertainty regarding the post-fire performance of FRP-confined RC columns. A comprehensive parametric experimental program was implemented to provide new insights into the post-thermal exposure behavior of said columns. The specimens were tested after exposure of moderately high temperatures (100-400 ℃) and extreme fire environments (+1000℃). The critical temperature for the FRP composites concrete was found to be in the 250-300℃ range depending on the type of fiber and polymer matrix. FRP-confined concrete specimens were suseptable to exploding during the thermal exposure protocol. The phenomenon was attributed expansion of the concrete being resisted by the shrinking confinement which has a negative thermal expansion coefficient. The onset of ignition of the polymer matrix was determined to be 300 ℃.

The performance of different innovative fire protection schemes was assessed. The use of proper insulation was found to be beneficial in reducing the degradation of specimens. The extent of the

reduction in degradation varies depending on the thermal properties and thickness of the fire protection system as well as the temperature and duration thermal exposure.

Additionally, for the first time, the post-thermal exposure behavior of hybrid carbon and glass FRP-confined concrete was investigated. The hybrid composite-confined specimens were found to be extremely susceptible to ignition and explosion at a temperature of 300℃ and above. This can be attributed to glass fiber fabric having a higher absorbtion of the epoxy matrix which acts as addiitonal fuel to the fire. Large-scale FRP-confined columns were tested under axial compression.

The results of the experimental program were used to develop simplified procedures to predict the residual behavior of FRP-confined columns post-thermal exposure. Nonlinear heat transfer simulations were conducted using ANSYS® Mechanical Transient-Thermal module to extract the thermal profile of the specimens exposed to temperatures and insulated with varying thicknesses of fire protection systems. Numerical simulations of post-fire seismic behavior of RC columns confined with FRP composites were also conducted via Opensees® to calibrate the design equations for FRP confined columns. The Opensees® *FRPConfinedConcrete02* material model was found to be accurate in predicting residual axial behavior of FRP-confined columns after exposure to elevated temperatures, provided that the material properties are known. Additionally, lateral cyclic simulation was performed on confined and unconfined RC-columns before and after high-temperature exposure. Both the confined and unconfined columns experience a reduction in their ductility and energy dissipation capacities after exposure to elevated temperature. The outcome of this study will increase the confidence level structural engineer via provided a wealth of information that will assist in predicting the residual strength of RC columns confined with FRP composites. Results also provide a confirmation on the necessity of using proper fire

protection systems to increase reliability of composites in repair and strengthening applications. The protocol used in building the Opensees® model can be included in this public-domain software to assist structural engineers in assessing the effect of fire and the resulting degraded mechanical properties associated with such events on the overall performance in any reinforced concrete structure. Results obtained from the experimental program revealed the necessity of changing the geometry and details of RC members such as columns when tested for fire rating. It was found that the bulk majority of published experimental work utilized specimens with unprotected end surfaces in contrary to the actual case of a typical RC column in a building or a bridge where the roof (or bridge deck) and the floor (or foundation such as pile cap) act as protective and insulative media. For this reason, and based on experimental program experience, it is strongly recommended to ad thick portions of concrete at the column ends to realistically simulate the fire damage and delay the premature local failure of specimen ends.

Finally, recommendations were made for future research work. This includes experimental testing of larger-scale columns, slabs, beams and beam-column joints strengthened with different types of FRP composites with and without thermal insulation. The other important topic is performing residual tests simultaneously or after a relatively short time of the end of the exposure time. This will provide a more realistic simulation of the behavior of such columns while specimens are still hot and degradation rate is high.

Chapter 1   INTRODUCTION

1.1   Background

The use of Fiber Reinforced Polymer (FRP) composites in construction applications has become popular in the last three decades or so due to several attractive features including lightweight, tailorability, relatively higher long-term performance and durability as compared to other conventional materials, and others. Numerous studies have been conducted, in the last three decades, on behavior of FRP composites in construction applications. FRP composite materials are utilized to enhance shear, moment, axial, and torsional behavior of concrete, wood, masonry and steel structural members. Composites are particularly beneficiary for seismic retrofitting of existing structures. The use of FRP strengthening of reinforced concrete (RC), steel, wood members for enhancing both strength and ductility for such members [1,2]. For instant, results of numerous studies confirmed the ability of FRP composites to enhance the ductility and energy dissipation of RC columns [3–7].

Carbon fiber reinforced polymer (CFRP) composites are one of the most widely used type of FRP composites used in structural repair and strengthening applications. Other composites such as E-glass fiber reinforced polymer (GFRP) and aramid reinforced polymer (AFRP) composites are also used in such applications. As compared to GFRP and AFRP, CFRP composites possess the highest ultimate strength and stiffness, however, its rupture strain is relatively low (e.g., 1-1.20%) in addition to its relatively higher cost.

Despite the unique and attractive features of FRP composites strengthening systems, there are still some concerns by the engineering community regarding the implementation of such systems.

Some of these concerns are typical of any new technology that requires a learning curve before it can be utilized properly. Another major concern is the lack of information on thermomechanical durability and degradation of FRP composites when subjected to elevated temperatures [8] and ultimately to fire [9]. Lack of understanding of the behavior of FRP composites under elevated temperature and fire have led to severe limitations being imposed on the use of such materials in repair and strengthening applications. These limitations arise not only due to the reduction in mechanical properties at elevated temperatures, including increased propensity to creep, but also due to limitations on continuous working temperature causing permanent damage to the material as a result of thermal and oxidative degradation.

The behavior of conventional building materials such as steel, concrete, and wood are well understood. For example, it is well known that concrete behaves well under elevated temperatures and acts as a good insulator. On the other hand, mechanical and physical properties of steel reinforcement are susceptible to degradation at elevated temperatures. However, minimum concrete cover code requirements ensure that the steel is well protected [1] . Composites, on the other hand, lose a great deal of their mechanical properties when subjected to high-temperature environments that equal or exceed their glass transition temperature (T_g). Glass transition temperature T_g, is defined as the *specific temperature at which the polymers change from a relatively rigid, "glass-like" substance to a relatively viscous, "rubbery" material*. This transition temperature varies from one thermoset polymer to another and depends on several factors, including polymer molecular weight, resin curing temperature, and rate of loading if the measurement process involves mechanical deformation [10]. Glass transition temperature, for most epoxies used in construction, ranges from $50 - 120\,°C$ [11]. Another concern is the

flammability of the epoxy matrix used in strengthening applications and its propensity to release toxic compounds in the event of a fire. Therefore, it is critical to examine thermomechanical behavior of FRP structural systems at elevated temperatures.

Known effects of fire on thermo-mechanical degradation of FRP composites led the American Concrete Institute (ACI) committee 440 [1] to impose limits on the amount FRP composites to be used for strengthening RC members to avoid catastrophic failure, especially in cases when no effective fire protection system is provided [1]. According to ACI committee 440 design guidelines [1], in the event of a fire, any FRP composites contribution to RC structural member is assumed to be lost unless it can be demonstrated that the FRP temperature remains below T_g. For this reason, FRP strengthening of concrete members is mostly used in bridge structures where fire does not pose a significant risk [8]. To ensure fire-safe design, ACI committee 440 [1] recommends the following conservative limitations on the strength of the column before FRP retrofitting:

$$(R_{n\theta})_{existing} \geq 1.0 S_{DL} + 1.0 S_{LL} \qquad \text{Eq. 1-1}$$

where: $(R_{n\theta})_{existing}$ is the nominal capacity of RC member before strengthening, and S_{DL} and S_{LL} are the dead and live loads imposed on the column. In addition, ACI 440 design guidelines document requires in this event that FRP strengthened RC member shall be designed to ensure that it can withstand service loading without FRP external reinforcement contribution. The justification for this harsh provision is to prevent sudden collapse in case the FRP system becomes ineffective due to several reasons including fire that is the main focus of this research study. This restriction makes FRP unattractive to the industry since such restrictions are overly

conservatives and can be quite costly. It is therefore very essential and beneficial to demonstrate that FRP-confined members such as columns can retain their strengthened capacity for a sufficient time during a fire when a reliable fire protection system is utilized.

Over the past two decades or so, several studies have been published on fire behavior of FRP-confined columns under service conditions [12–17]. These studies focused mainly axial performance of FRP-confined columns when subjected to higher temperatures. However, and as stated earlier, the majority of FRP composites strengthening applications are adopted in seismic repair and rehabilitation of structures with relatively few cases where composites are specified to strengthening reinforced concrete (RC) members in a non-seismic zone. For this reason, it is very crucial to assess the residual strength of repaired and retrofitted reinforced concrete members, such as RC columns, when exposed to fire followed by an aftershock or several aftershocks. In general, there are three potential scenarios that needs to be addressed in seismic-related applications:

(i) **SCENARIO 1:** *A Fire Event, Followed by an Earthquake, Resulting in Partial or Full Collapse*: This scenario has a low probability of occurrence that describes a rare coincidental case where a building catches fire just before the occurrence of the seismic event that may lead to a partial or a total collapse of the building depending on both the extent of post-earthquake fire damage and the intensity of the earthquake and aftershocks (refer to Figure 1-1-a),

(ii) **SCENARIO 2:** This scenario has a higher probability as compared to the preceding scenario, where the building is subjected to seismic forces that are followed by a fire event resulting in a partial or a full collapse (refer to Figure 1-1-b), and

(iii) SCENARIO 3: An earthquake triggering fire, resulting in partial or full collapse. This scenario may have the highest probability based on the historical data where during an earthquake event, fire may be initiated due to gas-leak, electrical, chemical, or blast sources (refer to Figure 1-1-c).

(a)

SCENARIO 1: *A fire event, followed by an earthquake, resulting in partial or full*

(b)

SCENARIO 2: *An earthquake event followed by Fire, resulting in partial or full*

(c)

SCENARIO 3: *An earthquake triggering fire, resulting in partial or full collapse*
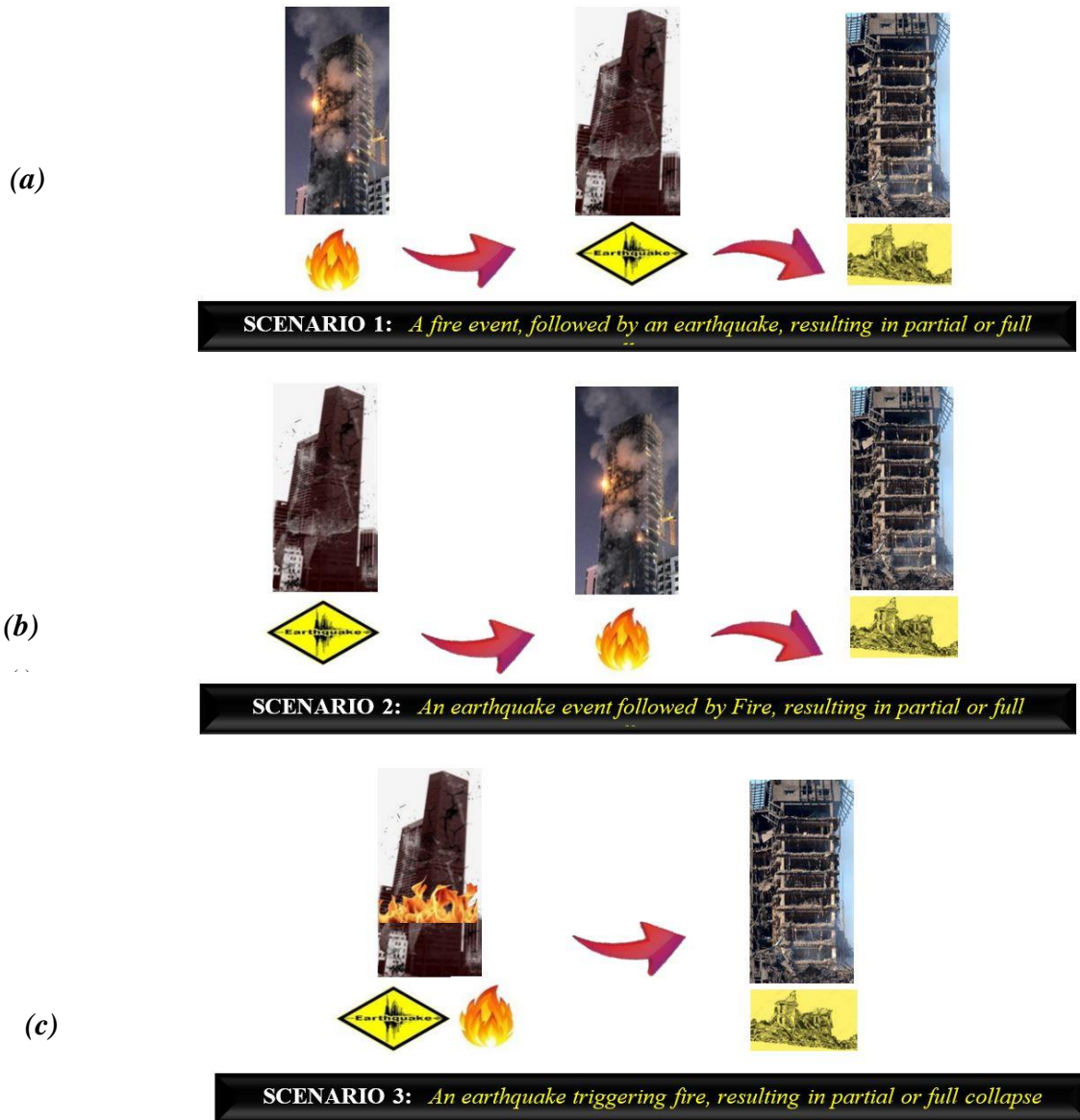
Figure 1-1: Main Fire/Seismic Scenarios

Other similar scenarios can potentially occur as a combination of these general scenarios that involve buildings with composite-retrofitted members such as columns, beams, and slabs. The difference between these cases and the general cases, in terms of fire exposure effects, is the sensitivity of polymeric composite to elevated temperatures that would accelerate the partial or complete collapse of such buildings. In addition, under the second scenario where a seismic event triggers fire, it is critical to quantify the extent of damage that determines both the residual axial and lateral capacities of the retrofitted columns, and accordingly determines its ability to withstand forces generated due to potential aftershocks.

Damage due to post-earthquake fire events can be worsened due to earthquake-induced damages in the structures' infrastructure systems such as gas and electrical systems that may lead to the occurrence of multiple fires at once which can impact fire management efforts. Fatalities due to post-earthquake fires comprised about 87% of the total fatalities in the 1923 Tokyo earthquake [18]. During the 1994 Northridge earthquake, a total of 110 fire events were reported [19].

Himoto [18] proposed an expression (refer to Eq. 1-2) that is based on historical data in Japan to predict the rate of post-earthquake fire ignition, r (km^{-2}), which is defined as the number of post-earthquake fires per building floor area:

$$r = 0.581895\theta'_{PGA}{}^2 - 0.029444\theta'_{PGA} \qquad\qquad \textit{Eq. 1-2}$$

where: θ'_{PGA} (cm/s) is the peak ground acceleration of the earthquake. The model calculates the fires that occur within 10 days of the earthquake including fires caused by potential aftershocks.

1.2 Related Research Work

The majority of published research focused mainly on the degradation of mechanical properties of composite strengthening systems when exposed to fire [11–15,17,20–23]. This information is very important to understand the effect of fire on the physical and mechanical degradation of composite-retrofitted columns that is considered be fundamental information that is needed to simulate behavior of retrofitted RC columns under the three aforementioned scenarios. As mentioned earlier, the main goal of this study is to determine, both experimentally and numerically, the residual strength of retrofitted columns under the three fundamental scenarios described in Figure **1-1**. Over the years, only a few studies assessed post-fire behavior of RC columns retrofitted with FRP composites. For example, Bénichou et al. [24] studied the impact of fire exposure on seismic resistance of fiber-reinforced polymer strengthened RC members. In 2012, Yaqub & Bailey [25] reported results of an investigation on seismic performance of shear critical post-heated reinforced concrete square columns wrapped with FRP composites. In this investigation, three groups of RC columns were evaluated experimentally: (a) unheated, (b) post-heated, and (c) post-heated columns repaired with GFRP or CFRP jackets. Results of Yaqub and Bailey study [25] indicated that the post-heated columns with a single-ply GFRP or CFRP composite jackets were not capable of restoring the original mechanical properties of unheated columns and that the unheated and post-heated columns failed in shear, while the failure mode of both GFRP and CFRP wrapped columns shifted from shear to flexural mode of failure. A recent article describing the results of a numerical model for post-earthquake fire resistance of CFRP-strengthened reinforced concrete joints based on experimental data is reported in Ref. [26]. Based on the in-depth literature review, these later three studies are the only papers related to the

assessment of the post-fire seismic performance of FRP-confined RC columns. It should be noted that the information described in these papers is limited to a certain number of composite plies and a specific test setup. It does not contain a general approach for identifying the residual axial strength of the retrofitted columns which very critical in determining the safety and vulnerability of a building after a combined event of fire and seismic loads. This issue is very critical for decision-makers and first responders for determining post-earthquake evacuation and rescue operations. This topic will be investigated, for the first time, in the proposed research. In addition, this research addresses the axial/lateral combined effects during the different potential scenarios.

1.3   Objectives & Motivations

The use of FRP composites in civil and structural application has a huge potential. FRP composites can be used to strengthen existing deficient or deteriorated structure and can extend the life of decaying infrastructure. However, there remains concerns and uncertainty when it comes to widespread applications due to their fire performance and degradation when exposed to elevated temperatures. Therefore, it is important to understand the post-thermal exposure behavior of structural systems strengthened with FRP composites

The main objective of this research is to study the residual behavior of heat-damaged FRP-confined reinforced concrete columns (FRP-CRCC) and to develop a predictive methodology simulate post-fire behavior of the strengthened CFRP columns.

1.4   Structure of the Dissertation

The second chapter of the dissertation focuses on presenting a summary of a literature review of the available literature related to the subject of this research.

Details and results of a parametric experimental program are presented in Chapter 3 through Chapter 7. The experimental program is composed of four interrelated levels of testing (refer to *Figure (1-2)*.
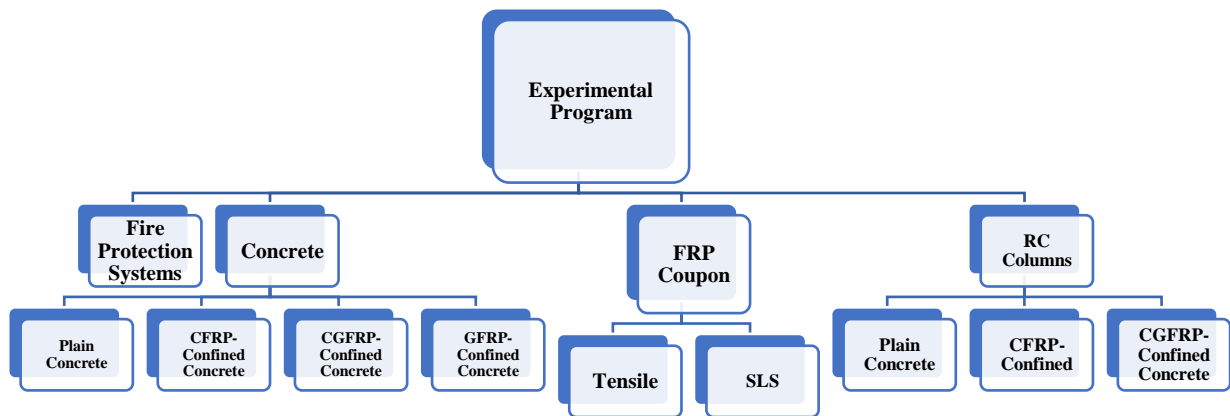
Figure 1-2: Experimental Program Summary

In order to extract meaningful information that can be used in developing a methodology to predict the post-fire behavior of RC columns confined with fiber reinforced polymer (FRP) composite jackets, experimental evaluation of different components was performed including:

1. FRP composite laminates characterization tests,

2. Tensile strength tests and Single-lap-shear (SLS) strength tests of FRP composite coupons after being exposed to both ambient and elevated temperatures,

3. Assessment of both pre- and post-fire compressive strength of small-scale FRP-confined and non-confined concrete specimens,

4. Assessment of different fire protection systems and their effect on maintain the residual strength of FRP-confined concrete specimens after exposure to moderate and extreme temperatures

5. Assessment of axial compression capacity of large-scale FRP-confined and non-confined reinforced concrete columns.

Based on the results obtained from the experimental program, analytical and design procedures are developed and presented in **Chapter** 8. The design procedures were capable of predicting the residual mechanical properties of FRP composites and FRP-confined concrete as described in Sections 8.1 and 8.2, respectively.

In **Chapter** 9, a description of the heat transfer simulations using ANSYS® Mechanical Transient-Thermal module are presented. **Chapter** 10, described analytical results performed using Opensees® computer code based on findings reported in **Chapter** 8 and **Chapter** 9. In this chapter, computer code was used to simulate post-fire exposure residual strength of FRP-confined columns. Conclusions of this study along with recommendations for future research that were identified from the outcomes of this study are presented in **Chapter 11.**

Chapter 2   LITERATURE REVIEW

The approach to studying seismic behavior and residual strength of fire-damaged FRP composites strengthened RC columns is divided into multiple sections. It should be noted, the scope of this research will focus on reinforced concrete columns with FRP composite jackets. First, it is essential to understand both the service and ultimate behavior of RC circular columns with FRP composite jackets under ambient conditions when subjected to a combined gravity and lateral loading for different applications including buildings and bridges. The second essential analysis is related to simulating the behavior of constituent materials of strengthened columns that includes both FRP composite laminates and both unconfined and confined reinforced concrete at both ambient and fire environments. The findings of the first two sections of the study will be used to develop an understanding of the post-fire seismic performance of FRP-jacketed RC columns. A summary of this approach can be found in Figure **2-1**.
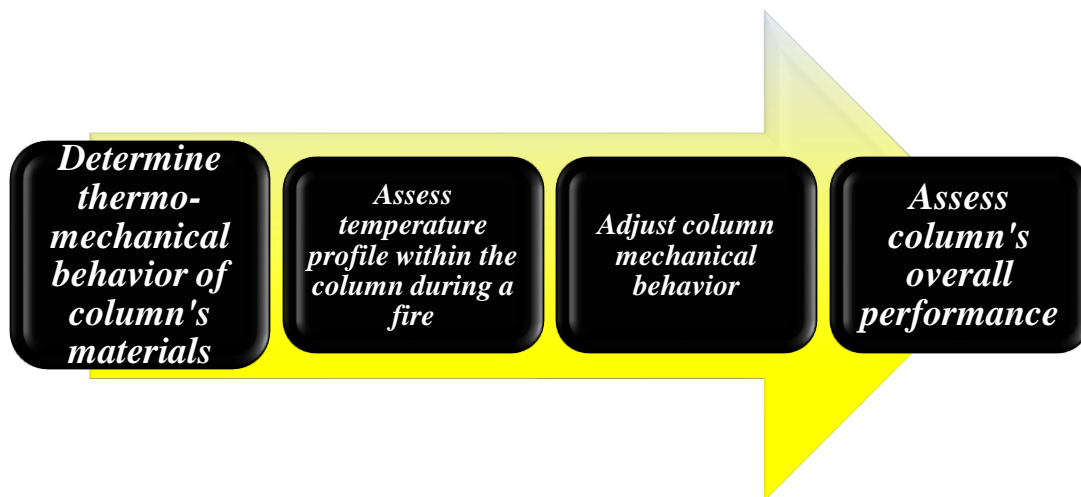
Figure 2-1: Research Approach of Study

2.1 Performance of FRP-Confined RC Columns under Ambient Conditions

In the past three decades or so, numerous studies have been published on the performance of FRP-confined reinforced concrete columns. Design guidelines and acceptance criteria have been established by ACI 440 committee [1] and the International Code Council Evaluation Services (ICC-ES) [27], respectively. There exist specifications on the design of structural elements incorporating FRP systems such those published by ACI committee 440 [1]. The following sections discuss axial behavior, combined axial and bending behavior, and seismic behavior of RC columns.

3.1.1. Axial Behavior: Understanding the behavior of axially loaded FRP-confined concrete is the first step in understanding the mechanics of confinement [5]. FRP confinement can be used to increase the axial capacity of conventional steel-reinforced concrete members. The FRP wrapping/jacketing where fibers are orientated in the hoop directions serves as a passive confinement that is activated only after cracking in the concrete occurs and the concrete dilates. Once activated, hoop stresses are developed in the external FRP composite jacket in a process similar to that spiral reinforcement [5, 28]. External confinement increases the ultimate strength and ductility of the reinforced concrete axial member. Although steel confinement does have similar effects on the performance of an RC column, ACI 318 does not account for the effect of transverse steel reinforcement when estimating the nominal axial capacity of the member. ACI 440.2R-17 [1] describes the nominal axial strength at zero eccentricity of a non-slender normal-weight FRP wrapped RC column, P_o, as follows:

$$P_o = 0.85 f_{cc}'(A_g - A_s) + f_y A_s \qquad \text{Eq. 2-1}$$

where all terms are as defined by ACI 318-19 [29] except for the new term f_{cc}' which is the confined compressive strength of concrete [29]. As per ACI 318-19 [29], the nominal axial capacity of an FRP-confined column, P_n, is obtained by multiplying the results from Eq. 2-1 by 0.85 and 0.80 for circular and rectangular columns, respectively. The value of confined compressive strength f_{cc}' can be obtained using many stress-strain models that have been developed in literature that is dependent on the effective lateral confining stress imposed on the column by the FRP jacketing at rupture, f_{le}. The effective lateral confining stress is directly proportional to the value of internal hoop stresses developed in the jacketing at rupture, f_{fe} [1, 5, and 28].

It is important to note that the maximum strain developed in the FRP jacketing, ϵ_{fe}, is less than the value of the ultimate strain of the FRP, ϵ_{fu}. This is due to factors such as spalling of the concrete which induces stress concentrations in the FRP jacketing. Youssef et al. [5] factored this strength reduction into a confined compressive strength (f_{cc}') equation. Lam and Teng [28], on the other hand, factored this strength reduction into the calculation of the effective internal stress in the FRP where $f_{fe} = E_f \epsilon_{fe}$. This value is incorporated into the equation for f_{le} which is developed from a free body diagram of a thin-walled pressure vessel (see Figure **2-2**) and is defined in Eq. 2-2. The CFRP effective rupture strain, ϵ_{fe}, is calculated using Eq. 2-3.

$$f_{le} = \frac{2 t_f f_{fe}}{D} = \frac{2 E_f t_f \epsilon_{fe}}{D} \qquad \text{Eq. 2-2}$$

$$\epsilon_{fe} = 0.58\epsilon_{fu} \qquad\qquad \text{Eq. 2-3}$$
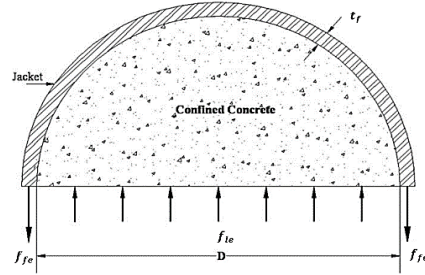
Figure 2-2: Internal Forces in FRP-Confined Column

where: E_f is the longitudinal modulus of elasticity of the FRP jacket with a total thickness, t_f, and D is the diameter of the wrapped column. The constant appears in Eq. 2-3 was obtained from experimental calibration. The value for the ultimate strength of a circular RC column with FRP composite jacket can be calculated in accordance with ACI 440 [1] using the following expression:

$$f'_{cc} = f'_c + 3.135 f_{le} \qquad\qquad \text{Eq. 2-4}$$

Note that the equation is applicable only for RC columns with circular cross-sections. Another alternative universal expression was developed at UCI by Youssef et al. [5] for FRP-confined circle columns is described as follows:

$$f'_{cc} = f'_c + 2.25 \left(\frac{f'_{lu}}{f'_c}\right)^{\frac{5}{4}} \qquad\qquad \text{Eq. 2-5}$$

where: $f'_{lu} = \frac{2t_f f'_{fu}}{D}$. Note that this expression factors in the strength reduction of the FRP composite jacket in the equation and is thus simpler to use.

3.1.2. Seismic Behavior: Results of numerous published research indicated that the use of FRP confinement greatly increases the seismic performance of RC columns. It showed significant improvement in both strength and ductility of columns with deficient steel spiral reinforcement both under relatively high and low axial loading [3, 29]. Unlike steel spiral reinforcement, FRP jackets provide confinement to the entire cross-section and length of the column and results in decoupling stiffness and strength [3, 21, 31].

The enhancement in ductility that FRP confinement provides to concrete columns is one of its main benefits. One way to measure the ductility of columns is through the drift ratio of the column, $\delta_u = \Delta_u/H$, where Δ_u and H are the ultimate deflection and height of the column, respectively. The confinement ratio, more than the FRP fracture strain, has a positive effect on the ultimate drift ratio of the column, where a larger confinement ratio leads to a higher drift ratio. The effective confinement ratio, λ_{fe}, is typically used to compare the amount of FRP confinement between non-identical columns and is defined by:

$$\lambda_{fe} = \frac{f_{le}}{f_c'} = \frac{2E_f t_f \epsilon_{fe}}{D f_c'} \qquad \text{Eq. 2-6}$$

Ozbakkaloglu and Saatcioglu [32] suggested an expression for predicting the drift ratio of FRP-confined concrete columns subjected to an axial load. Adjusting the expression to incorporate the shape and confinement effective factors used in Eq. 2-6 will yield the expression found in Eq. 2-7 after simplification. P_{ou} is the nominal axial capacity of the unconfined column and can be calculated using Eq. 2-8 and $P/P_{ou} \geq 0.2$. The maximum lateral deflection based on the drift ratio, $\Delta_{u\delta}$, can be calculated using the expression in Eq. 2-9

$$\delta_u = 1 + \left[\frac{\lambda_{fe}}{4 \cdot P/P_{ou}} \right] \times 100 \qquad\qquad Eq.\ 2\text{-}7$$

$$P_{ou} = 0.85 f_c'\left(A_g - A_s\right) + A_s f_y \qquad\qquad Eq.\ 2\text{-}8$$

$$\Delta_{u\delta} = \left[1 + \left[\frac{\lambda_{fe}}{4 \cdot P/P_{ou}} \right] \times 100 \right] \cdot H \qquad\qquad Eq.\ 2\text{-}9$$

However, the drift ratio increases with increasing confinement only up to a certain confinement ratio beyond which the ultimate drift ratio starts to decrease [6,21]. Gu et al. [21] explained that the decrease in drift ratio can be attributed to the increase in frictional bond between the steel and concrete which reduces the strains induced in the longitudinal reinforcement.

On the other hand, the curvature ductility index, μ_Φ, increases with increasing confinement [6]; where $\mu_\Phi = \Phi_u/\Phi_y$. The maximum curvature of a column, Φ_u, is the summation of the yield curvature, Φ_y, and the plastic curvature, Φ_p, and can be calculated by [1, 33]:

$$\Phi_u = \Phi_p + \Phi_y = \frac{\theta_p}{L_p} + \frac{\epsilon_{sy}}{d - c_y} \leq \frac{\epsilon_{ccu}}{c_u} \qquad\qquad Eq.\ 2\text{-}10$$

Where θ_p is the maximum rotation in the plastic hinge and L_p is the length of the plastic hinge region that is estimated to be equal to the column cross section, D [3, 6, 31]. ϵ_{sy} and c_y are the steel strain and the depth of neutral axis at yield, respectively, and ϵ_{ccu} and c_u is the ultimate strain in the confined concrete, and neutral axis when that strain is reached, respectively.

Youssef et al. [34] developed a detailed model using an experimental database of 37 full-scale columns that accurately predicts the ultimate displacement of FRP-confined columns. They also developed a more detailed model for predicting the length of the plastic hinge region in FRP-

confined columns. The drift model has the advantage of incorporating the plastic hinge length and column curvature into the expression. The Paulay and Priestley [33] plastic hinge model was modified to incorporate the effect of FRP confinement as follows:

$$L_p = 0.8\lambda_{fe}H + 0.022f_{sy}d_b \qquad \text{Eq. 2-11}$$

where: d_b is the diameter of the longitudinal rebar, and f_{sy} is longitudinal steel yield strength.

The model provides a more accurate prediction of the ultimate drift ratio of the columns in the database compared to other models [32, 34]. The ultimate drift ratio model is a modified version of the Paulay and Priestly [33] model and is shown in Eq. 2-12. The expressions for calculating Φ_y and Φ_u are given Eq. 2-13 and Eq. 2-14, respectively.

$$\delta_u = \frac{\Phi_y H}{3} + \frac{(\Phi_u - \Phi_y)L_p(H - 0.5L_p)}{H} \qquad \text{Eq. 2-12}$$

$$\Phi_y = \frac{2.45\epsilon_{sy}}{D} \qquad \text{Eq. 2-13}$$

$$\Phi_u = \frac{0.013 + 0.05\lambda_{fe}}{0.18D + \frac{P}{P_o}(0.7 - 0.25\lambda_{fe})D} \qquad \text{Eq. 2-14}$$

Similar to unconfined columns, FRP-confined columns exhibit a decrease in deformability with an increasing ratio of axial load to column axial capacity (P/P_o) [3, 21, 30]. This is supported by the relation given in Eq. 2-14.

The incorporation of FRP also increases the column energy dissipation capacity [3, 6, 21]. Energy dissipation is defined as the area encased by the moment-displacement curve (hysteresis) of a column. According to Gu et al. [21], at low axial loading, stiffness of the FRP jacket makes no

difference in the energy dissipation capacity of a column. However, at high axial loading, a large confinement stiffness provides larger energy dissipation. The authors however did not provide sufficient explanation for this phenomenon. At high axial loading, an increase in effective confinement stiffness, $E_l = 2E_f t_f / D$, is more significant than confinement ratio, λ_f [6,21]. It is important to note that for an identical FRP strengthening system, an increase in one value leads to a proportional increase in the other value. Hence, it can be said that an increase in confinement ratio will lead to an increase in energy dissipation for FRP-confined circular columns with the same $E_f, t_f, and\ D$.

2.2 Effect of Fire on Constituent Materials

To understand the seismic behavior of fire-damaged FRP-confined RC columns, one must first understand the effects of fire on the constituent materials of such columns. It is important to understand the influence of elevated temperatures on the mechanical properties of the column materials (thermo-mechanical) and post-cooling (residual) behavior. In order to perform accurate heat transfer modeling, thermal conductivity and specific heat of FRP composites, concrete, and steel need to be understood and identified. Thermal conductivity is the material's capacity to transfer heat (thermal energy) to another material via conduction. A higher thermal conductivity leads to a higher heat transfer. Specific heat is defined as the amount of energy required to raise a unit mass of material by a unit of temperature. Performing heat transfer analysis of the column will be used to predict the column's internal temperatures when exposed to fire. This information will also be used to obtain the changes in mechanical properties of different materials that allow for better modeling of the fire-exposed column's seismic performance.

Assessing fire performance of a structural member, such as RC column, can be achieved by conducting standardized tests described in ASTM E119 standard [36]. This ASTM standard procedure is discussed in more detail in Chapters 6 and 7. It is impossible to accurately predict the temperatures that could occur in a real fire; therefore, ASTM E119 specifies a *time-temperature curve* for such a standardized test (refer to Figure **2-3**). Henceforth, the term "standard fire" will refer to the fire specified by ASTM E119 [36]. Figure **2-4** presents a comparison between the time-temperature curve of ASTM E119 standard [36] and a typical actual fire curve [37].

2.2.1   Effect of Fire on Reinforced Concrete

Concrete is the most widely used construction material in the world. One of the benefits of concrete that makes it popular is its favorable performance during fires. ACI 216 [10] specifies fire resistance requirements for both concrete and masonry structural members that includes concrete cover requirements to ensure adequate fire endurance of an RC structural member. In general, fire rating of a structural member is determined by the number of hours that it can withstand a fire until it can no longer withstand its design load. In other words, a fire rating of 5 hours means that the structure fails after five hours of fire exposure. The required fire rating for columns is typically 4 hours [36].

2.2.1.1   Reinforced Concrete Thermal Properties

As mentioned earlier, concrete has a low thermal conductivity that decreases with increasing temperature. This property makes concrete a good insulator that allows for RC structures to achieve a favorable fire rating without the need for insulation, as compared to steel structures [37]. The specific heat of the concrete is also temperature-dependent, and it is influenced by the amount

of moisture in the concrete, especially in the temperature range of 100-115℃. A specific heat value $(c_{c,peak})$ of 1.47 kJ/kg·K is used to account for the moisture evaporation heat within that temperature range. Concrete density changes slightly at elevated temperatures due to moisture evaporation and other chemical reactions. Table *2-1* provides details on concrete thermal properties as defined by both Eurocode 4 [38] and Lie [37].

Steel, on the other hand, has high thermal conductivity (heat-sink) and thus, the temperature gradient inside the steel is considered uniform. Due to its relatively small mass as compared to a concrete section (ρ_c ranges from 1% to 8%), steel reinforcement plays little role during the heat transfer process. It is thus safe to assume that the temperature of the steel is the same as that of the surrounding concrete.

2.2.1.2   *Mechanical Properties of Reinforced Concrete at Elevated Temperatures*

The mechanical properties of both steel and concrete are affected when exposed to elevated temperatures. For example, concrete strength at elevated temperature varies greatly depending on the type of aggregates [36, 38]. The concrete modulus of elasticity, on the other hand, is not affected by aggregate type. The elastic modulus never completely recovers after cooling. Additionally, the lower the cement-to-aggregate ratio, the less degradation occurs in concrete which means that cement is affected more than aggregates by exposure to elevated temperatures. The water content in concrete can help concrete retain its compressive strength at moderately high temperatures as moisture migrates from the core of the specimen. This process can be delayed in concretes with low porosity such as high-strength concrete. Calcium silicate hydrate (C-S-H) starts to decompose at around 560 ℃ [39]. This decomposition along with water evaporation and

other changes in the chemical structure causes an increase in pore size of the concrete which further contributes to the degradation of its mechanical properties. In 2015, Lim [40] conducted an experimental study to evaluate both micro- and nano-structural changes of cement paste exposed to elevated temperatures. In these tests, cement paste specimens with a w/c ratio of 0.35, were heated until 1,000 ºC and their behavior was assessed. Results showed that the nanostructure of cement paste changes to a more loosely packed globular structure when exposed to 300 ºC. Results also indicated that microcracks were developed at 500ºC at the interface and became more intense as the temperature increased to 700ºC and 900ºC as paste porosity increases. Figure *2-5* shows scanning electron microscope (SEM) images of fractured surfaces of cement paste specimens at different temperatures.
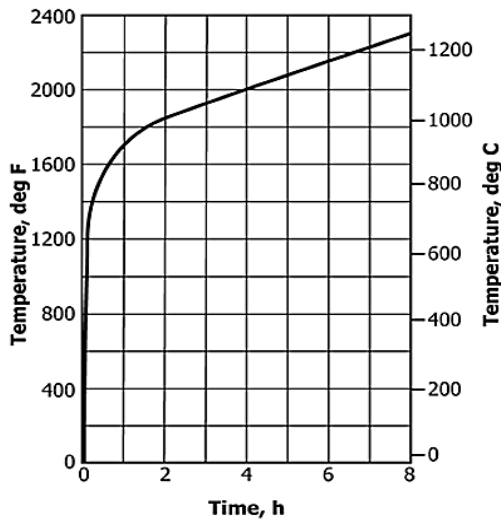
Figure 2-3: ASTM E119 Standard Fire Time-Temperature Curve [36]
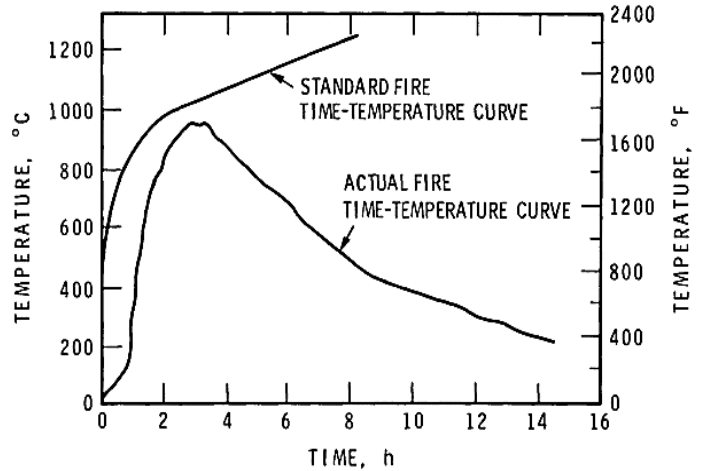
Figure 2-4: Time-Temperature Curve for ASTM-Standard vs. Actual fire [37]

Also, published research showed that loaded concrete exhibit less strength deterioration under elevated temperatures as compared to none-loaded concrete [13, 38].

It is known that mechanical properties of steel deteriorate greatly at elevated temperatures ($T >$ 200℃) [37]. Additionally, steel exhibits significant viscoelastic behavior (creep) at temperatures beyond 450℃ which is well within the temperature range of a standard fire. The critical temperature for steel (corresponding to a 50% reduction in yield strength) is 593℃ [12, 23]. For these reasons, steel requires adequate fire protection. Minimum concrete cover provisions exist in part to ensure that steel rebars are fully encased in concrete and are therefore adequately insulated. Dai et al. [15] were able to numerically simulate the performance of fire insulation by transforming it to an equivalent concrete layer. Figure **2-6** plots the normalized mechanical properties of steel and concrete with respect to time; where: f_c , f_{ct}, and E_c are the compressive strength, the tensile strength, and elastic modulus of concrete respectively; f_{sy} and E_s are the yield strength and elastic modulus of steel.
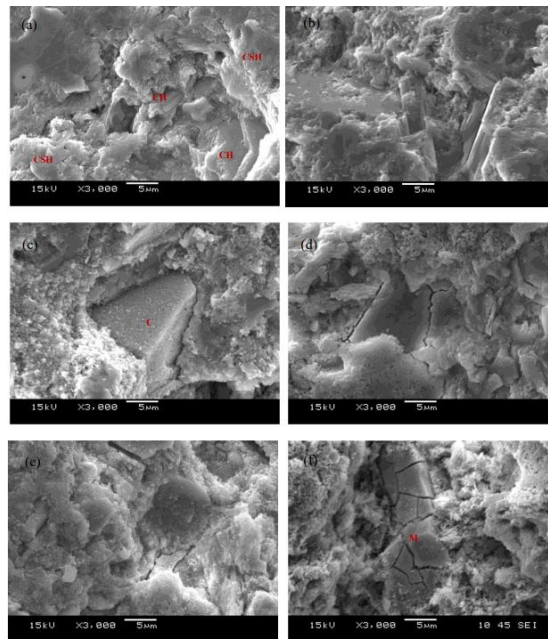
Figure 2-5: SEM images of fractured surfaces of cement paste (a) at room temperature (control sample), (b) 105 ℃, (c) 300 ℃, (d) 500 ℃, (e) 700 ℃ and (f) 900 ℃ with w/c of 0.35 [40]

Table 2-1: Thermal Properties of Concrete

Material Temperature (°C)	Density (kg/m^3)	Thermal Conductivity ($W/m \cdot$ °C)		Specific Heat ($J/kg \cdot$ °C)	
	Eurocode 4	Lie, 1992 [37]	Eurocode 4	Lie, 1992 [37]	Eurocode 4
20	2,300	1.49	1.33	783	900
100	2,300	1.44	1.23	957	1,470
115	2,300	1.43	1.21	989	1,470
200	2,254	1.38	1.11	1198	1,000
300	2,200	1.31	1.00	12273	1,050
400	2,185	1.25	0.91	12357	1,100
500	2,165	1.19	0.82	1848	1,100
600	2,145	1.13	0.75	1259	1,100
700	2,125	1.06	0.69	1271	1,100
800	2,105	1.00	0.64	1283	1,100
900	2,084	1.00	0.60	1296	1,100
1,000	2,064	1.00	0.57	1308	1,100
1,100	2,044	1.00	0.55	1321	1,100
1,200	2,024	1.00	0.55	1334	1,100

Many detailed methods for evaluating the fire resistance of concrete elements exist. One popular manual is ASCE Structural Fire Protection by Lie et al. [37]. The manual specifies the minimum required column dimension, D in inches, to achieve a fire rating of R, which is a measure of fire endurance in hours. The relationship for a normal-weight concrete circular column with siliceous aggregates is given by:

$$D = 3.2f(R + 0.75)$$

Eq. 2-15

where: f is an overstrength factor that considers the bracing conditions of the columns and effective length factor, k, as defined by ACI 318-19 [2]. Other equations exist for different types of aggregates and cross-sections. The manual also provides the minimum cover requirement to ensure the steel does not reach excessive temperatures.

2.2.1.3   RC Heat-Damaged Residual Mechanical Properties

Numerous studies have established that heated steel reinforcement tends to retain most of its mechanical properties post-cooling [41,42]. Concrete on the other hand exhibits a reduction in mechanical properties after being exposed to elevated temperatures. The increase in pore size due to moisture evaporation and the decomposition of C-S-H leads to permanent damage to the mechanical properties of concrete. Ma et al. [39] describe the heat-damaged residual compressive strength of concrete as experiencing three stages:

1) $Ambient < T < 300°C$: constant strength with a possible slight increase due to post-curing of concrete
2) $300°C < T < 800°C$: a steep reduction in compressive strength
3) $T > 800°C$: almost zero compressive strength
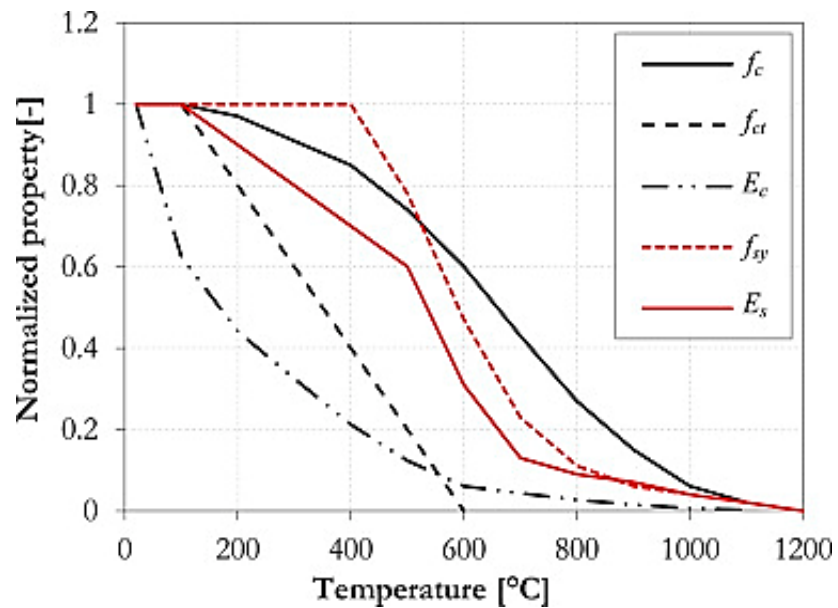
Figure 2-6: Mechanical Properties of Concrete and Mild Steel with Respect to Temperature [13]

Lie et al. [41] used available experimental data to provide the following relations to describe the residual strength of concrete, f'_{cr}, based on the highest temperature attained by the concrete, T:

$$\frac{f'_{cr}}{f'_c} = \begin{cases} 1 - 0.001T & ,0°C < T < 700°C \\ 1.375 - 0.00175T & ,500°C < T < 700°C \\ 0 & ,T > 700°C \end{cases} \qquad Eq.\ 2\text{-}16$$

Chang et al. [43] tested the residual mechanical properties of 108 cylinders that were exposed to temperatures in the range of $100 - 800°C$. The authors developed a relationship for f'_{cr} expressed in Eq. 2-17. They also provide a relationship for the peak strain of the heat-damaged concrete, ϵ_{cur} as can be shown in Eq. 2-18.

$$\frac{f'_{cr}}{f'_c} = 1.008 + \frac{T}{450\,ln\left(\frac{T}{5800}\right)} \geq 0 \qquad ,20°C < T < 800°C \qquad Eq.\ 2\text{-}17$$

$$\frac{\epsilon_{cur}}{\epsilon_{cu}} = \begin{cases} 1 & ,20°C < T \leq 200°C \\ (-0.1f'_c + 7.7)\left[\frac{exp\,(-5.8 + 0.01T)}{1 + exp\,(-5.8 + 0.01T)} - 0.0219\right] + 1 & ,200°C < T \leq 800°C \end{cases} \qquad Eq.\ 2\text{-}18$$

Chang et al. [43] also obtained the stress-strain curves of heat-damaged concrete cylinders and observed that the difference between the initial tangent modulus (E_o) and the peak secant modulus (E_p) decreases with increasing exposure temperatures. It was also noted that as temperatures increases the descending branch flattens. A summary of experimental residual stress-strain curves of heat-damaged 40.0 MPa concrete is presented in Figure *2-7*.

2.2.2   *Effect of Fire on FRP Composites*

Different manufacturing processes and composition of FRP composites produce different mechanical and hygrothermal characteristics of the final FRP product. It is therefore important to focus on characterizing the fire performance of FRP composites that will be used in this proposed study.
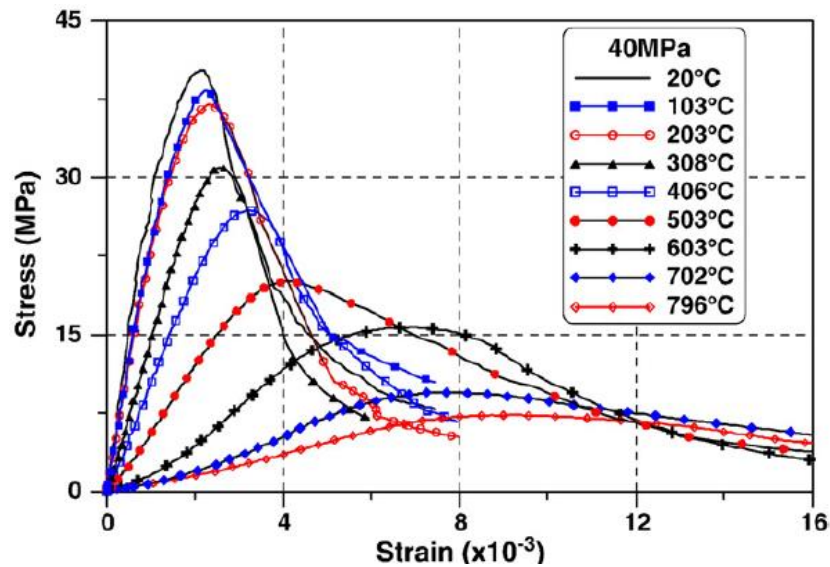
Figure 2-7: Residual Stress-Strain Curves of Heat-Damaged Concrete [43]

Fiber-reinforced polymer composites are used by different industries such as aerospace, civil, naval, transportation, and renewable energy. Each industry typically uses a different manufacturing process for FRP depending on the application. Some of the FRP manufacturing methods are filament winding, Vacuum-Assisted Resin Transfer Molding (VARTM) process, and pultrusion. However, for the repair and rehabilitation of RC members, the wet layup lamination method is the preferred process [1, 43]. The wet layup process is performed by spreading a layer of epoxy-based room-temperature cure primer on the exterior surface of the RC column before starting with a layer of epoxy resin. Saturated unidirectional or multidirectional woven synthetic fabrics (e.g., E-glass, carbon, or aramid fiber fabrics) are then applied to the specified location with specified fiber orientations depending on the structural design. Each saturated fabric is squeezed firmly to remove any excess resin to maintain the target fiber volume fraction (V_f). This process can be repeated until the desired number of composite plies is achieved. Finally, the

laminate is allowed to cure for at least 48 hours depending on the resin characteristics, surrounding temperature, and relative humidity.

Although E-glass and aramid composite systems are used in construction applications, however, the most widely used type in construction is carbon fiber reinforced polymer (CFRP) due to favorable mechanical properties and durability features. E- and S-glass are often used because of their relatively low cost as compared to CFRP composites. However, glass fiber composites have a lower on-axis elastic modulus (about one-tenth of steel) as compared to carbon fiber composites, in addition to their susceptibility to long-term creep and degradation in alkaline environments such as fresh concrete. Moreover, carbon fiber composites have been found to exhibit superior durability at elevated temperatures as compared to glass and aramid fibers composites [13]. Comparisons between the tensile strength of carbon, glass, and aramid at elevated temperatures are presented in Figure *2-8*.

Epoxies that are typically used in the aerospace industry are cured at high temperatures and are called high-cured epoxies (HCE) and can withstand large temperatures before experiencing a reduction in thermomechanical properties [45]. However, in cases such as repair of structural columns, cold-curing or room-temperature curing epoxies (CCEs) are preferred over HCEs because their ease of installation does not demand ideal and high quality-control conditions such as those at laboratory or shops [46]. The majority of fabrics that are typically used for columns strengthening applications are unidirectional because it is sufficient to provide the hoop stresses needed for confinement.

Considering all these variations in FRP composition, the available literature must be compared to FRPs with similar compositions as much as possible. The focus of this study will be on wet laid externally bonded unidirectional fiber-reinforced polymer composites with a cold curing epoxy matrix.

2.2.2.1 FRP Thermal Properties

For unidirectional FRP composites, fibers control thermal conductivity in the longitudinal direction. While carbon fiber shows high resistance to thermal degradation, it does have high thermal conductivity compared to glass and aramid fibers. Polymers on the other hand have relatively low thermal conductivity and they control the thermal conductivity in the transverse direction of the FRP. The thermal conductivity of carbon/epoxy $48.44 - 60.55 \ W/m \cdot \ ^\circ\text{C}$ in the longitudinal direction and $0.87 \ W/m \cdot \ ^\circ\text{C}$ in the transverse direction [13]. *Figure 2-9* shows the variation in thermal properties of CFRP with respect to temperature.
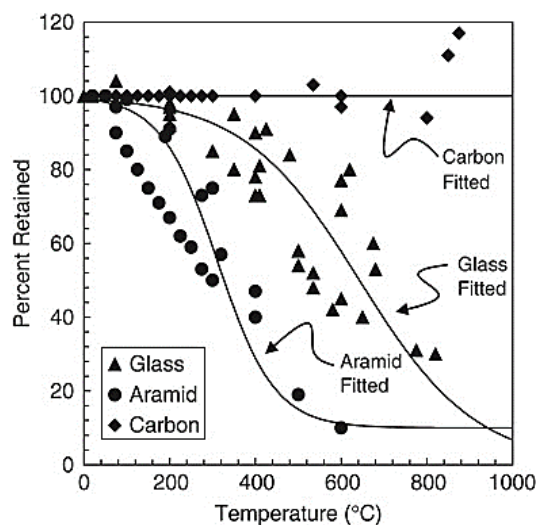
Figure 2-8: Tensile Strength of Glass, Aramid, and Carbon Fibers vs. Temperature [13]
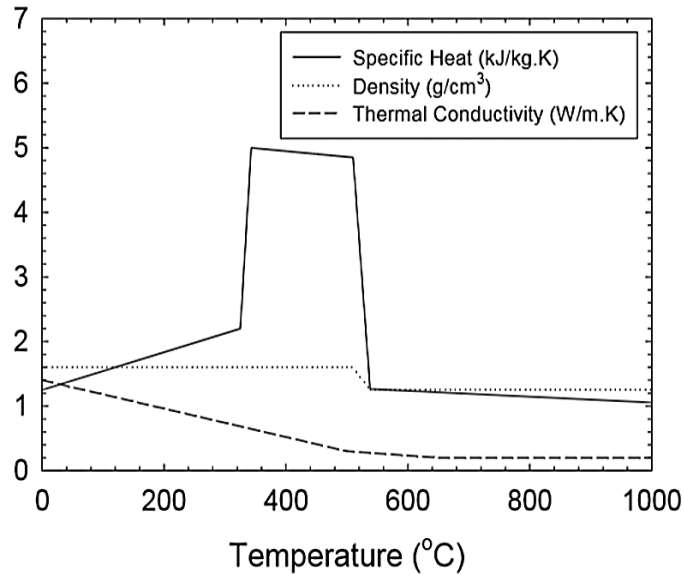
Figure 2-9: Specific Heat, Density, and Thermal Conductivity of CFRP vs. Temperature [13]

2.2.2.2 *FRP Mechanical Properties at Elevated Temperature*

One of the most important FRP composites property to be considered for fire endurance is its glass transition temperature (T_g). As discussed earlier, glass transition temperature is defined as the midpoint within a temperature range where FRP polymer matrix changes from a plastic state into a flexible, viscoelastic state. The glass transition temperature is typically in the range of $50 - 120\ ℃$. The value of T_g can be experimentally determined through either Dynamic Mechanical Analysis (DMA) or Differential Scanning Calorimetry DSC [12].

Mechanical properties of the FRP polymeric composites drop drastically beyond T_g, although strength degradation can start well before T_g [44,47,48]. Hence, the mechanical properties of FRPs at elevated temperatures are highly dependent on the laminate's fiber volume fraction (*fibers volume/laminate volume*). The typical fiber volume fraction range for a typical wet layup

laminate is 30% to 40%. Hawileh et al. [44] found that CFRP lost 61% of its elastic modulus and 46% of its ultimate strength at 300 ℃. The degradation of CFRP mechanical properties during fires is sensitive to oxidation [49]. Proper insulation will reduce the amount of oxygen that comes in contact with the laminate. This means that fibers away from the exposed surface will not experience the same loss in mechanical properties. The negative effects due to exposure to high temperatures are more pronounced in the epoxy as opposed to the fibers themselves [50]. Therefore, mechanical properties that are dependent on the matrix are most affected by elevated temperatures. Matrix dependent properties of FRP include interlaminar shear strength and stress transfer between fibers. The matrix in FRP composites is responsible for load transfer from the matrix to the fibers and from fibers to other adjacent fibers [51].

Another factor affecting the mechanical properties of FRPs is the difference in coefficient of thermal expansion between fibers and resin which weakens the fiber/matrix interface. This can weaken the stress transfer between fibers and increases the risk of delamination [50].

Figure *2-10* shows the change in FRP mechanical property under elevated temperatures [47]. The mechanical property of an FRP is assumed to remain close to its value at room temperature, $P_{initial}$, and then start degrading beyond T_{cr} until it reaches P_R at the point of the melting temperature of the polymer matrix, T_m. $T_{central}$ and $P_{central}$ are the points at which the graph is nearly symmetrical.
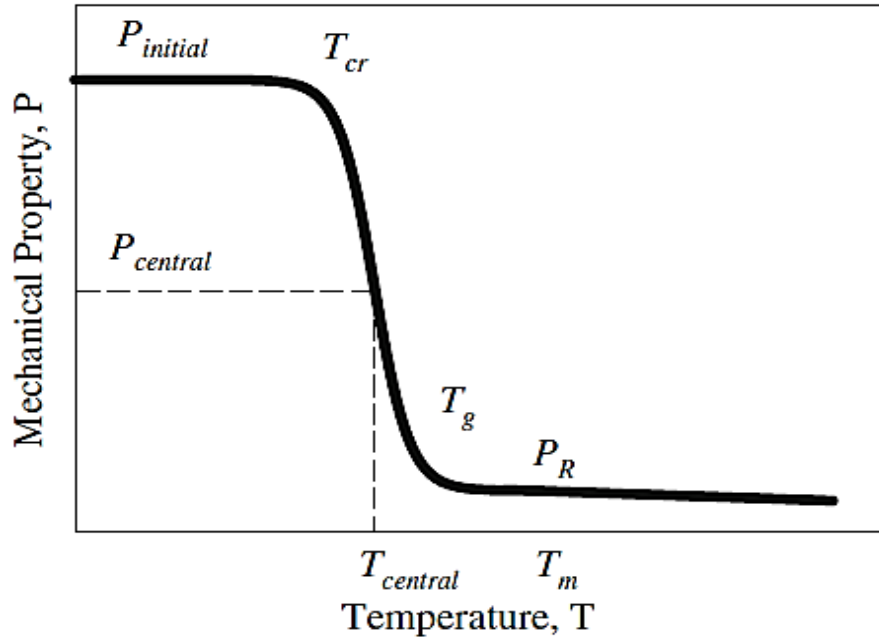
Figure 2-10: Typical Plot of FRP Mechanical Properties vs. Temperature

A polynomial mathematical function is suggested by Kulkarni and Gibson [52] for calculating the mechanical property of an FRP, $P(T)$, at temperature T and is given by the following equation:

$$\frac{P(T)}{P_{initial}} = 1 - \left[\begin{array}{l} a_1 \left(\dfrac{T - T_{initial}}{T_g - T} \right) \\ + a_2 \left(\dfrac{T - T_{initial}}{T_g - T} \right)^2 \\ + a_3 \left(\dfrac{T - T_{initial}}{T_g - T} \right)^3 \end{array} \right] \qquad Eq.\ 2\text{-}19$$

Gibson et al. [53] expanded on this relationship with a hyperbolic tangent function that is given by:

$$P(T) = R^n \left[\frac{P_{initial} + P_R}{2} - \frac{P_{initial} - P_R}{2} \tanh\{k_m(T - T_{central})\} \right] \qquad Eq.\ 2\text{-}20$$

where: k_m is a parameter obtained from experimental curve fitting; R is the remaining epoxy content, with a value of 1.0 denoting no decomposition and a value of 0.0 denoting total mass loss; n depends on the stress state. It recommended that $n = 0$ for matrix dependent properties and $n = 1.0$ for fiber dependent properties [53].

Bisby [13] introduced the following semi-empirical equation to predict the reduction in the mechanical properties of FRP with respect to temperature:

$$\frac{P(T)}{P_{initial}} = \left(\frac{1-a}{2}\right)\tanh[-b(T-c)] + \left(\frac{1+a}{2}\right) \qquad Eq.\ 2\text{-}21$$

where: a is an assumed constant that is based on the residual mechanical property value, and b and c are empirical constants. Table **2-2** summarizes the coefficients that Bisby [13] derived based on previous experimental data.

Table 2-2: Coefficients for mechanical properties of CFRP and GFRP at elevated temperatures

Material	Property	Coefficients		
		a	*b X10^-3*	*c*
CFRP	Tensile Strength	0.10	5.83	339.54
	Elastic Modulus	0.05	8.68	367.41
GFRP	Tensile Strength	0.10	8.10	289.14
	Elastic Modulus	0.05	7.91	320.35

2.2.2.3 Heat-Damaged Residual Mechanical Properties

Very few experiments have been conducted in examining the post-heated residual mechanical properties of FRP composites used in construction [41, 53, 54]. A summary of residual strength values of published CFRP post-heated residual experimental results is presented in **Table 2-3.** All published experimental studies were performed under steady-state conditions where FRP composite laminates were exposed to a temperature T_{ex} ($23°C - 400°C$) for a specified period,

t_{ex}, before being completely cooled down. The specimens were then tested under ambient conditions and failure strength was recorded. The normalized residual property, $k = P_T/P_{23°}$, is recorded for better comparison between different types of FRP composites.

The effect of exposure duration on the residual strength of heated CFRP composites is plotted in Figure *2-11*. It is expected to see a larger strength reduction for longer exposure at an elevated temperature. Test results of the t_{ex} for 60.0 and 180.0 minutes confirm that hypothesis. Still, more tests need to be conducted before a conclusive statement can be made.

Naser & Uppala [58] developed a model for predicting the residual mechanical properties of heated FRP composites based on Refs. [41, 43, and 53].

Nguyen et al. [55] performed an experimental study focusing on evaluating residual tensile strength of twelve pultruded CFRP composite specimens that were exposed to temperatures ranging from $200 - 600°C$ for a duration of 60 minutes. Coefficients for Eq. 2-21 were calibrated by Bisby model [13] to predict the residual ultimate strength and Young's modulus of heated FRPs. The calibrated coefficients are presented in Table *2-4*.

Table 2-3: Residual strength of CFRP composites due to different temperature exposure

	Source	Fabrication	T_g (°C)	t_{ex} (min.)	Specimen	$P_{23°}$ (MPa)	Normalized Residual Strength				
							23°	100°	200°	300°	400°
1	Foster et al., 2008 [54]	Layup	78	180	Coupon	986	1	0.96	0.92	0.9	0.46
			85	180		3800	1	0.88	0.84	0.48	0.4
2	Hawileh et al., 2015 [44]	Layup	58[b]	45	Coupon	1485	1	0.86	0.66	0.54	-
3	Kim et al., 2014 [56]	Layup	71	180	Coupon	2070	1	0.75	0.68[c]	-	-
4	Al-Salloum et al., 2011	Layup	88	60	Wrapped	38.8	1	0.99	0.81	-	-

	[57]			120	Concrete	38.8	1	0.99	0.78	-	-
				180		38.8	1	0.95	0.73	-	-
5	Hamad et al., 2017 [42]	Pultruded	-	180	Bars	1572	1	0.933	0.8[a]	0.54[a]	0.27[a]
6	Nguyen et al., 2018 [55]	Pultruded	100-125	60	Coupon	2389	1	0.88[a]	0.79	0.7	0.6

[a] *Interpolated*   [b] *Reported by manufacturer*   [c] *One outlier removed*
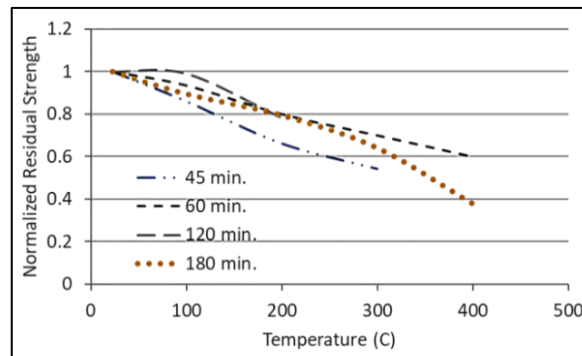
Figure 2-11: Residual Strength of CFRP vs. Temperature for different t_{ex}

A comparison between models developed in Refs. [13, 54, and 57] were compared to the experimental results presented in *Table* **2-3**. The comparison presented in Figure **2-12** shows that the model by Nguyen et al. [55] provides the most accurate prediction of the residual strength of heated CFRP composites across all temperatures.

Table 2-4: Coefficients for predicting the residual mechanical properties of CFRPs exposed to elevated temperatures [13]

Property	Coefficients		
	a	*b*	*c*
Residual On-axis Ultimate Strength	0.1133	0.0039	350
Residual On-axis Modulus of elasticity	-0.0154	0.0129	536.9

Experimental values of the residual stiffness reported by Refs. [41, 43, and 54] were compared to predictions from the calibrated Bisby model [13] as suggested by Nguyen et al. [55] (see Table **3-3**). The comparison is presented in Figure *2-13*. It is expected to see a larger strength reduction

for longer exposure at an elevated temperature. Experimental results for the t_{ex} of 60.0 minutes and 180.0 minutes confirm that hypothesis. Still, more tests need to be conducted before a conclusive statement can be made.
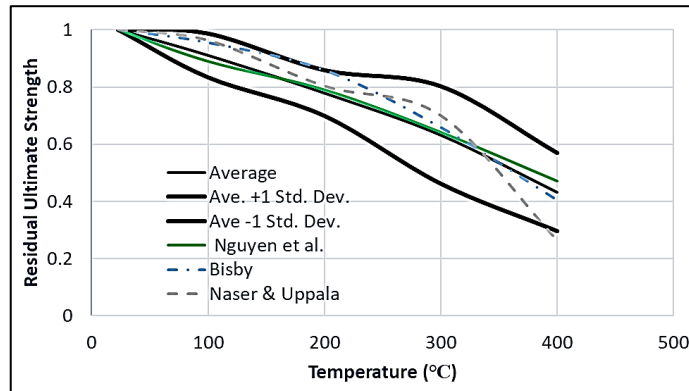
Figure 2-12: A Comparison of Residual Strength Prediction Models Results for CFRP

2.2.2.4   *Effect of Elevated Temperatures on Epoxy Adhesives*

Bond strength is the critical property when assessing fire behavior of RC column confined by FRP composites because it largely depends on the resin properties [22]. The use of adhesive as opposed to mechanical fasteners reduces the probability of delamination caused by stress concentrations [59]. The use of FRP composite jackets is achieved by external bonding and single-lap shear bonding process. The FRP wrapping is continuously bonded to the concrete column using an adhesive. FRP is then bonded onto itself with an overlap in what is essentially a single-lap adhesive joint. The single-lap method is often used for ease of installation and when shear transfer between the concrete and the FRP is not needed. Typically, shear transfer is not needed for axial confinement, however, it is useful for seismic applications. The bond between the FRP composite laminates and concrete can be assumed to be lost once the confined concrete dilates.

For bonded single-lap joints using an epoxy adhesive, strength decreases with increasing adhesive thickness. The joint strength increases with increasing overlap length up to a point before remaining constant [50]. No generalized formula exists to predict the joint strength with respect to geometric parameters such as overlap length and bond line thickness. Each type of adhesive is unique in this way and requires independent testing to find the optimum joint configuration [50].

Chowdhury et al. [47] tested single-lap splice adhered GFRP specimens at elevated temperatures under steady-state and transient conditions. They recorded a single lap-splice shear strength loss of around 30% at 45°C (T_g-30) and 77% at 75°C (T_g). All tested coupons failed in the lap-splice region. For CFRP composites, Cree et al. [60] evaluated their tensile and lab-splice strength characteristics when subjected to elevated temperatures. The evaluation was performed using both steady-state and transient temperature tests. Results indicated that the adverse effect of elevated temperature exposure on bond strength was greater than on both tensile strength and tensile modulus of the CFRP composites.
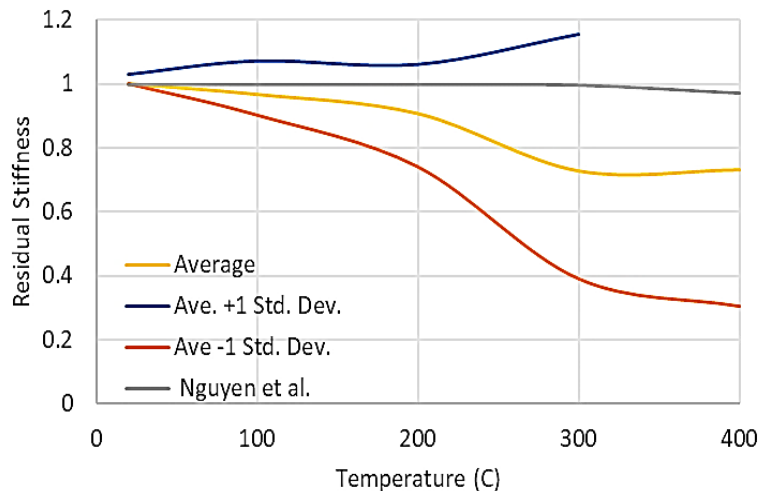
Figure 2-13: Experimental Residual Stiffness and Model Prediction Comparison

Foster and Bisby [54] tested the residual mechanical properties of two epoxies that were exposed to temperatures up to 300°C under steady-state conditions. The residual single-lap shear (SLS) strength and the residual tensile strength of the heated epoxies were tested and are presented in *Table 2-5*. The results suggest the residual shear strength of epoxies is not as severely affected by elevated temperatures as tensile strength. More tests are needed to test these findings.

Table 2-5: Residual mechanical properties of heated epoxies

Source	T_g (°C)	t_{ex} (min.)	Specimen	Property	P_o (MPa)	20	100	200	250	300
Foster *et al.,* 2008 [54]	78	180	Coupon	Tensile Strength	72.4	1	1.05	1	0.55	-
	85				55.2	1	1.05	0.1	-	-
	78		SLS	Shear Strength	-	1	0.95	0.88	0.72	0.12
	85				-	1	0.96	0.84	0.88	0

2.2.2.5 Environmental and Health Considerations

Another risk, on top of thermomechanical degradation, is the environmental and health hazard risks posed by possible combustion of the FRP composites during a fire. When exposed to fire, the decomposition of the epoxy releases volatile toxic gasses that pose health and structural risks through heat production [20, 60]. The thermal decomposition temperature of the epoxy polymer is approximately $4T_g$ [43, 46]. Therefore, the value of R in Eq. 2-20 can be taken as 1.0 if the CFRP's temperature is maintained below $4T_g$.

At temperatures close to 500°C, carbon fibers near the fire-exposed surface start to decompose due to oxidation. This process rapidly increases at temperatures above 550°C. Similar to modulus degradation, thermal decomposition of sub-surface fibers is reduced due to lack of air diffusion caused by escaping gasses that are produced by the already decomposed epoxy matrix [49].

Epoxy not only supports combustion but can also produce copious quantities of dense black smoke at elevated temperatures. Some additives can be incorporated into epoxy resin to enhance its flammability and smoke generation characteristics (fire and smoke retardant additives). However, these additives decrease the mechanical properties of the epoxy and are therefore not popular in the industry [23].

2.3   Effect of Fire on FRP-Confined RC Columns

The preceding sections provided an understanding of the fire behavior of the hybrid column's constituent materials. This information is essential to understand and be able to analyze the behavior of FRP-jacketed columns. Figure *2-14* shows the tensile strength versus temperature of concrete and steel based on approximations proposed by Lie [37] and for CFRP and GFRP composites based on formulations developed by Bisby [13]. This figure is very important in understanding the behavior and mechanical properties degradation pattern of the different possible components of a typical FRP-strengthened column subjected to fire. As shown in this figure concrete strength will only start to degrade at about 450$^{\mathrm{o}}$C. At the same temperature, the residual strength percentage of steel, CFRP, and GFRP composites already reached about 42%, 30%, and 18% of their corresponding room temperature strength, respectively. Also, at a temperature of 600$^{\mathrm{o}}$C (red fire temperature starts from about 550$^{\mathrm{o}}$C to 1,100$^{\mathrm{o}}$C), both CFRP and GFRP composites retain only about 15% of their room temperature strength values, and the residual strength of the steel is about 25%. At that same temperature, concrete, that is considered to be a good thermal insulator, is capable of maintaining about two-third of its room temperature strength. One also can see that both steel and GFRP are able to retain the same residual strength of about 65% at a temperature of about 280$^{\mathrm{o}}$C, while the corresponding temperature for CFRP

and steel for retaining about 67% of their room temperature strength is about 330°C. However, this relatively better performance of GFRP as compared to CFRP will end once the temperature exceeds 330°C. This is an important observation that can be used as a guideline for selecting the column composite jackets when exposed to elevated temperature. For example, if the maximum design exposure temperature is 330°C, GFRP composites, which is more economical than CFRP composites, is the optimum selection, provided that other mechanical design criteria are met. In addition, up to a temperature of 200°C, both CFRP and GFRP have the same strength retention.

The bulk majority of previous research on assessing the fire performance of FRP-confined RC columns focused on their fire performance while axial loads are applied. According to ASTM E119 [36], the fire endurance failure criteria of a column are satisfied when a column can no longer withstand its service load. Other failure criteria that are suggested by researchers are: (i) temperature in the FRP-concrete interface exceeds FRP composites glass transition temperature, T_g; and (ii) temperature in the outer surface of the FRP exceeds the *ignition temperature* of FRP constituent materials [62]. The second criteria are controlled by the epoxy matrix and can be taken conservatively to be 350 ℃. As shown in **Table 2-5** epoxy adhesives can recover up to 88% of their shear strength after being exposed to a temperature of 200℃. This means that the temperature in the FRP-concrete interface can be allowed to reach a temperature exceeding its glass transition temperature (i.e., $T > T_g$) if the column does not reach the unstrengthened capacity during the fire event.

Experimental procedures adopted by the majority of published research on the performance of fire-damaged FRP-confined columns are based on ASTM and ISO standards. The columns are

loaded with a sustained gravity load, typically service loading based on specification by ACI 440 committee [1], and are exposed to a standard fire regime; this is called transient-state testing. The goal of this procedure is to measure the fire endurance rating of the structural element. However, one issue that is consistent in all published studies is the declaration that it is difficult to define the point at which the FRP composite jacket becomes ineffective during exposure to a standard fire. Steady-state testing can be more valuable in determining the mechanical behavior of FRP strengthened columns at different temperatures.
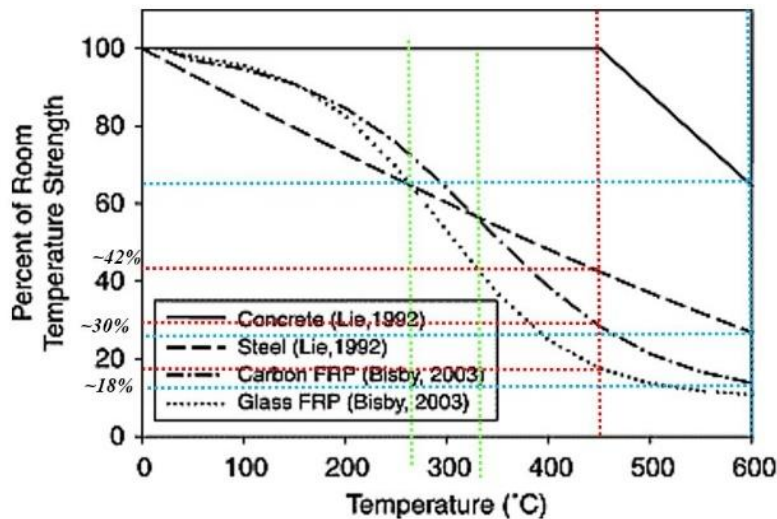
Figure 2-14: Temperature Dependent Tensile Strength of Concrete, Reinforcing Steel, CFRP and GFRP [13]

The satisfactory fire rating of a building is achieved when structural elements can withstand service loads during a fire for a minimum duration. The minimum fire endurance requirement for a structural element depends on the vitality of the element type for the structure's integrity. Columns require the highest fire rating (up to four hours) as compared to slabs (as low as two hours) [37].

Results of several research studies have shown that with proper thermal insulation, FRP composites strengthened concrete members can achieve a satisfactory fire-endurance [13, 14, 23, 62, 63]. It is important to note that all columns evaluated in the previous studies were only subjected to service loading based on the unstrengthened capacity of the columns based on safety provisions provided by ACI 440 [1] in Eq. 1-1. So, the main goal of the insulation in these studies was to provide protection for both the concrete and the internal steel reinforcement. Bisby [13] commented that it is difficult to determine when the FRP composite jacket became ineffective.

The majority of published studies reported results of transient tests where axially loaded FRP-confined columns were exposed to a standard fire until failure. This type of testing is driven by fire insulation industry with their interest is focused on proving that their products can achieve the current code fire rating requirements. However, very few studies provided improvements on residual strength predictions that assist in alleviating concerns regarding fire performance of structural members strengthened with FRP composites.

The main procedure for predicting the performance of an FRP columns during a fire is performed in two steps. The initial step involves determining internal temperature of FRP-confined column materials. This step requires the utilization of heat transfer models. Which means the thermal properties of FRP, concrete, and steel are required. The second step involves modifying temperature-depended mechanical (thermos-mechanical) properties of the materials using temperatures acquired from the heat transfer of the adjacent materials.

Heat transfer in the column can be described by the heat diffusion differential equation for a differential volume in Cartesian coordinates and is given by [65]:

$$\frac{\partial}{\partial x}\left(k\frac{\partial T}{\partial x}\right) + \frac{\partial}{\partial y}\left(k\frac{\partial T}{\partial y}\right) + \frac{\partial}{\partial z}\left(k\frac{\partial T}{\partial z}\right) + \dot{q} = \rho C_P \frac{\partial T}{\partial t} \qquad Eq.\ 2\text{-}22$$

where: k refers to the thermal conductivity of a material; T and t are the temperature and time respectively; $\dot{q}$ represents heat generation in the material; ρ and C_P are material's density and specific heat respectively. Columns are commonly assumed to be infinitely long for heat transfer purposes with success [13,37]. A model proposed by Bisby [13, 61] has been found to accurately predict the thermal and structural response of columns with FRP composite jackets.

The critical interfaces in the heat analysis are (i) FRP-fire and (ii) FRP-concrete interfaces. Considering that steel, surrounded by concrete, has little influence on these two interfaces, many FRP strengthened concrete heat transfer models do not factor in the influence of steel [11,63,66]. However, steel temperatures are important to know for mechanical property considerations; steel temperature can be assumed to be the same temperature as that of the concrete in the same location. It is, therefore, important to understand the thermal properties of concrete, FRP, and the thermal insulation being utilized. The two main materials properties in question are: (i) thermal conductivity, and (ii) specific heat.

2.4   Seismic Performance of Fire-Damaged FRP-Confined RC Columns

Based on the literature review conducted in this study, it was found that very limited publications are available related to seismic performance of fire-damaged FRP-confined RC columns. The only published paper found during the literature review is a limited experimental study presented by Bénichou et al. [24]. Two insulated FRP-confined confined columns (one square and one circular) were exposed to a CAN/ULC-S101-07 standard fire for four hours. During the heating

regimen, the columns were subjected to a sustained axial load with a value slightly greater than their unstrengthened axial capacity (P_{ou}). Temperature readings were recorded at various locations in the cross-section of the column during the duration of the fire test. The columns were then left to cool until they reached room temperature. Through forensic evaluations, the researchers deemed the FRP to be ineffective. This is not surprising given that the FRP-insulation interface reached temperatures close to 800℃ and Concrete-FRP recorded temperatures were just under 600℃. Both temperatures are above the decomposition temperature of the epoxy meaning that the entire matrix most likely decomposed. After cooling, the same axial load was applied to the columns and a lateral displacement was applied slowly. The square column failed after two displacement cycles. The circular column did not fail after three displacement cycles; the axial load was increased until the circular column fails. A simplified simulation of the square column was used to estimate the performance of the unstrengthened column without fire damage. The results found that the tested column behaved the same as the unstrengthened and undamaged column model. These findings are similar to those reported in fire endurance tests FRP-confined columns. Figure *2-15* shows a comparison between the experimental and numerical lateral response of the square column.

Yaqub and Bailey [67] conducted an experimental study on seismic performance of shear critical post-heated reinforced concrete columns wrapped with FRP composites after heating. However, the focus of the study was on RC square columns with FRP composite jackets installed after the heating regimen and only limited specimens were evaluated. Another published paper that discusses the residual performance of FRP-retrofitted RC columns after being subjected to cyclic

loading damage is presented by Shan et al. [68], however, fire damage was not included in their study.

Based on the in-depth literature review, it is clear that there is a lack of information on the subject of this research.
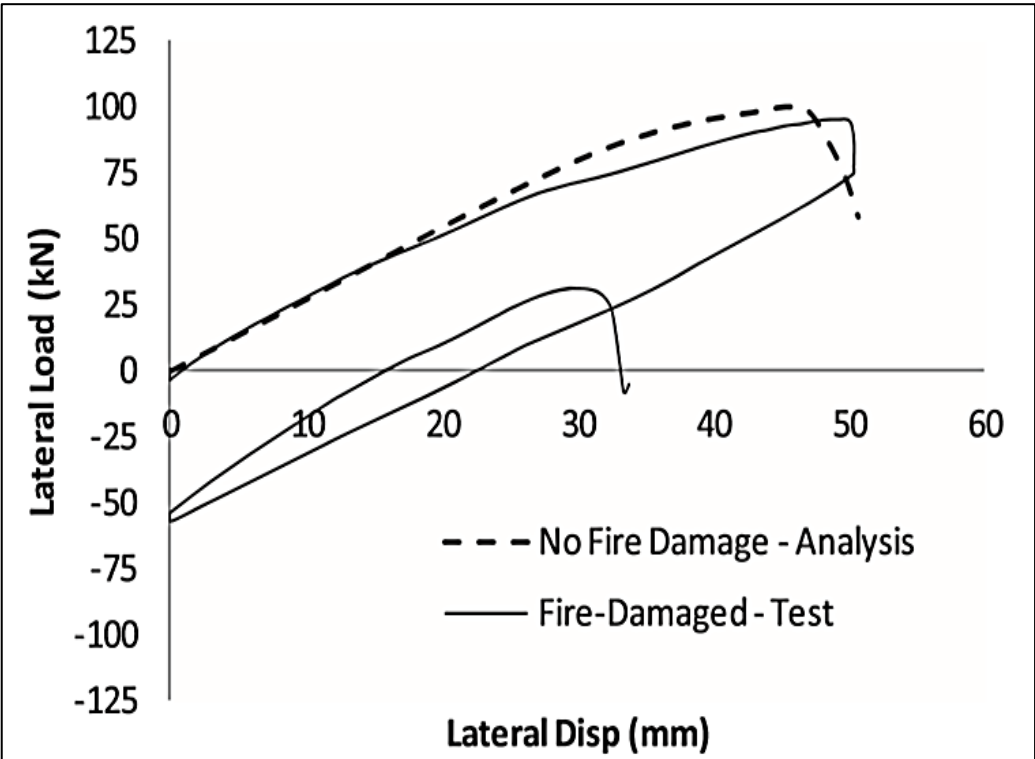
Figure 2-15: Experimental and Numerical Lateral Response of the Square Column [24]

Chapter 3   SMALL-SCALE CONCRETE EXPERIMENTS PART I

3.1   General

In this chapter, a description of different thermal insulation schemes that were utilized for

protecting small-scale concrete specimens is presented. The objective of this assessment is to

examine the effectiveness of different insulating systems in protecting the FRP-composite jacket

exposed to elevated temperatures. All FRP composites and insulation materials used in this study

phase was manufactured by DYMAT® company. The CFRP composites used in this experimental

phase were DYMAT® DHC-190 carbon fiber system and the two-part room temperature cure

DYMAT® D epoxy resin. This epoxy system is made up of an epoxy resin (Part A) and a

hardener or a catalyst (Part B) that is mixed with a ratio of 1:3 (A:B). A summary of the

mechanical properties of the CFRP materials is presented in **Table 3-1**.

Table 3-1: Mechanical Properties of: (a) DYMAT DHC-190 and (b) DYMAT D

(a) Carbon Fibers	
Long. Ultimate tensile strength, f_{carbon} (GPa)	4.83
Long. Tensile modulus, E_{carbon} (GPa)	280
Long. Rupture Strain, ϵ_{carbon}	0.0165
Fabric thickness, t_{carbon} (mm)	0.37
(b) 2-Part Epoxy	
Tensile strength, f_{epoxy} (MPa)	90.0
Shear modulus, E_{epoxy} (GPa)	5.0

The effectiveness of three different fire protection systems was examined. This was achieved by

subjecting insulated and uninsulated concrete specimens to thermal exposure protocols followed

by mechanical testing. Control unconfined and confined specimens were also tested without

thermal exposure in order to quantify the extent of strength degradation. System A consists of

DYMAT™-RS and DYMAT™ Dymatherm. System B consists of DYMAT™ FIRECOAT insulation. System C consists of DYMAT™ REARLOCK along with FireSet60.

All thermal exposure experiments covered in this chapter were performed at the fire test lab of the Karadeniz Technical University (KTU) in Trabzon, Turkey as a collaborative research effort established by Prof. Mosallam. The fire tests are conducted using the KTU calibrated furnace (shown in **Figure 3-1**).

Figure 3-1: KTU Medium-Scale Calibrated Furnace

Capacity	$6\ m^3$	Width	$2.0\ m$
Operating Temperature	1,100 °C	**Length**	1.5 m
Heating Power	210 kW	**Height**	2.0 m

Table 3-2: Specifications of KTU Heating Furnace

3.2 Fire Protection System "A"

DYMAT™RS is a 0.01 thick high-temperature resistance cloth. Dymatherm™ is a textured blanket insulator with a nominal thickness of 2.0 mm. Both materials are good insulators, and their negligible thickness makes the system a suitable candidate for a fire protection system.

A total of 48 small-scall concrete cylindrical specimens (200 mm. diameter and 450 mm. height) were fabricated to examine the effectiveness of fire protection system A. Four concrete samples were left unstrengthened and without thermal exposure to serve as reference samples. The remaining 44 specimens were divided into two groups. The first group was confined with a CFRP laminate, and the second group was confined with a GFRP laminate. The parameters that were examined are FRP type, exposure temperature, and insulation type. The goal is to examine the effectiveness of four different fire protection configurations (*T1, T2, T3*, and *T4*). This was achieved by comparing the ultimate strength of insulated specimens to the ultimate strength of the unprotected specimens. To reduce the possibility of experimental errors, two samples were tested for each unique parametric configuration. A summary of the test matrix for System (A) specimens is presented in **Table 3-3**.

3.2.1 Specimen Fabrication for System A

The concrete specimens were cast into cylindrical molds then moist cured for 7 days. The casting procedure is presented in **Figure 3-2**. All specimens, except for the reference specimens, were

strengthened with 2 CFRP plies with an overlap length of 200 mm. Before application of the FRP, the concrete surface is cleaned of any dust and degree and the surface is dried thoroughly. A primer layers of the epoxy is then applied directly to the concrete to ensure proper adhesion between the confining fabric and the surface of the concrete. The fabric is then impregnated with the epoxy via a roller. Finally, the fabric is rolled on the concrete specimen while ensuring there are no void or excessive resin content. The application process is depicted in **Figure 3-3**.

After the FRP has been cured, four different application configurations of DYMAT™RS and Dymatherm were applied to the specimens. The application of the fire protection materials was done in accordance with the instructions provided by the manufacturer. The insulation was tied with a metal wire to ensure a tight fit. A representation of the fire protection configuration of System **A** is presented in **Table 3-4**. The steps of application of the insulation materials are represented in **Figure 3-4**.

Table 3-3: System (**A**) Test Matrix and Naming Convention

Exposure Temperature	Specimen ID				
20	Ref-1 Ref-2 Ref-3 Ref-4	CFRP-1	CFRP-2	GFRP-1	GFRP-2
200	--	CFRP-200-1	CFRP-200-2	GFRP-200-1	GFRP-200-2
		CFRP-T1-200-1	CFRP-T1-200-2	GFRP-T1-200-1	CFRP-T1-200-2
		CFRP-T2-200-1	CFRP-T2-200-2	GFRP-T2-200-1	CFRP-T2-200-2
		CFRP-T3-200-1	CFRP-T3-200-2	GFRP-T3-200-1	CFRP-T3-200-2
		CFRP-T4-200-1	CFRP-T4-200-2	GFRP-T4-200-1	CFRP-T4-200-2
400	--	CFRP-400-1	CFRP-400-2	GFRP-400-1	CFRP-400-2
		CFRP-T1-400-1	CFRP-T1-400-2	GFRP-T1-400-1	CFRP-T1-400-2
		CFRP-T2-400-1	CFRP-T2-400-2	GFRP-T2-400-1	CFRP-T2-400-2
		CFRP-T3-400-1	CFRP-T3-400-2	GFRP-T3-400-1	CFRP-T3-400-2
		CFRP-T4-400-1	CFRP-T4-400-2	GFRP-T4-400-1	CFRP-T4-400-2
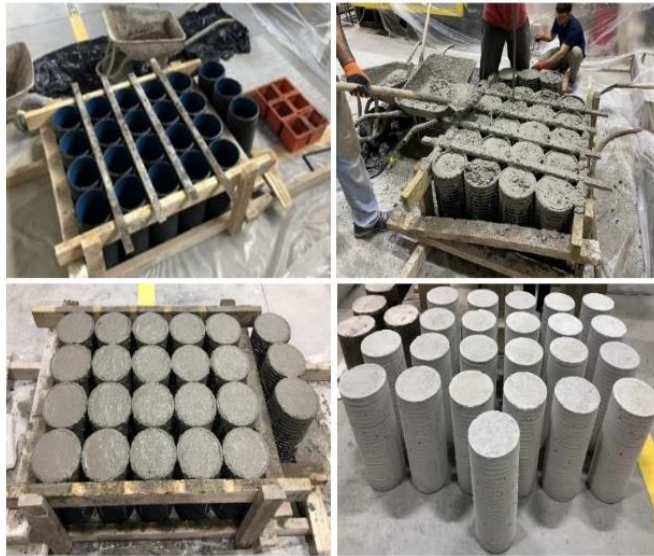
Figure 3-2: Casting of Small-Scale Specimens (System *A*)
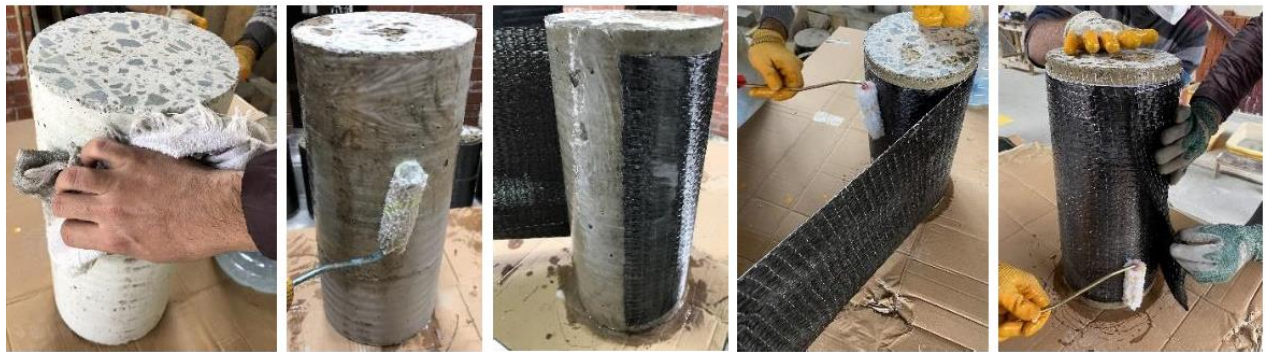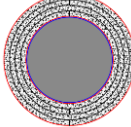
(a)   CFRP Composite System

(b)   GFRP Composite System

Figure 3-3: Application of (a) CFRP, and (b) GFRP Confinement to Concrete Specimens

Table 3-4: Insulation Configuration for System A

Configuration ID	Configuration Information			Schematic Drawing of Configuration
	DYMAT RS	Dymatherm	DYMAT RS	
T1	✗	2 plies	✓	
T2	✗	4 plies	✓	
T3	✓	2 plies	✓	
T4	✓	4 plies	✓	

a) System A, Type 1

(b) System A, Type 2

c) System A, Type 3

d) System A, Type 4

Figure 3-4: Application Steps of Insulation Materials for System A

3.2.2 Thermal Exposure Protocol for System-A

Two thermal exposure protocols were utilized for specimens in System A. Protocol 1 involved exposing the specimens to a temperature of 200°C while Protocol 2 the specimens are exposed to a temperature of 400°C. The specimens are placed in the furnace at room temperature and the protocol is initiated once the doors are closed with a ramp rate of $2.5°C/min$ until the target temperature is reached. The temperature is then held constant for a duration of 60 minutes. The target temperature for Protocol-1 was reached in 134.0 minutes while the temperature for Protocol-2 was reached in 214 minutes.
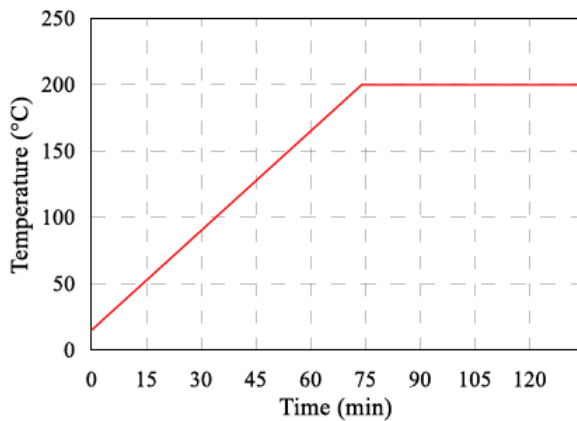
(a) Protocol-1
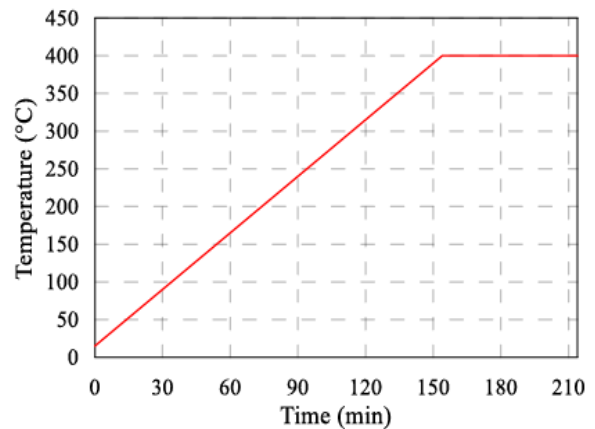
(b) Protocol-2

Figure 3-5: Time-Temperature of Thermal Exposure Protocols (System A)

Thermocouples were placed between the insulation and the FRP confinements to measure the maximum temperature that the FRP is exposed to. The test specimens were placed on the car-bottom of the furnace at room temperature in a symmetrical configuration (see **Figure 3-6**). The same figure also displays the location of thermocouples. The furnace is equipped with a

ventilation system which was activated for heating Protocol 2 to protect from the toxic gases that are released from the polymer matrix at elevated temperatures. The placement of thermocouples and their ID designation are referenced in **Table 3-5**.
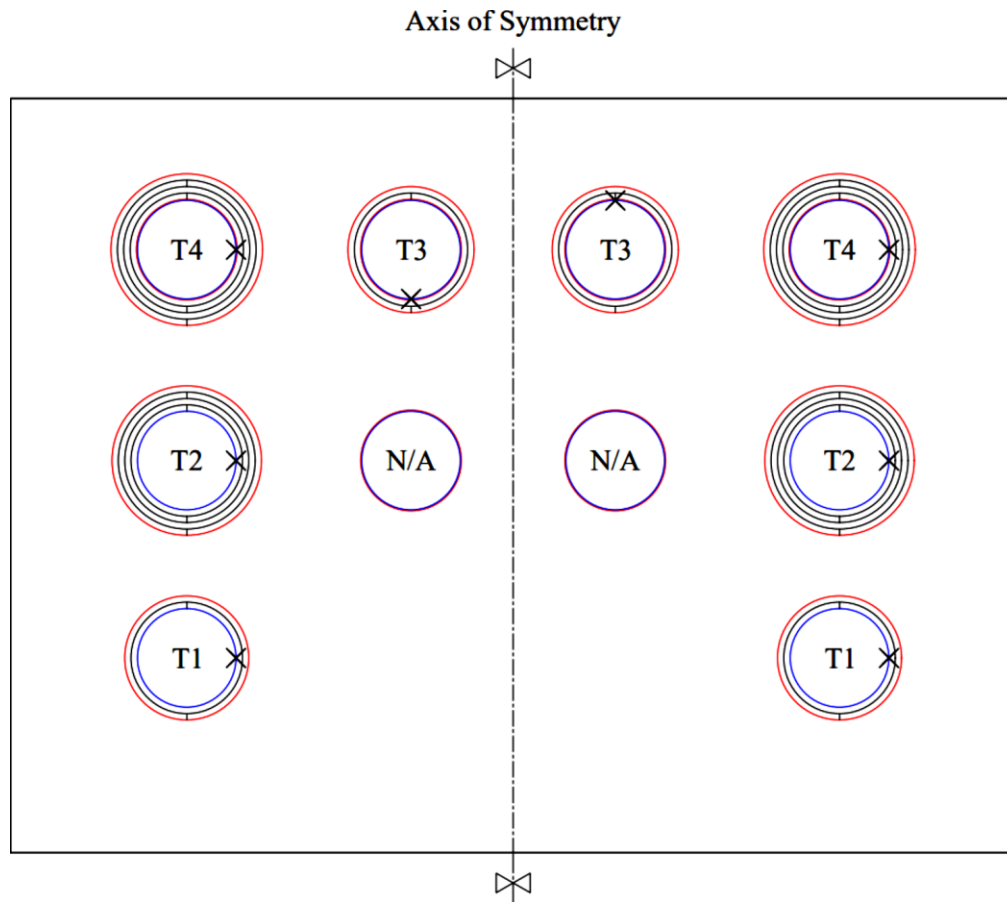
Figure 3-6: Placement Configuration of Sample and Location of Thermocouples

Table 3-5: Thermocouple Designation for Fire Protection System **A**

Thermocouple ID	Insulation Scheme (System-A)
TC-1, TC-2	T1 (2 layers of Dymatherm + DYMAT RS)
TC-3, TC-4	T2 (4 layers of Dymatherm + DYMAT RS)
TC-5, TC-6	T3 (DYMAT RS + 2 layers of Dymatherm + DYMAT RS)
TC-7, TC-8	T4 (DYMAT RS + 2 layers of Dymatherm + DYMAT RS)
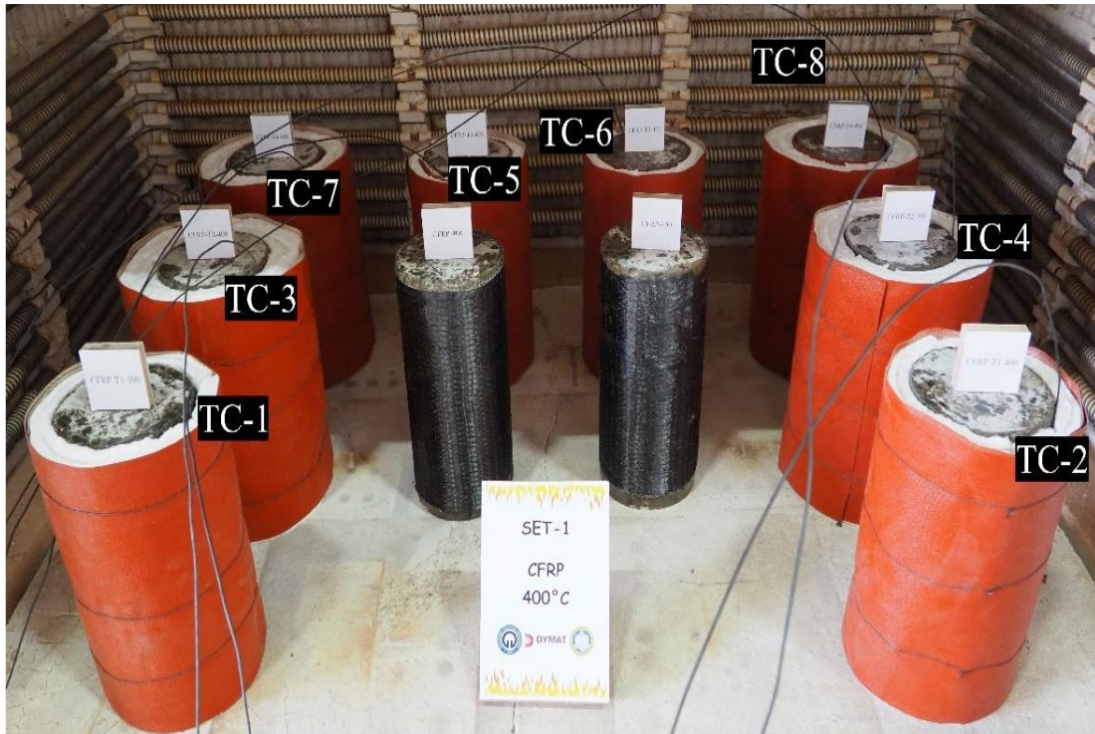
Figure 3-7: *Thermocouple attachments at measurement stations*
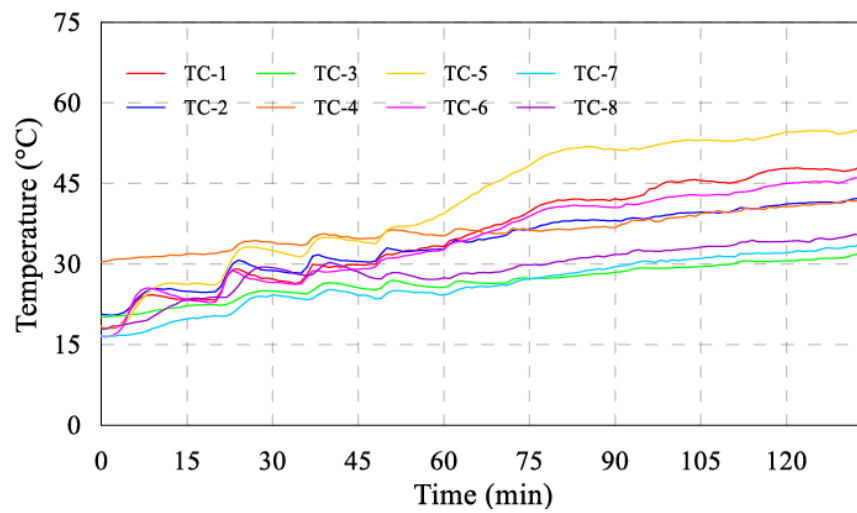
(a) CFRP specimens exposed to Protocol-1 (200℃)
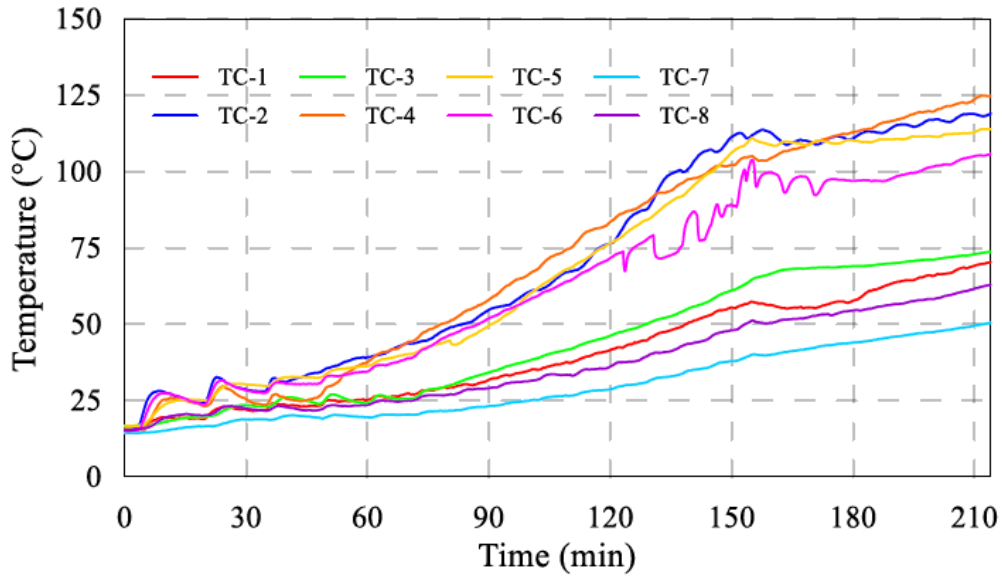
(b) CFRP specimens exposed to Protocol-2 (400℃)
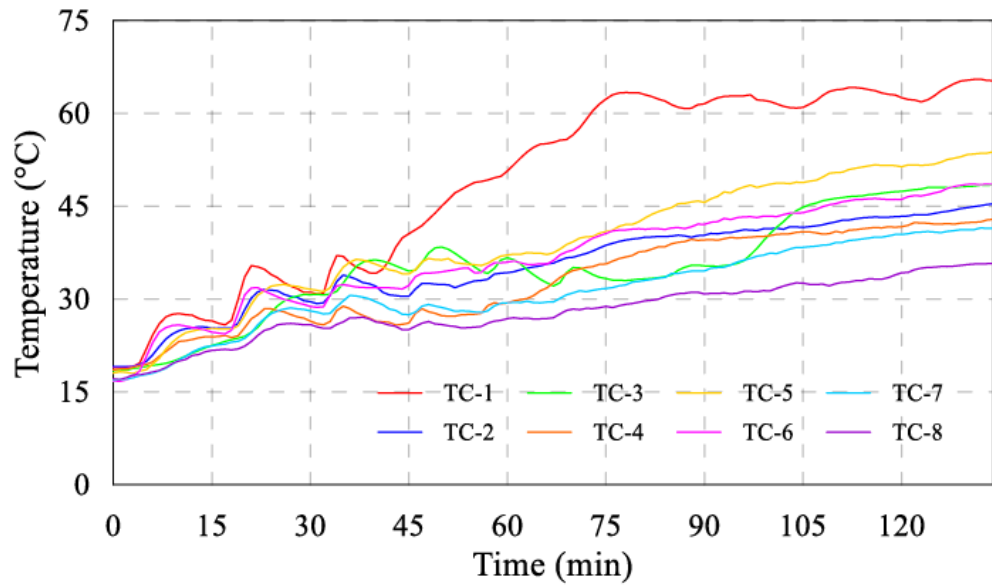
(c) GFRP specimens exposed to Protocol-1 (200℃)
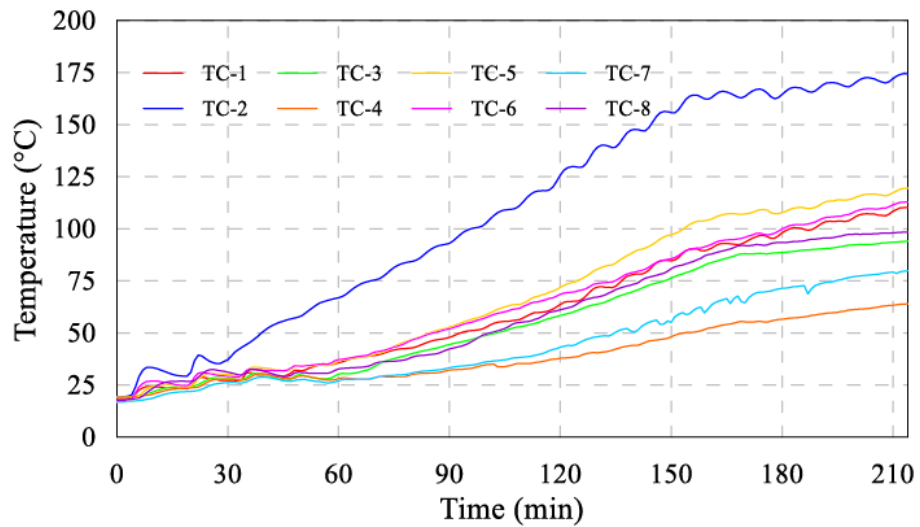
e) GFRP specimens exposed to Protocol-2 (400℃)

Figure 3-8: Temperature variation at FRP-Insulation interface for specimens insulated with System (A) During Heating Protocols

Figure 3-9: View of CFRP System-A specimens after exposure to Thermal Protocol-2 (400℃)

(a) View of GFRP set

(b) Close-up of unprotected specimens

Figure 3-10: View of GFRP System-A specimens after exposure to Thermal Protocol-2 (400℃)

3.2.3   Experimental Results of System A

The samples were tested under uniaxial loading after being cooled down. The uniaxial compression loading was implemented at a rate of 0.6 MPa/s. The obtained data is presented in. The pre-test and post-test conditions of the CFRP and GFRP specimens are presented in Figure 3-11 and Figure 3-12 respectively.

CFRP (1)   CFRP (2)

CFRP-200 (1)   CFRP-200 (2)

N/A

CFRP-400 (1)

CFRP-400 (2)

CFRP-T1-200 (1)

CFRP-T1-200 (2)

CFRP-T1-400 (1)

CFRP-T1-400 (2)

CFRP-T2-200 (1)

CFRP-T2-200 (2)

CFRP-T2-400 (1)

CFRP-T2-400 (2)

CFRP-T3-200 (1)
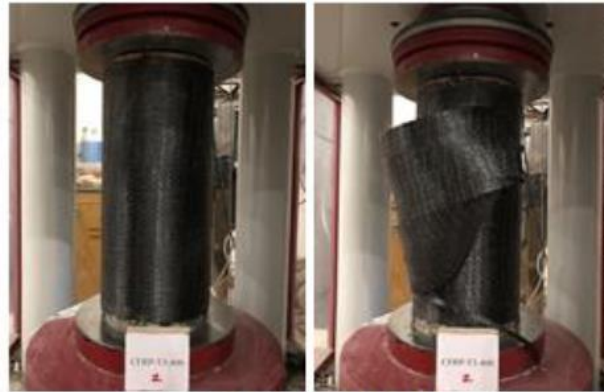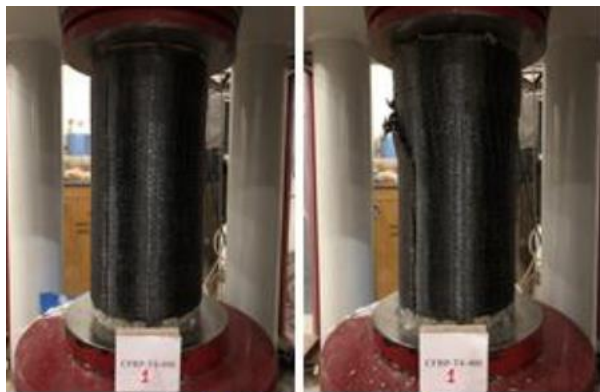
CFRP-T3-200 (2)

Figure 3-11: View of CFRP System-A specimens before and after uniaxial compression testing

GFRP (1)

GFRP (2)

GFRP (3)

GFRP-200 (1)

GFRP-200 (2)

GFRP-400 (1)

GFRP-400 (2)

GFRP-T1-200 (1)

GFRP-T1-200 (2)

GFRP-T1-400 (1)
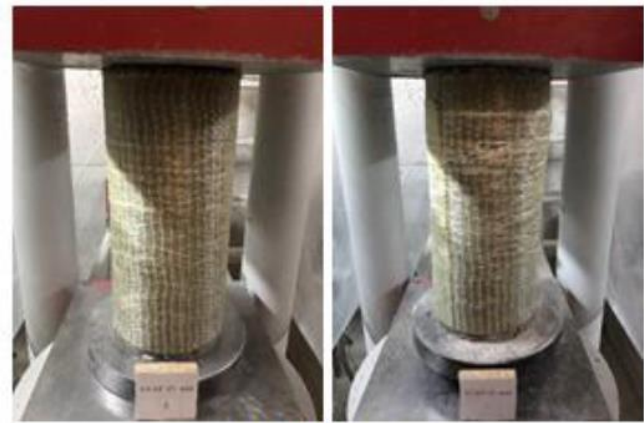
GFRP-T1-400 (2)

GFRP-T2-200 (1)

GFRP-T2-200 (2)

GFRP-T2-400 (1)

GFRP-T2-400 (2)

GFRP-T3-200 (1)

GFRP-T3-200 (2)

GFRP-T3-400 (1)

GFRP-T3-400 (2)

GFRP-T4-400 (1) GFRP-T4-400 (2)

GFRP-T4-200 (1) GFRP-T4-200 (2)
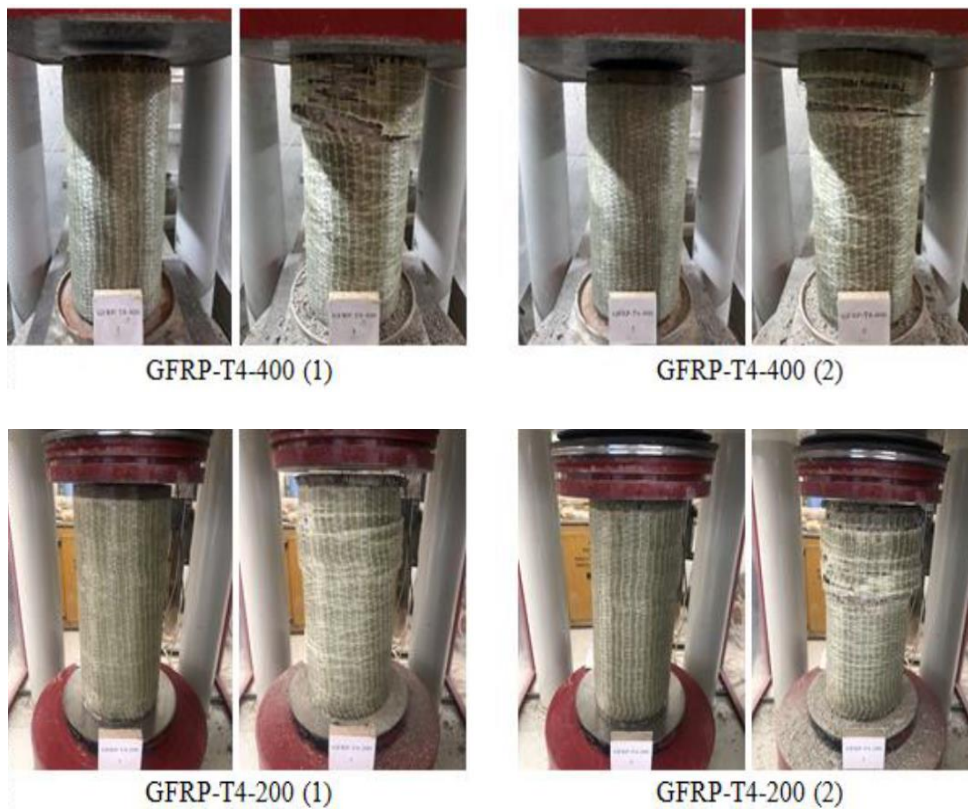
Figure 3-12: *Samples of GFRP System A specimens before and after uniaxial testing*

Table 3-6: Uniaxial Compression Results (System A – CFRP)

Specimen ID	No.	Height (mm)	Max. Load (N)	Max. Stress (MPa)
Ref. Set-1	1	500	668591.38	21.28
Ref. Set-1	2	495	649674.38	20.68
Ref. Set-1	3	450	700831.81	22.31
CFRP	1	450	1756729.38	55.92
CFRP	2	450	1735335.88	55.24
CFRP-200	1	450	1289973.88	41.06
CFRP-200	2	450	1454258.5	46.29
CFRP-400	1	450	833603.38	26.53
CFRP-400	2	450	916042.94	29.16
CFRP-T1-200	1	450	----------------	------
CFRP-T1-200	2	450	1557017.88	49.56
CFRP-T1-400	1	450	1369665.63	43.60
CFRP-T1-400	2	450	1287087.5	40.97
CFRP-T2-200	1	450	1414657.88	45.03
CFRP-T2-200	2	450	1543619.5	49.13
CFRP-T2-400	1	450	1268892	40.39
CFRP-T2-400	2	450	1257975.88	40.04
CFRP-T3-200	1	450	1601409.75	50.97

Specimen ID	No.	Height (mm)	Max. Load (N)	Max. Stress (MPa)
CFRP-T3-200	2	450	1486868.38	47.33
CFRP-T3-400	1	450	1366398.38	43.49
CFRP-T3-400	2	450	1387070.25	44.15
CFRP-T4-200	1	450	1509295.13	48.04
CFRP-T4-200	2	450	1621360.13	51.61
CFRP-T4-400	1	450	----------------	------
CFRP-T4-400	2	450	1394817.25	44.40

Table 3-7: Uniaxial Compression Results (System A – GFRP)

Specimen ID	No.	Height (mm)	Max. Load (N)	Max. Stress (MPa)
Ref. Set-2	1	450	687895.25	21.90
Ref. Set-2	2	450	684841.50	21.80
GFRP	1	450	2005733.75	63.84
GFRP	2	450	2001496.63	63.71
GFRP	3	450	1671547.75	53.21
GFRP-200	1	450	1570035.25	49.98
GFRP-200	2	450	1577176.13	50.20
GFRP-400	1	450	954730.01	30.39
GFRP-400	2	450	970123.81	30.88
GFRP-T1-200	1	450	1862531.00	59.29
GFRP-T1-200	2	450	1963454.75	62.50
GFRP-T1-400	1	450	1605668.01	51.11
GFRP-T1-400	2	450	1668456.00	53.11
GFRP-T2-200	1	450	1855110.46	59.05
GFRP-T2-200	2	450	1906632.58	60.69
GFRP-T2-400	1	450	1620038.00	51.57
GFRP-T2-400	2	450	1690797.00	53.82
GFRP-T3-200	1	450	----------------	------
GFRP-T3-200	2	450	1942309.38	61.83
GFRP-T3-400	1	450	1540871.00	49.05
GFRP-T3-400	2	450	1594078.00	50.74
GFRP-T4-200	1	450	1946177.13	61.95
GFRP-T4-200	2	450	1997536.63	63.58
GFRP-T4-400	1	450	1592911.00	------
GFRP-T4-400	2	450	1693166.00	53.90
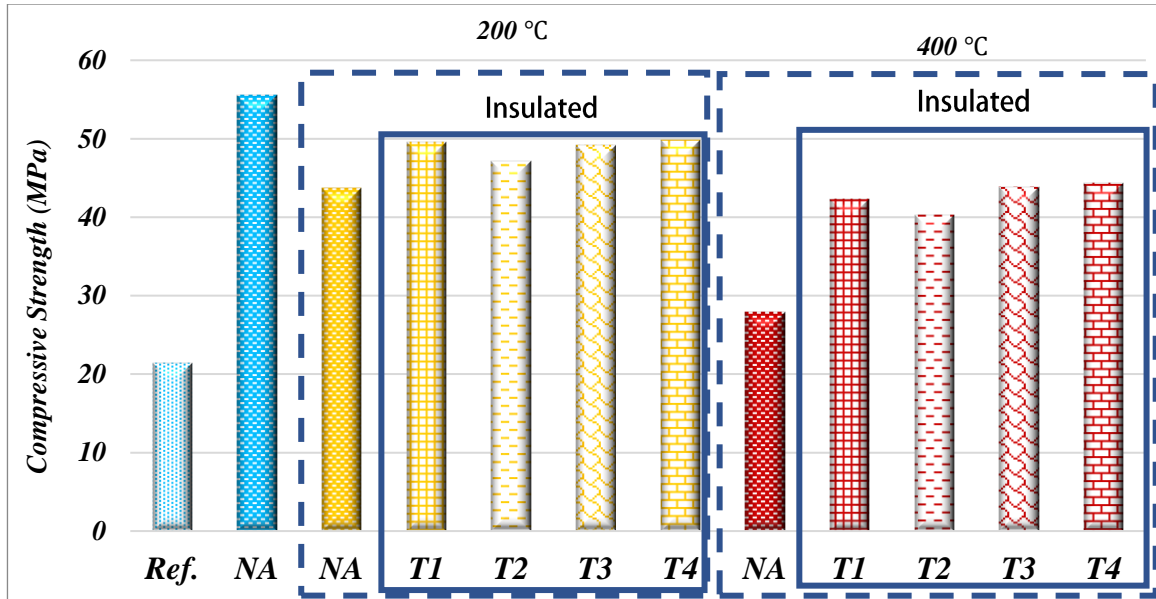
Figure 3-13: A Comparison of compressive strength of CFRP specimens (System **A**)

3.3 Fire Protection System B

A total of 14 small-scale concrete cylindrical specimens were fabricated for the experimental portion dedicated to Insulation System B. Three specimens were left as built, seven specimens were confined with CFRP composites, and another 7 specimens were confined with GFRP composites. In both case specimens were wrapped with two layers of unidirectional fiber with an overlap length of 200 mm. DYMAT™BT-D epoxy (Parts "A" and "B") was used for the FRP matrix.
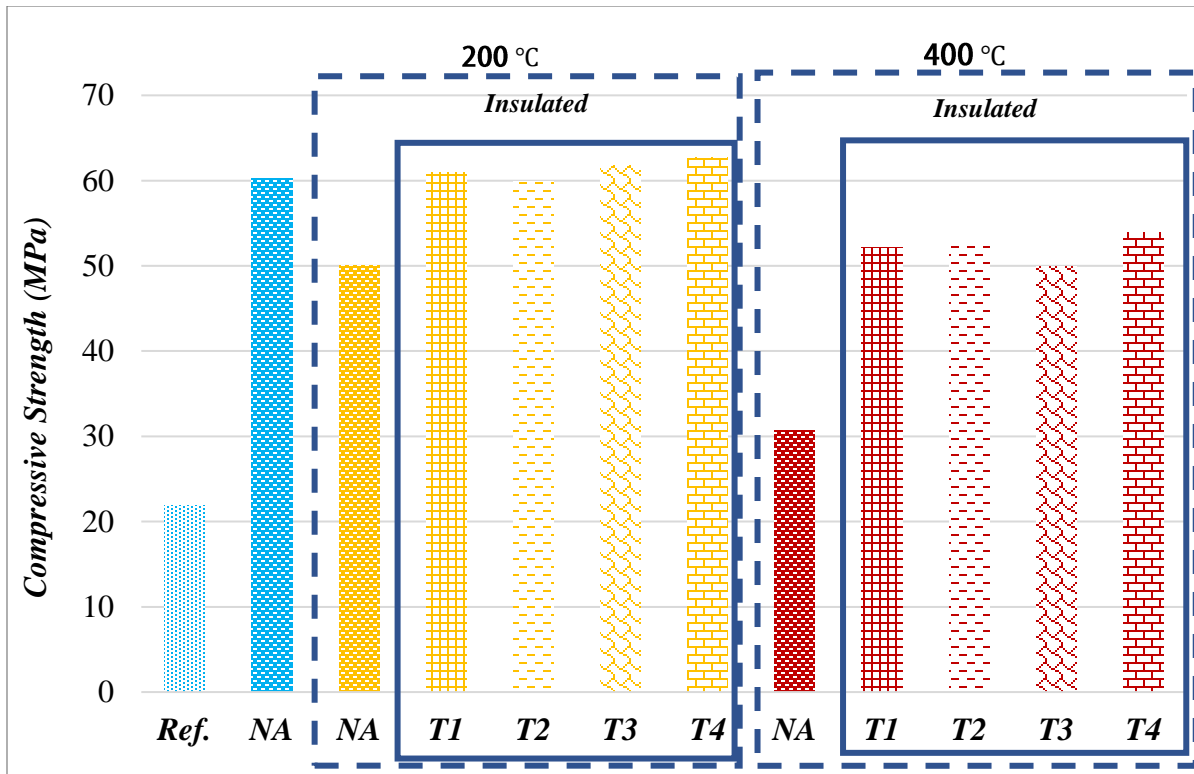
Figure 3-14: *Comparison of compressive strength of GFRP specimens (System-A)*

System B (FIRECOAT) consists of DYMAT™ DCF-D and FireFree 88 (DYMAT™D8). DYMAT™ DCF-D is a polymer material made up of Part "A" epoxy resin and Part "B" curing agent and presented. FireFree88 is a proprietary white viscous insulating material. The application process of System **B** is presented in **Figure 3-15**.

The concrete surface was cleaned and dried prior to application of DYMAT™ DCF-D. Part A and Part B were mixed using a mechanical mixer with 1:1 ratio by volume. The compound was applied to the specimens using paint rollers with each layer weighing 310 grams. The layers are left to dry completely before adding another layer using the same procedure or going on to apply

the next insulating material. DYMAT™D8 was mixed with a clean wooden stick before being applied with a brush paint roller.
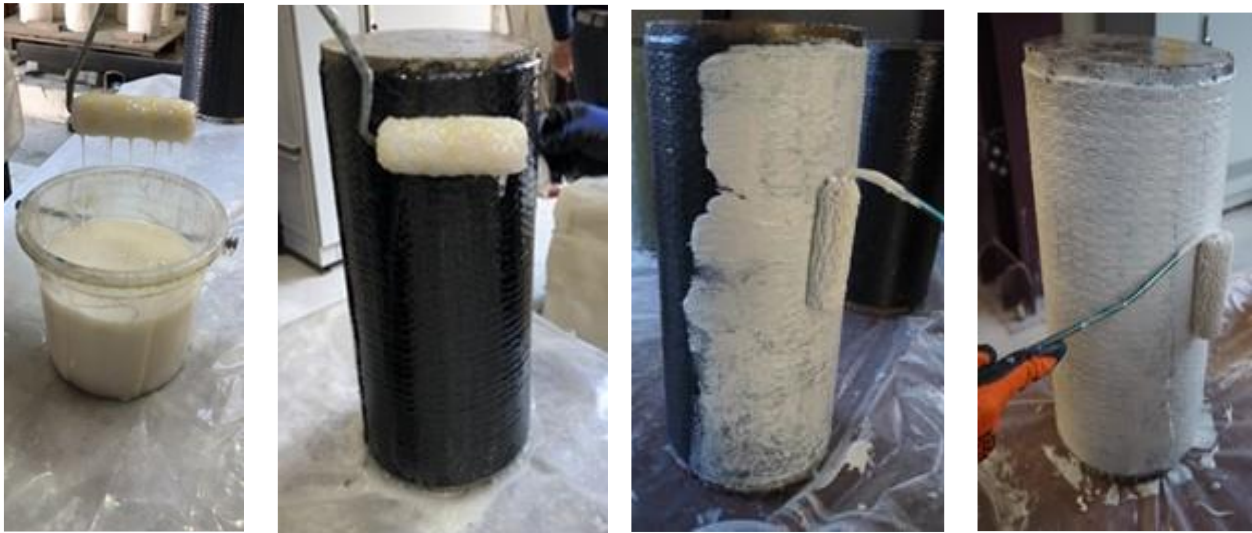
DYMAT™ DCF-D Epoxy Resin   FireFree 88 (DYMAT™D8).

Figure 3-15: *Application of components of Fire Protection System B*

Each layer weighed 55.2 grams. The next layer is then applied once the preceding layers sets and reached a gel-like state. This procedure is repeated until the final layer is applied. Two different configurations of System B were utilized (T1 and T2) with varying number of layers for each material. The number layers used for each fire protection material is presented in **Table 3-8**.

Table 3-8: *System B Insulation Layer Configurations*

Insulation Configuration ID	DYMAT® DCF-D Epoxy Resin	FireFree 88 (DYMAT®D8)
T1	1 layer	3 layers
T2	2 layers	6 layers

Table 3-9: System **B** Test Matrix

Heat Exposure Regimen	Heating Duration (minutes.)	Specimen ID		
Room Temperature	**--**	**Ref**	**CFRP**	**GFRP**
ASTM E119	**30**	Ref-30	CFRP-30	GFRP-30
			CFRP-T1-30	GFRP-T1-30
			CFRP-T2-30	GFRP-T2-30
	60	Ref-60	CFRP-60	GFRP-60
			CFRP-T1-60	GFRP-T1-60
			CFRP-T2-60	GFRP-T2-60

3.3.1   *Thermal Exposure Protocol for System B:*

The specimens in system B were exposed to ASTM E119 standard fire for 60 minutes and 30 minutes as can be seen in **Figure 3-16**.
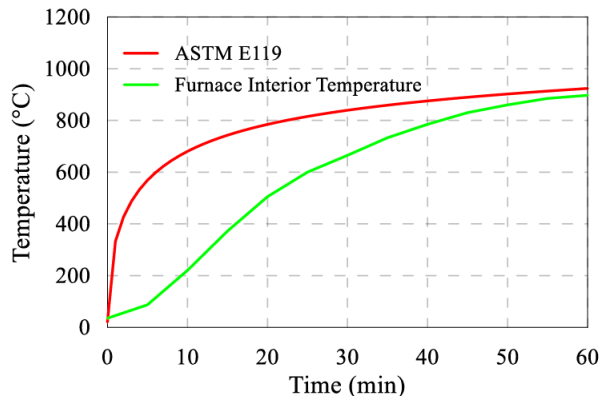
(a)   System-B 60 minutes Thermal Exposure Protocol
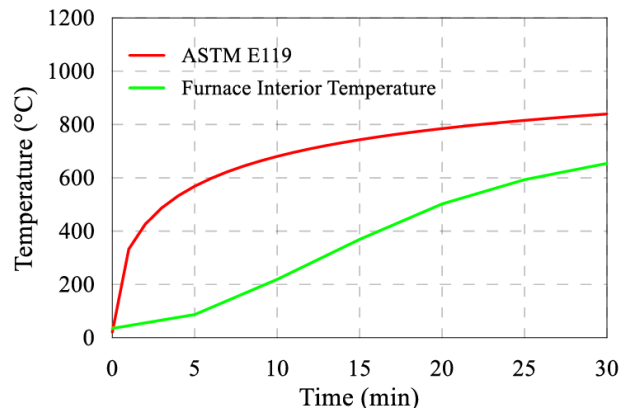
(b) System-B 30 minutes Thermal Exposure Protocol

Figure 3-16: Thermal Exposure Protocol for System **B**
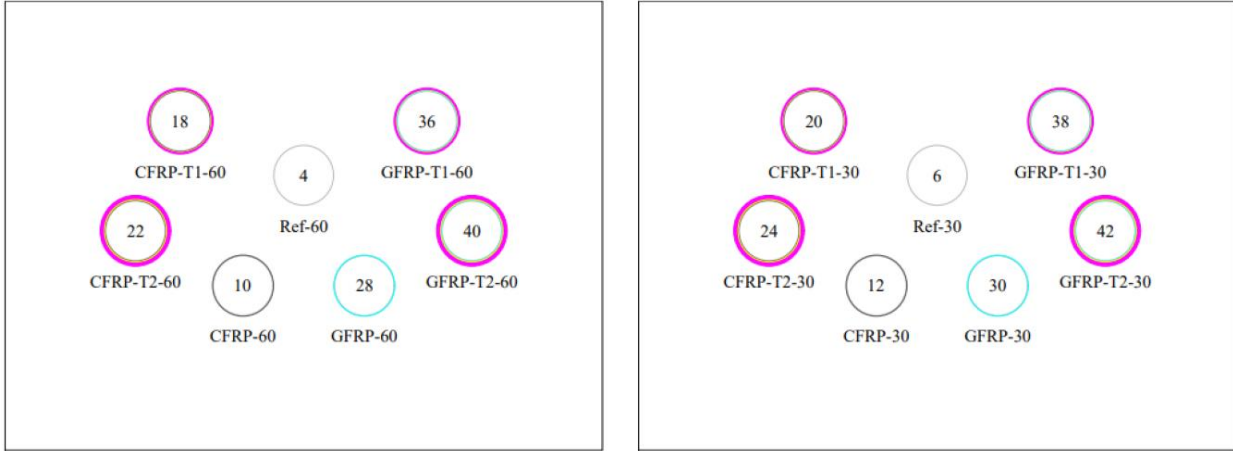
Figure 3-17: Configuration of specimens in the furnace System-B

During fire exposure of 60 minutes some specimens experienced severe damages as can be seen in

Figure *3-18*. So, they were excluded from rest of the experiment. Upon completion of temperature test, the furnace door was opened, and using a dual laser portable pyrometer (AST TI 1500), the surface temperature of specimens was measured. Then, the samples were placed outside the furnace and cooled naturally to be prepared for compression tests. In this stage, visual observations of tested specimens were recorded and backed up using photographs and video so that can be used in further evaluations. Using the data obtained from compressive tests and recorded visual observations, the effectiveness of each insulation method was evaluated.

3.3.2   Experimental Results of System-B

A summary of the experimental results for fire protection System B are presented in **Table 3-10**.

CFRP-30   CFRP-T1-30   CFRP-T2-30

GFRP-30   GFRP-T1-30   GFRP-T2-30

Figure 3-18: Post-Thermal Exposure View of Specimens in System B (60 minutes)

Table 3-10: Uniaxial Compression Results (System B)

| Material | Specimens | | Max. Load (N) | Max. Stress (MPa) |
	No	ID		
Ref	1	Ref	945281.56	30.09
	6	Ref-30	560723.19	17.85
	4	Ref-60	536824.31	17.09
CFRP	7	CFRP	2705007	86.10
	12	CFRP-30	1088490.13	34.65
	10	CFRP-60	576904	18.36
	20	CFRP-T1-30	1137223.13	36.20
	18	CFRP-T1-60	587583.44	18.70
	24	CFRP-T2-30	2371450.25	75.49
	22	CFRP-T2-60	-----------	------
GFRP	25	GFRP	2143591	68.23
	30	GFRP-30	734890.63	23.39
	28	GFRP-60	603850.81	19.22
	38	GFRP-T1-30	972557.44	30.96
	36	GFRP-T1-60	675841.88	21.51
	42	GFRP-T2-30	1636213.25	52.08
	40	GFRP-T2-60	440795.81	14.03

Chapter 4   EVALUATION OF FIRE PROTECTION SYSTEMS UNDER LONG-PERIOD EXTREME FIRE ENVIRONMENTS

This set of experiments aimed to obtain the differences between hot and cold compressive tests, fire performance of insulation systems under 4 hours of ASTM E119 fire exposure and performing SEM to obtain the changes in properties of all fire exposed materials. To perform the fire tests, a total of 11 specimens were used. Due to shortage of concrete specimens, they were just wrapped with CFRP (except reference sample).

Table 4-1: Specifications of the specimens

Non-Wrapped Specimens		
(#2) Ref-200		
CFRP-Wrapped Specimens		
(#5) CFRP		
(#6) CFRP-200		
Insulated Specimens		
System A	**System B**	**System C**
(#9) CFRP-T3-200	(#13) CFRP-B-T1	(#15) CFRP-C-T1
(#10) CFRP-T4-200	(#14) CFRP-B-T2	(#16) CFRP-C-T2
(#11) CFRP-A-T3		
(#12) CFRP-A-T4		

4.1   Experiment – 1 : Temperature Test

To perform the first temperature test, a total of 4 specimens comprising 1 unwrapped specimen and 3 CFRP wrapped specimens were used. From the CFRP wrapped specimens, two of them were insulated using T3 and T4 of System A, and one specimen remained uninsulated. The

Table 4-2: Utilized Insulation Schemes

Insulation System	Insulation Type ID	Layer Information			Schematization
A	**T3**	Dymat®RS	Dymatherm 2 layers	Dymat®RS	
	T4	Dymat®RS	Dymatherm 4 layers	Dymat®RS	
B	**T1**	~~FCI APP11 A&B Components 1 layer~~ *	FireFree 88 (Dymat®D8) 3 layers	-	
	T2	~~FCI APP11 A&B Components 2 layers~~ *	FireFree 88 (Dymat®D8) 6 layers	-	
C	**T1**	-	Acrylic Vella Fino 2 layers	-	
	T2	Fire Set 60 1 layer	Acrylic Vella Fino 1 layer	-	

* This material has lost its properties so it couldn't be used.

specimens were exposed to temperature with a heating rate of 2.5 °C/min and after reaching 200°C remained constant for 1 hour. Before performing the temperature test, thermocouples were embedded into FRP surfaces of the insulated specimens to measure the temperature developments and evaluate the effectiveness of the insulation types. Also, a pyrometer was used to measure the surface temperature of the exterior material of each specimen before and after the test. The details of the conducted test and temperature readings are presented in the following tables and figures.

Table 4-3: Details of Fire Test 1

Test ID	DYMAT-AC125
Temperature Test No	1
Insulation System	A
Date	22.03.2022
Heating Regime	2.5°C/min to 200°C, then remains constant for 1 hour
Starting Time	15:50
Finishing Time	18:04
Test Duration	134 minutes
Cooling Duration	70 minutes
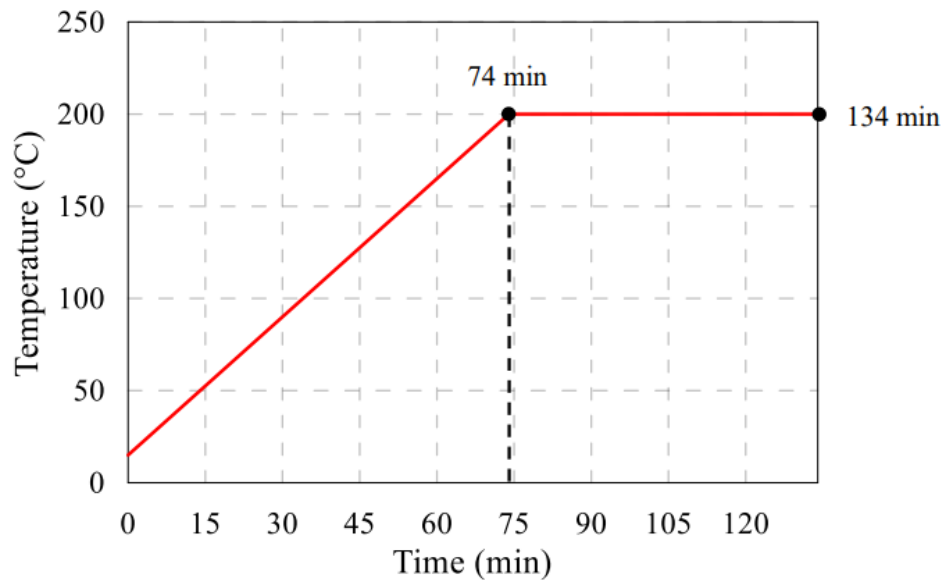
Figure 4-1: *Furnace Temperature during Test-1*

Table 4-4: Environmental Conditions during Test-1

	Pre-Test Stage	Post-Test Stage
Room Temperature (°C)	10.1	12.1
Humidity (%)	70	75

Table 4-5: Pyrometer measurements for Test – 1

Spec. No	Spec. ID	Stage	Surface Temperatures (°C)					Configuration
			S1	S2	S3	S4	Average	
2	Ref-200	Pre-Test	8.6	8.1	8.2	8.1	8.25	
		Post-Test	117	132	128	124	125.25	
6	CFRP-200	Pre-Test	8.6	8.1	8.0	8.2	8.23	
		Post-Test	110	123	118	128	119.75	
9	CFRP-T3-200	Pre-Test	10.0	9.9	9.5	9.8	9.80	
		Post-Test	135	138	118	103	123.50	
10	CFRP-T4-200	Pre-Test	11.7	10.7	10.4	10.4	10.80	
		Post-Test	138	148	134	121	135.25	

Configuration: S3, S4, S2, S1 arranged around circle. Emissivity 0.93
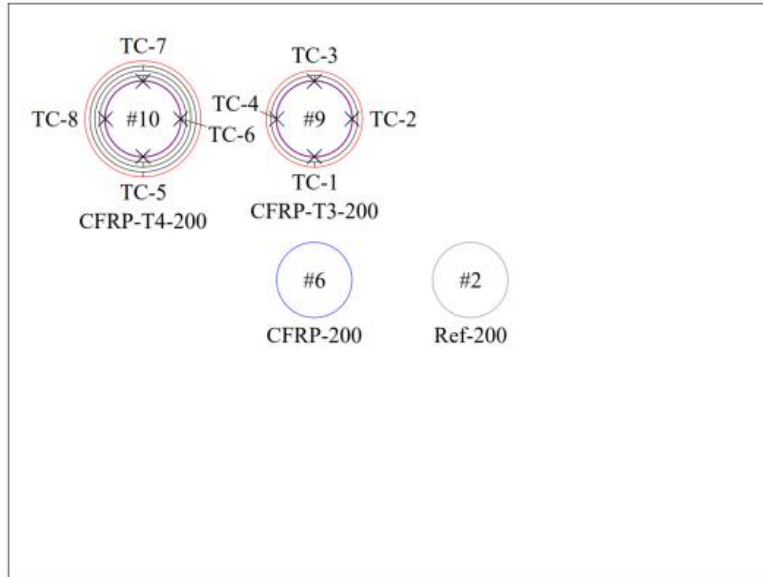
Figure 4-2: *Location of specimens in the furnace & thermocouple measurement stations in Test-1*
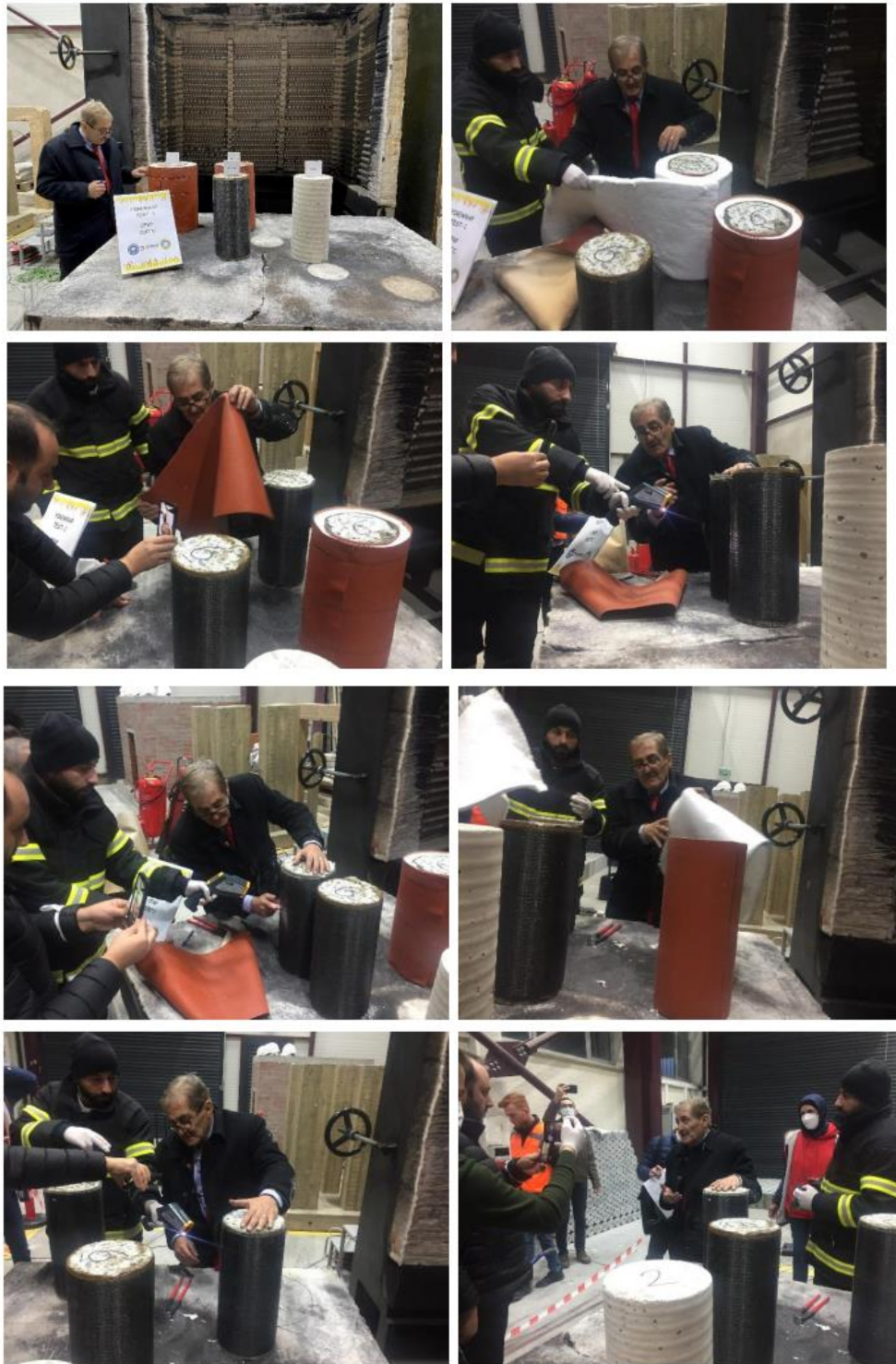
Figure 4-3: Post-test controls and measurements
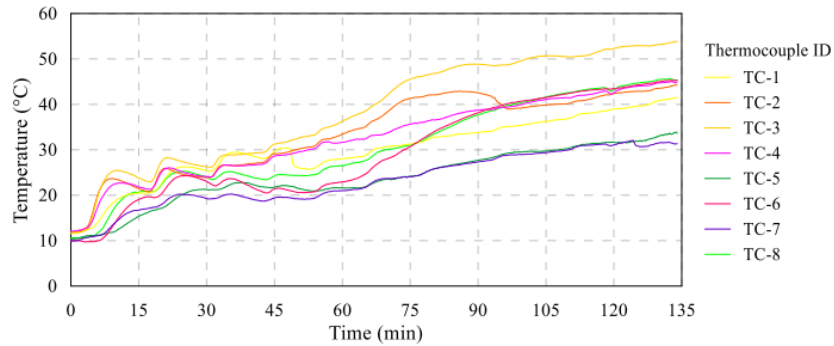
Figure 4-4: Thermocouple readings during Test-*2*

4.2   Experiment – 1 : Compression Tests

As it was aimed to conduct a hot specimen compressive test, after 70 minutes of cooling, specimens were prepared for compressive tests. Before conducting a compression test on each specimen, the surface temperature was measured. All specimens were subjected to the same loading rate of 0.6 MPa/s. Later, the obtained values were compared with the results of cold specimen compression test presented in previous technical reports. The general overviews of the hot specimen compression tests and the obtained values are presented in the figures and tables below.

Table 4-6: Compression Results for Test-1

Specimen		Surface Temperature (°C)	Time		Max. Load (N)	Max. Stress (N/mm²)
No	ID		Start	Finish		
1	Ref	---	---	---	945281.56	30.09
7	CFRP	---	---	---	2705007.00	86.10
4	Ref-200	72.0	---	19:15	516354.38	16.44
6	CFRP-200	63.8	---	19:27	2063345.13	65.68
9	CFRP-T3-200	17.4	22:22	22:24	2350391.50	74.82
10	CFRP-T4-200	16.1	22:36	22:37	2395627.83	76.26

#4 Ref-200

#6 CFRP-200

#9 CFRP-T3-200

#10 CFRP-T4-200

Figure 4-5: Compression tests for hot specimens

Although the use of CFRP significantly improved the compressive strength of specimen (from 30.09 to 86.10 MPa), a fire exposure of 134 minutes decreased the compressive strength of CFRP wrapped specimen by 24%, and this value reached 65.68 MPa. The strength of CFRP-T3-200 and CFRP-T4-200 specimens decreased from 86.10 MPa by 13%, and 11% and reached 74.82 MPa, and 76.26 MPa respectively. There were no significant differences between the compression test results obtained from the hot specimen and cold specimen and the obtained reduction are similar to the reductions obtained from compressive tests on cold specimens (refer to section **Error! Reference source not found.** on System A). However, this observation is related to the hot compressive test on specimens having a maximum temperature of 72°C. So, this difference might be more significant in the compressive test on specimens with higher temperatures and demands further evaluations.

4.3   Experiment – 2 : Temperature Test

To conduct the second test, a total of 7 CFRP wrapped specimens comprising 1 non-insulated and 6 insulated specimens were used. The 6 insulated specimens were divided into three groups of two, and each group was insulated with two different insulation types of Systems A, B, and C. This test was performed with respect to 4 hours of ASTM E119 standard fire curve. Before performing Test – 2, thermocouples were just embedded into FRP surfaces of the System A insulated specimens in a similar manner to Test – 1. Also, a pyrometer was used to measure the material surface temperatures before and after fire test. The post-fire pyrometer measurement was done in 2 phases. The first phase was performed right after opening the furnace door. The second phase was conducted within four different intervals of cooling period. The details of the conducted test and temperature readings are presented in the following tables and figures.

Table 4-7: Details of Fire Test-2

Test ID	DYMAT-AC125
Temperature Test No	2
Insulation System	A, B and C
Date	23.03.2022
Heating Regime	ASTM E119 Standard Fire Curve
Starting Time	12:35
Finishing Time	16:50
Test Duration	4 hours
Cooling Duration	25 hours 46 minutes
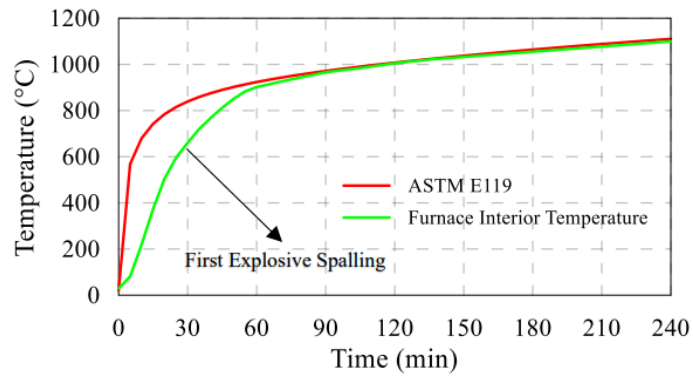
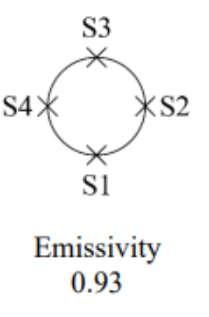***Figure 4-6:*** *Furnace Temperature during Test-1*
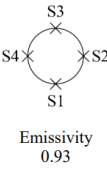
Table 4-8: Environmental conditions during Test – 2

	Pre-Test Stage	Post-Test Stage
Room Temperature (°C)	13	22
Humidity (%)	76	76

Figure 4-7: *Opening the furnace door and first measurements of surface temperature after Test-2*

Table 4-9: Pyrometer measurements for Test – 2

Spec. No	Spec. ID	Stage	Surface Temperatures (°C)					Configuration
			S1	S2	S3	S4	Average	
5	CFRP	Pre-Test	11.8	11.7	11.6	11.4	11.625	
		Post-Test	670	510	510	580	567.5	
11	CFRP-A-T3	Pre-Test	12.6	11.9	11.9	12.4	12.2	
		Post-Test	380	190	250	250	267.5	
12	CFRP-A-T4	Pre-Test	12.1	12.3	12.1	12.4	12.225	
		Post-Test	410	310	260	275	313.75	
13	CFRP-B-T1	Pre-Test	11.9	11.8	11.8	11.8	11.825	
		Post-Test	560	450	470	530	502.5	
14	CFRP-B-T2	Pre-Test	11.9	11.8	11.6	11.6	11.725	
		Post-Test	320	380	430	220	337.5	
15	CFRP-C-T1	Pre-Test	11.8	11.8	11.8	11.8	11.8	
		Post-Test	290	400	470	470	407.5	
16	CFRP-C-T2	Pre-Test	12.2	11.8	11.8	11.7	11.875	
		Post-Test	380	300	530	360	392.5	

Configuration: S3, S4, S2, S1

Emissivity 0.93
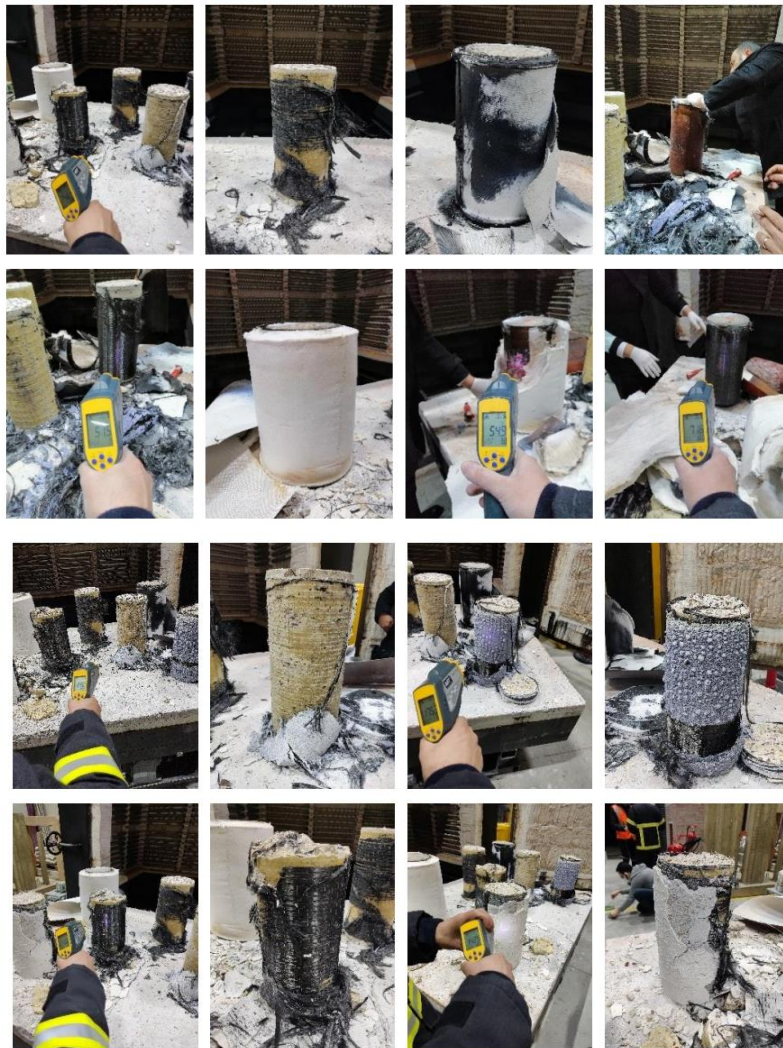
Figure 4-8: General overview of specimens and temperature measurement during cooling period

Table 4-10: Pyrometer measurements during cooling period for Test – 2

Spec. No.	Spec. ID	Measurement Location	Surface Temp. for Different Measurement Time (°C)			
			17:35	18:00	18:35	19:00
5	CFRP	Concrete	280	250	205	170
		FRP	320	285	245	185
11	CFRP-A-T3	Concrete	400	245	208	182
		Outer RS Material	150	120	115	93
12	CFRP-A-T4	Concrete	300	220	185	160
		Outer RS Material	100	120	110	85
13	CFRP-B-T1	Concrete	290	255	215	175
		FRP	435	300	240	210
		FireFree88	260	255	140	120
14	CFRP-B-T2	Concrete	220	250	233	205
		FRP	---	270	200	170
		FireFree88	260	215	180	290
15	CFRP-C-T1	Concrete	280	180	220	175
		FRP	400	280	215	210
		Vella Fino	300	350	265	230
16	CFRP-C-T2	Concrete	300	250	215	185
		FRP	340	277	220	200
		Fire Set 60	250	190	145	140
		Vella Fino	200	172	160	125
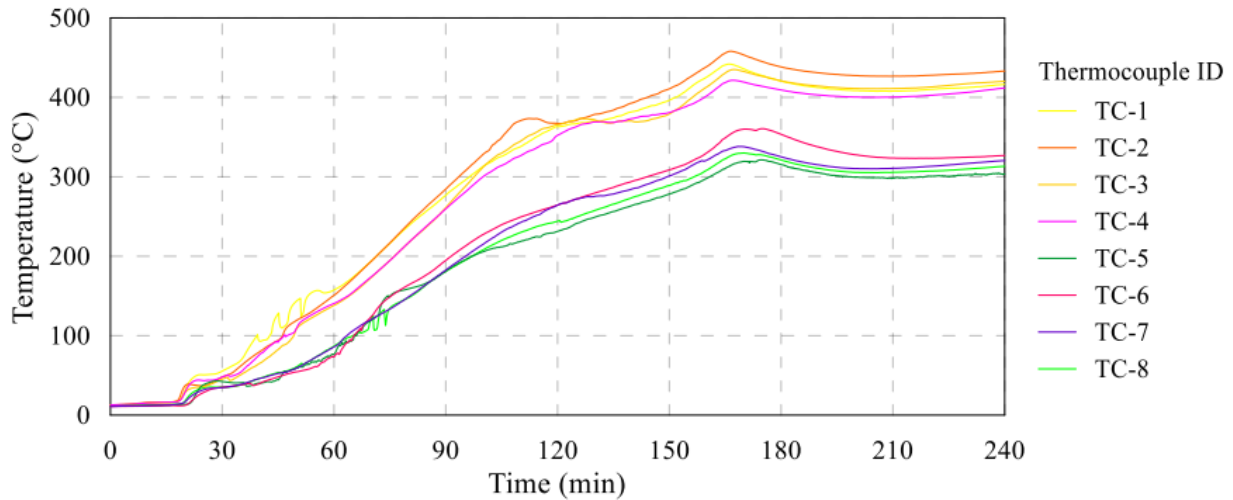
Figure 4-9: Thermocouple readings during Test-*2*

4.4 Experiment – 2 : Compression Tests

As the specimens were extremely hot, compression tests could not be conducted on the same day and after 24 hours specimens were still hot. Due to the long exposure duration 3 specimens

experienced explosive spalling (System C and B). To retrofit the exploded specimens with gypsum, they were temporarily excluded from compression tests. The rest of the 4 specimens were prepared for compression test. All specimens were subjected to the same loading rate of 0.6 MPa/s. Before each compression test, the temperature of specimen's surface was recorded. Below figures and tables demonstrate the general overview of the compression tests and obtained values. It should be noted that specimens with system were still hot when they were tested.

Table 4-11: Results Related to Heated Specimen in Test – 2

Specimen		Surface Temperature (°C)	Time		Max. Load (N)	Max. Stress (N/mm^2)
No	ID		Start	Finish		
5	CFRP	16.0	18:59	19:00	202920.00	6.46
11	CFRP-A-T3	33.8	19:11	19:11	667840.94	21.26
12	CFRP-A-T4	36.9	19:20	19:21	977897.19	31.13
13	CFRP-B-T1	18.4	19:32	19:33	209496.20	6.67

* Specimens insulated with System A were still hot during compression tests

Despite superior performance during 1-hour fire exposure, System C displayed a severe level of damage whereby it could not withstand a 4-hour fire load. So, the high fire performance of System C is limited to 60 minutes of fire and in case of long fire exposure, this system loses its specifications and will not protect the specimen. During the 4 hours of ASTM fire exposure, System C insulated specimens experienced explosive spalling. Thus, the post-fire strength data related to this system could not be obtained. The comparison between the results from 1 hour and 4 hours of fire exposure points out that for a 1-hour fire duration System C has the best fire performance. But for a longer exposure duration, System A insulated specimens will perform better than the other two systems.

Although the use of CFRP significantly improved the compressive strength of specimens (from 30.09 to 86.10 MPa), 4 hours of fire exposure significantly decreased the strength of the specimens. This reduction was more tangible in system B insulated specimens. After 4 hours of fire exposure, the strength of the CFRP-B-T1 specimen decreased by 92% and reached 6.67 MPa. The strength values of system A insulated specimens were also significantly decreased. For the CFRP-A-T3 specimen, a reduction of 75% was observed and its strength decreased to 21.26 MPa. For the CFRP-A-T4 specimen, a reduction of 63% was observed and its strength value reached 31.13 MPa. Fire exposure of 4 hours has changed the physical properties of all insulation materials. However, System A insulation was still wrapped around the specimens and slowed down the cooling process of the concrete part. Thus, after a cooling period of 25 hours, CFRP-A-T3 and CFRPA-T4 specimens were still hot while the rest of the specimens returned to their initial temperature. From the strength results obtained from 4-hour fire exposed specimens, it can be observed that specimen CFRP-A-T4 has the best performance.

Evaluation of FRP and concrete bond performance (or debonded specimens) demonstrated that specimen CFRP-A-T4 with the highest post-fire load-carrying capacity experienced cohesive failure in the concrete substrate while the failure mechanism for the rest of the specimens was an adhesive failure at the adhesive/concrete interface. The results indicate that for long fire exposure, System A outperformed the other two systems. Thus, System A is a suitable option for a prolonged exposure duration. Within system A, T4 demonstrated a higher fire performance than T3.

Chapter 5   SMALL-SCALE CONCRETE EXPERIMENTS PART II

A total of 171 standard concrete cylinders were fabricated to test the post-thermal exposure compressive behavior of FRP-confined cylinder. The 100x200 mm and 150x300 mm. concrete cylinders were cast and confined with FRP laminates. The effect of different parameters on the compressive behavior was examined. These parameters are reinforcement type number of plies (C1, C2 and G4), stacking sequence (C2G1, C2G1 and CGCG), cylinder size (20:100x200mm; and 30:150x300mm), heating temperature and duration (23-400 and 23(180)-400(180) for 90- and 180-min. thermal exposure duration respectively), bond overlap length (50mm and 150mm), and if cylinders are protected (NA,1P,2P,3P). The heating duration was 90 minutes unless noted otherwise (e.g., 300 vs. 300(180)).   The naming convention for cylinder notation is further explained in **Table 4-1**.

Table 5-1: Specimen Notation Convention

Test type	Type of Reinforcement	Cylinder Height	Temperature	Overlap	Protection
C	C1, C2, CGCG C2G2, C1G4, G4, AS	20, 30	23-400(na/180)	50/150	NA,1P,2P,3P

Some specimens were left unstrengthened from each cylinder size to examine the thermomechanical properties of as-built concrete. The experiment was designed to examine the effect of multiple parameters on the residual post-heated strength of FRP-confined concrete.

5.1 Small-Scale Concrete Specimen Fabrication

The concrete cylinders were cast on 6/15/2021 using ready-mix concrete from a local manufacturer. The aggregates used were made up of igneous rocks. The concrete mix design is presented in **Table 5-2**.

Table 5-2: Concrete Mix Design

Component	*Weight (kg)*
Cement	420
Coarse Aggregates	810
Fine Aggregates	820
W/C Ratio	0.44
Super-plasticizer	12

The air content (3.75%), temperature (30.7°C) and the slump (4.5 cm) were measured for quality assurance. The cylindrical specimens were cast according to ASTM C192M and C39M. The concrete cylinders were demolded after 24 hours, and their surface was ground to ensure a level surface for compression testing and were placed in a curing tank for 7 days before being removed to air dry. The cylinders were left to cure at room temperature until they reach their 28-day strength.

After curing for 28 days in water tank, cylinders were confined with carbon and E-glass/epoxy laminates. Specimens were fabricated using the hand wet-layup method using Sikadur-300 epoxy for the matrix. The surface of the specimens was first cleaned using an acetone-soaked cloth to remove any dirt. The epoxy was mixed according to the manufacturer's instruction for 10 minutes. A primer epoxy coating was then applied to the surface. The carbon and E-glass fabrics

were then saturated with the epoxy and rolled-over with a roller to ensure proper impregnation of

the fibers.

(a)

(b)

(c)

(d)

Figure 5-1: Casting of Concrete Cylinders: a) Air Content Reading; b) Concrete Temperature; c) Slump Measurement; d) Prepared Specimens

5.2   Small-Scale Concrete Specimen Thermal Exposure Protocol

The experiment examined the affect Each configuration group was exposed to temperatures of 23, 300, and 400 ℃. Most configurations were also exposed to a temperature of 200 ℃. A few configurations were exposed to temperatures of 100, 150, and 250 ℃. Cylinders were placed in the furnace at room temperature and were heated up to required temperature and held at that temperature for 90 and 180 minutes. Once heating is finished the furnace is shutoff and the furnace door is left open to allow the specimens to cool down to room temperature. Some cylinders were cast with a thermocouple located in the center of cylinder to measure the temperature of the concrete. Additional thermocouples were placed in the oven to record the heating temperature. A view of post-thermal exposure of the specimens can be found in Figure 5-2 and

Figure **5-3**.

Figure 5-2: Ignition of the CGFRP-Confined Specimens at a temperature of 300℃

a)

b)

c)

d)

Figure 5-3: Samples of CFRP-confined specimen post-thermal exposure damages

5.3 Post-Thermal Exposure Compressive Test Procedure

The cylinders were tested in Forney© FX700 model compression machine with a stress-controlled testing rate of 0.25 MPa/second. The machine had a 3000 kN capacity. Two 50-mm vertical strain gauges were installed on all cylinder as-built concrete cylinders on opposite directions at mid-span. Two 50-mm horizontal strain gauges were installed on the as-built concrete cylinders in the hoop direction at mid-span. Four 10-mm horizontal strain gauges were installed on the CFRP and GFRP confined concrete cylinders at midspan starting from the bond going around in the hoop direction.

5.4 Small-Scale Concrete Experimental Results

The results of the small-scale testing of the unconfined As-built concrete specimens are presented in **Table** *4-3*.

Strain readings were recorded at a rate of 1 Hz. However, all stress strain diagrams display readings at a sampling rate of 0.05 Hz except for the last 10 readings which are displayed at a rate of 1 Hz. The initial reading display rate was chosen to easily differentiate between readings of specimens. The 1.0 Hz rate was chosen to better capture any sudden changes that might occur near failure of the specimens.

5.4.1 As-built Concrete:

The modulus of elasticity of concrete, is calculated in accordance with ASTM C469 through the following equation:

$$E_c = (S_2 - S_1)/(\epsilon_2 - 0.00005)$$

Eq. 5-1

where E_c is the modulus of elasticity of concrete, S_2 is the applied stress corrosponding to 20% ultimate load, S_1 is the applied stress corrosponding to a strain of 0.00005, and ϵ_2 is the strain induced by a stress of S_2.

Table 5-3: Result Summary of As-built Small-Scale Concrete Specimens

Height, mm.	Exposure Period, min.	Temperature, °C	Ultimate Strength, MPa	f'_{ccT}/f'_c
200	90	23	44.47	1.00
			45.13	1.02
			43.49	0.98
		100*	39.93	0.90
		150*	37.71	0.85
		200	38.50	0.87
			40.59	0.91
			35.88	0.81
		250	33.27	0.75
		300	35.82	0.81
			37.85	0.85
		400	28.47	0.64
			27.29	0.62
			29.92	0.67
300	90	23	45.96	1.04
			43.63	0.99
			42.96	0.97
		100*	39.77	0.90
		150*	37.56	0.85
		200	34.60	0.78
			38.11	0.86
			33.75	0.76
		250*	33.14	0.75
		300*	30.93	0.70
		400	33.78	0.76
			36.56	0.83
			32.55	0.74
	180	23	40.08	0.99
			40.85	1.01
		100*	36.42	0.90
		150*	34.40	0.85
		200	33.62	0.83
			32.76	0.81
		250	34.90	0.86
			33.63	0.83
			34.76	0.86
		300	29.92	0.74
			26.28	0.65

			27.73	0.69
		400	27.21	0.67
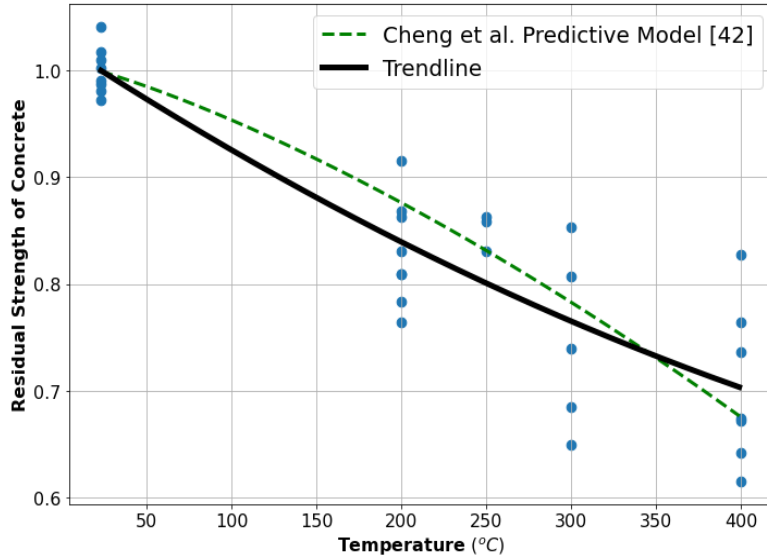
Figure 5-4: Residual compressive strength of concrete post- exposure to elevated temperatures
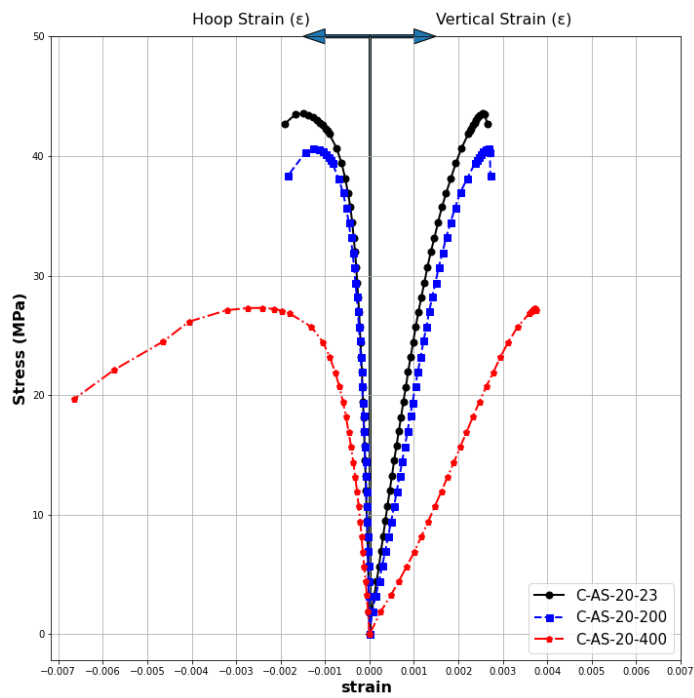
Figure 5-5: Stress-Strain diagram for C-AS-20 cylinders after being exposed to different temperatures.
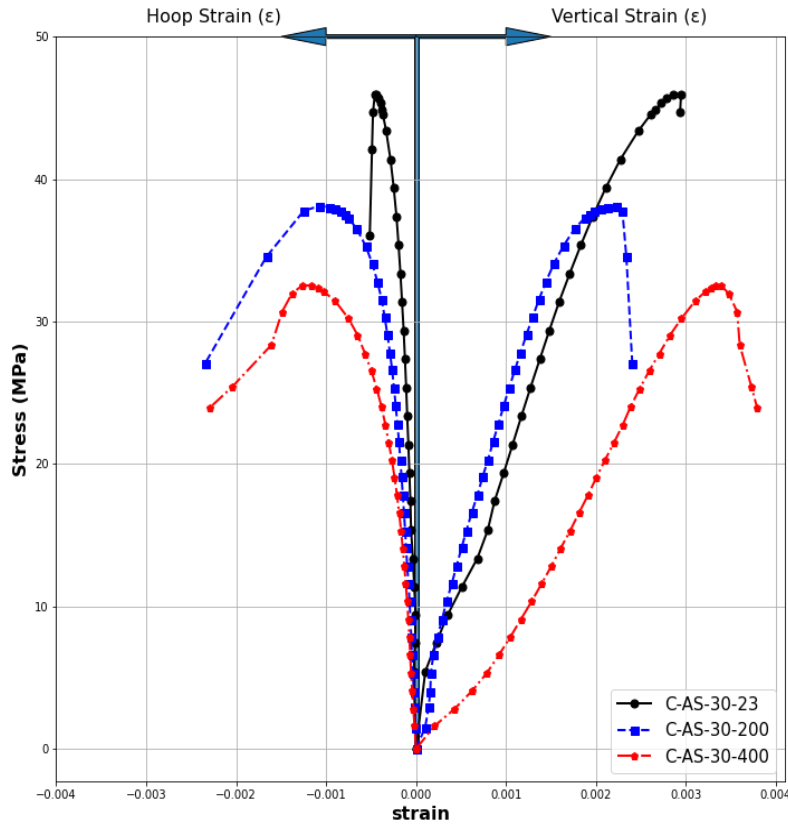
Figure 5-6: Stress-Strain diagram for C-AS-30 cylinders after being exposed to different temperatures.

5.4.2   CFRP-confined Concrete:

The stress-strain model of FRP-confined concrete was assumed to consist of two branches per the model proposed by Youssef et al. [5] and is presented in **Figure 4-6**. The modulus of the second branch, E2, was calculated by getting the average tangent in the stress-strain starting from stress reading corresponding to the maximum strength of unconfined concrete and ending at maximum stress of confined concrete (Point B to Point C in **Figure 4-6** respectively).
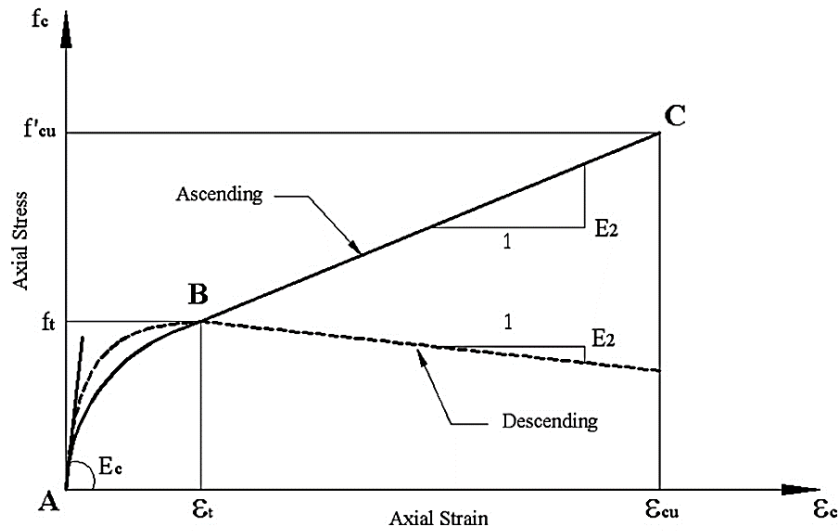
Figure 5-7: Stress-Strain for FRP-confined Concrete (Youssef et al. 2007)

The tangent at any given point was calculated using the following expression:

$$E_{2n} = (S_n - S_{n-1})/(\epsilon_n - \epsilon_{n-1})$$

Where S_n is the applied stress at a given reading n, S_{n-1} is the applied stress at the previous

reading n-1, ϵ_n is the strain induced in the specimen by stress S_n, and ϵ_{n-1} is the strain induced in

the specimen by stress S_{n-1}.

At a temperature of 200 ℃ the bond between the concrete and CFRP was still maintained. The

two layers CFRP confined specimens exhibited rupture in the inner layer and debonding in the

outer layer. At heating regimens above 250 ℃ the bond between concrete and CFRP was

observed to be lost.

CFRP confined Cylinders reinforced with 1 layer lost all their matrix at 400 ℃ which is above the

decomposition temperature of the epoxy matrix. Specimens that were confined with two layers

either maintained their matrix or exploded during heating. Their ability to retain their matrix can be due to an increase in their epoxy content compared to those confined with a single layer. Ignition of CFRP was only noticed during 300 ℃ regimen. Meaning that ignition temperature is expected to be in the range of 250-300 ℃.

5.4.2.1 Specimens C-C1-20-50

C-C1-20-50 specimens were fabricated with a single layer of carbon fiber and an overlap of 50 mm. The 20 refers to 200 mm. height of the specimens that were used. The effect of elevated temperature on the stress-strain diagrams and reduction of mechanical properties is presented in **Figure *4-7*** and **Figure *4-8*** respectively. There is a clear strength and stiffness degradation with an increase of exposure temperature.
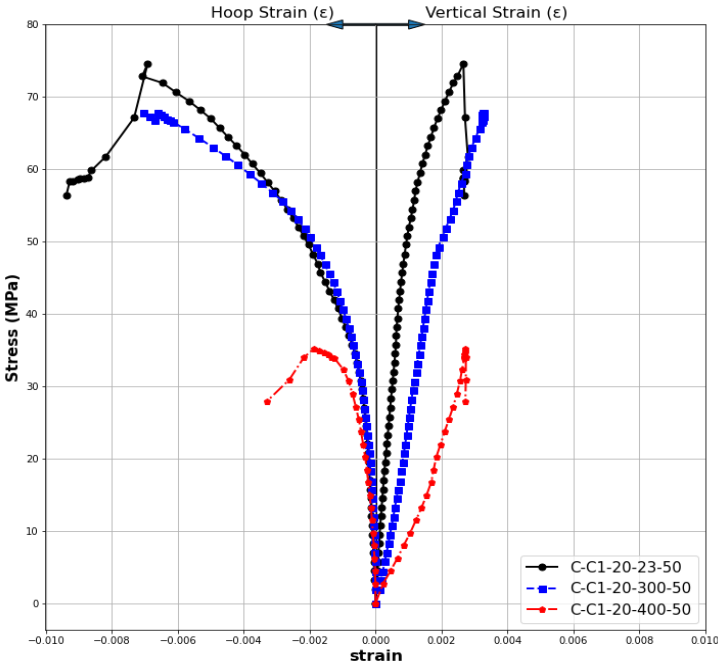
Figure 5-8: Stress-Strain diagram for C-C1-20-50 specimens after being exposed to different temperatures.
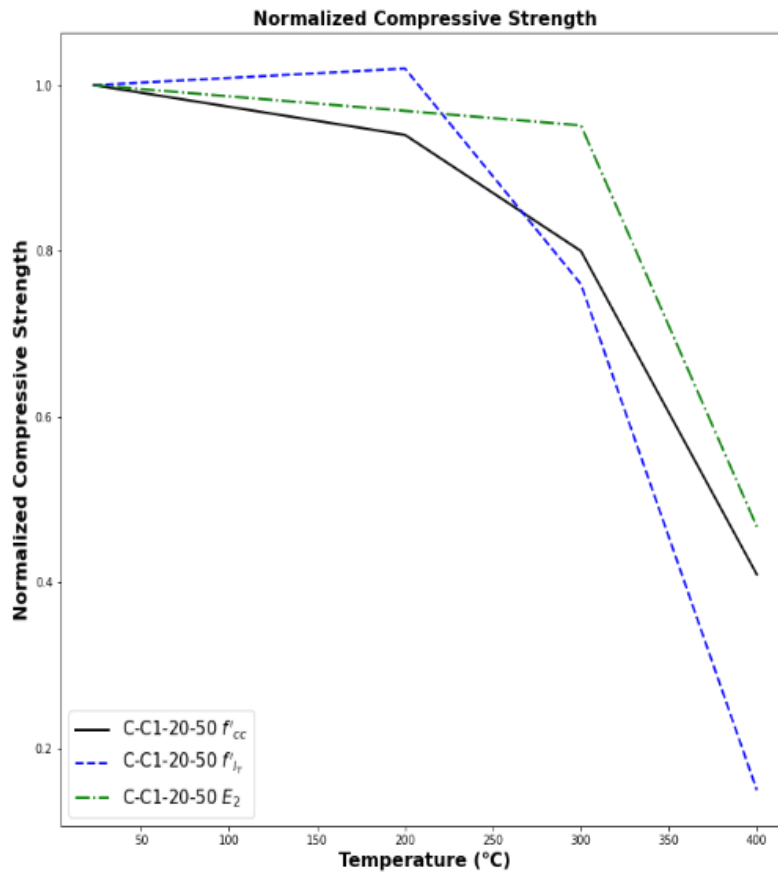
Figure 5-9: Effect of elevated temperature on the mechanical properties of C-C1-20-50 specimens.

5.4.2.2   Specimens C-C1-20-150

C-C1-20-50 specimens were fabricated with a single layer of carbon fiber and an overlap of 50 mm. The 20 refers to 200 mm. height of the specimens that were used. The effect of elevated temperature on the stress-strain diagrams and reduction of mechanical properties is presented in **Figure *4-9*** and **Figure *4-10*** respectively. There is a clear strength and stiffness degradation with an increase of exposure temperature similar to C-C1-20-150 specimens.
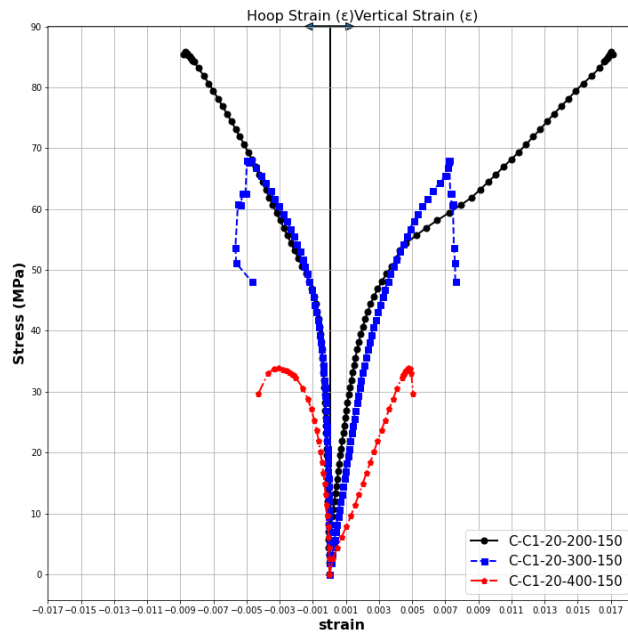
Figure 5-10: Stress-Strain diagram for C-C1-20-150 specimens after being exposed to different temperatures.

Figure 5-11: Effect of elevated temperature on the mechanical properties of C-C1-20-150 specimens.

5.4.2.3   Specimens C-C2-20

These specimens were fabricated by laminating two layers of carbon fiber on 100x200 specimens. The effect of elevated temperature on the stress-strain diagrams and reduction of mechanical properties is presented in **Figure *4-11*** and **Figure *4-12*** respectively. This group displayed a reduction in compressive strength with an increase in exposure temperature. However, f_{lT} increased at a temperature of 200 ℃.

Figure 5-12: Stress-Strain diagram for C-C2-20 specimens after being exposed to different temperatures.

Figure 5-13: Effect of elevated temperature on the mechanical properties of C-C2-20 specimens.

5.4.2.4   Specimens C-C2-30

These specimens were fabricated using two layers of carbon fiber fabric and 150x300 mm. concrete specimens. The stress diagrams presented in **Figure *4-13*** display a clear strength, vertical stiffness , and lateral stiffness degradation with an increase of exposure temperature. However, specimens the residual modulus of the specimens increased after temperature exposure of 250 ℃ as can be seen in **Figure *4-14***.

Figure 5-14: Stress-Strain diagram for C-C2-30 specimens after being exposed to different temperatures.
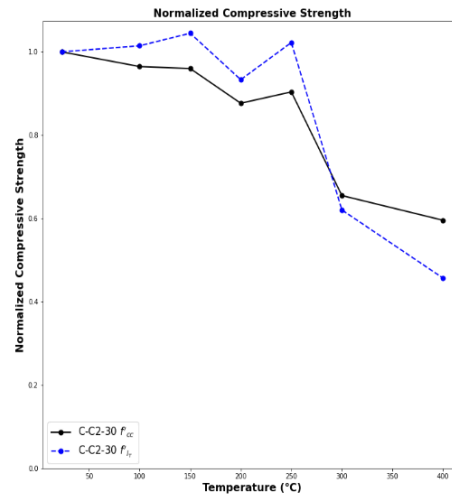
Figure 5-15: Effect of elevated temperature on the mechanical properties of C-C2-30 specimens.

5.4.2.5   Specimens C-C2-30-T180

These specimens were fabricated in the same way as C-C2-30 except that the elevated temperature exposure duration was for 180 minutes. The stress-strain diagrams for different exposure temperatures are presented in **Figure *4-15***. There was a clear increase in f_{lT} after exposure temperature of 200℃ then it drops sharply at temperature of 250℃ and 300℃.

5.4.3   CGFRP-confined Concrete:

A large portion of the small-scale experimental program was dedicated to examining the residual behavior of hybrid-composite-confined concrete specimens. The combination of both carbon and glass was examined by utilizing different stacking sequences and number of layers. The theory behind the hybrid use of both fabrics is to get the benefits of both fabrics. The glass fabric is theoretically meant to act as a sacrificial layer to protect carbon. Additionally, glass fiber has a higher ultimate strain which could lead to an increase in ductility for the confined concrete specimens.
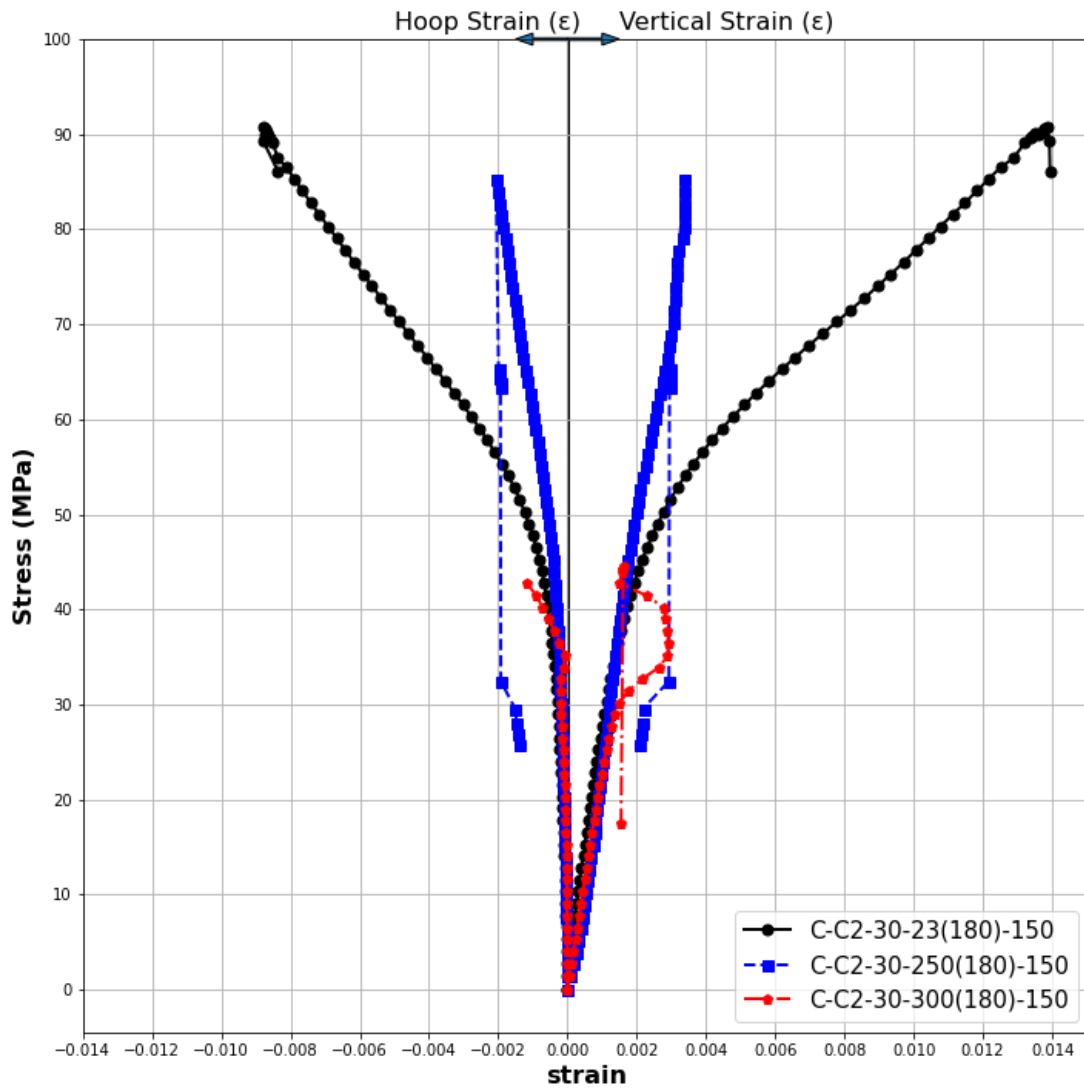
Figure 5-16: Stress-Strain diagram for C-C2-30-T180 specimens after being exposed to different temperatures.

5.4.3.1 *Specimens C-C1G4-30-T180*

This group was fabricated by confining the specimens with one layer of carbon followed by four layers of glass. The specimens were exposed to an elevated temperature for a duration of 180 minutes. The stress strain diagram presented in **Figure *4-16*** shows that there is a clear stiffness with increasing temperatures. However, the ultimate capacity and strengthening of CGFRP does not decrease until after a temperature of 250 ℃ as can be seen in **Figure *4-17***. The jump in stiffness at exposure temperature 300 ℃ is unrealiable as can be seen from the unpredictibaly of the stress-strain diagram of specimen C-C1G4-30-300(180)-150.
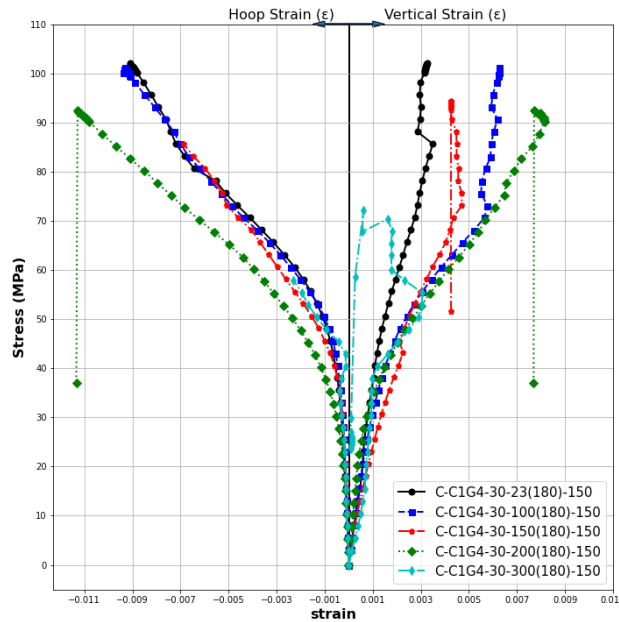
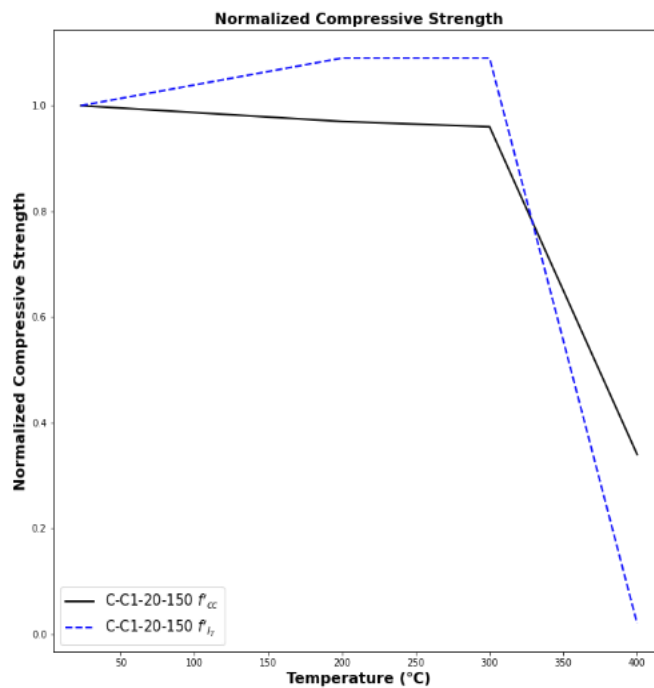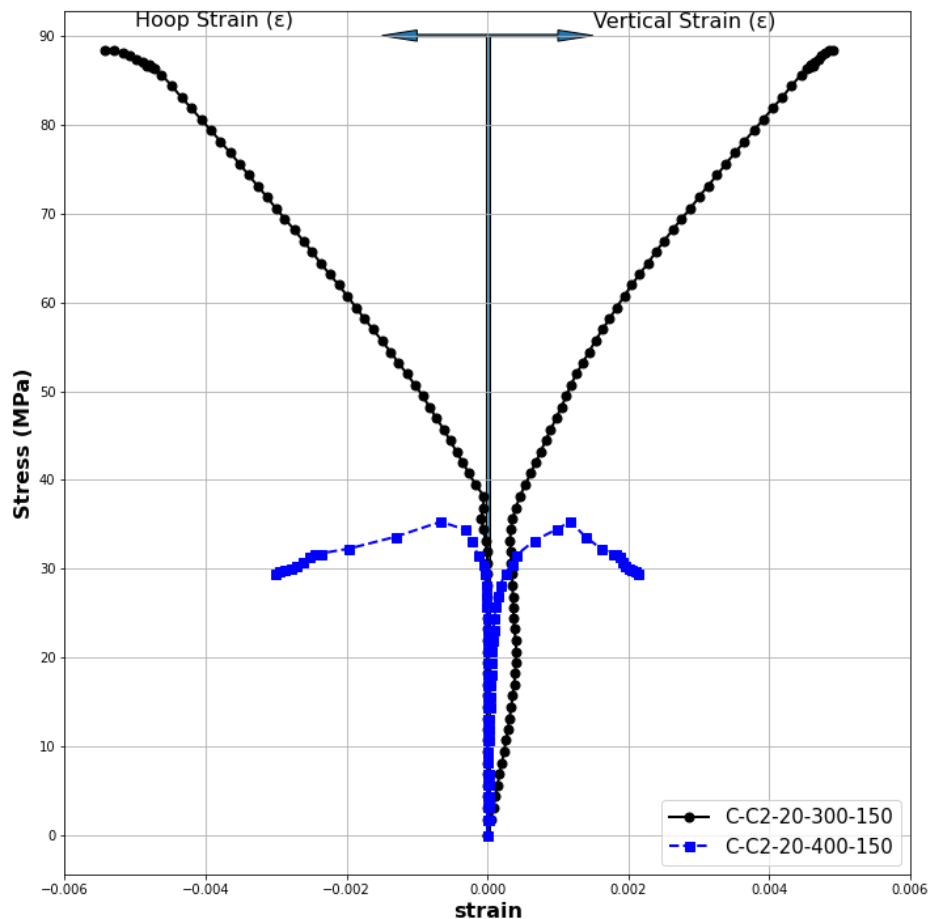**Figure 5-17:** Stress-Strain diagram for C-C1G4-30-T180 specimens after being exposed to different temperatures.
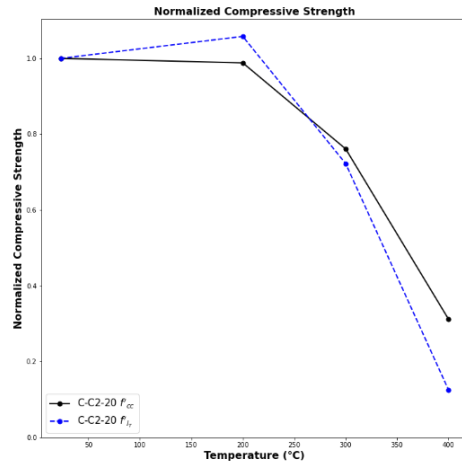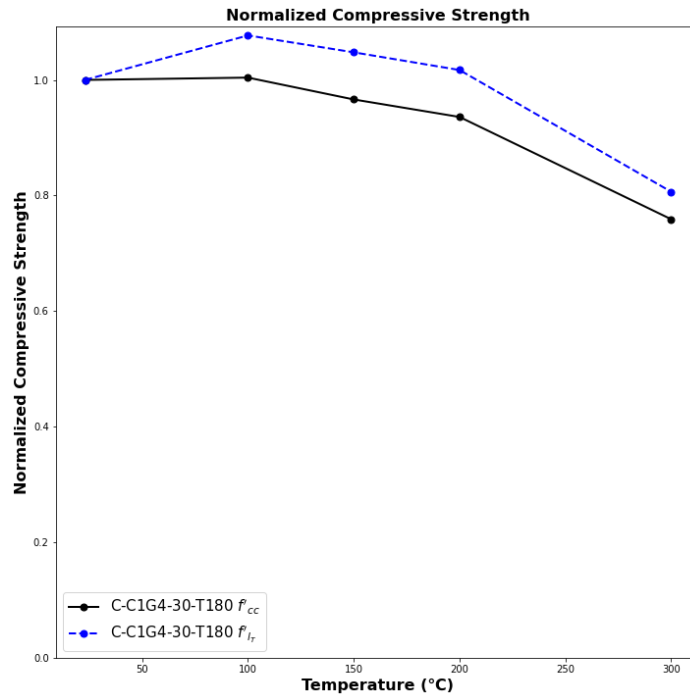
Figure 5-18: Effect of elevated temperature on the mechanical properties of C-C1G4-30-T180 specimens.

5.4.3.2   Specimens C-C2G2-30-T180

This group was fabricated by confining the specimens with two layers of carbon followed by two layers of glass. The specimens were exposed to an elevated temperature for a duration of 180 minutes. A comparison of the stress-strain diagram
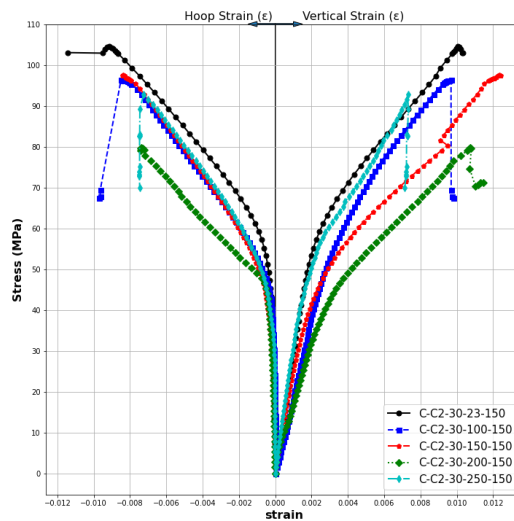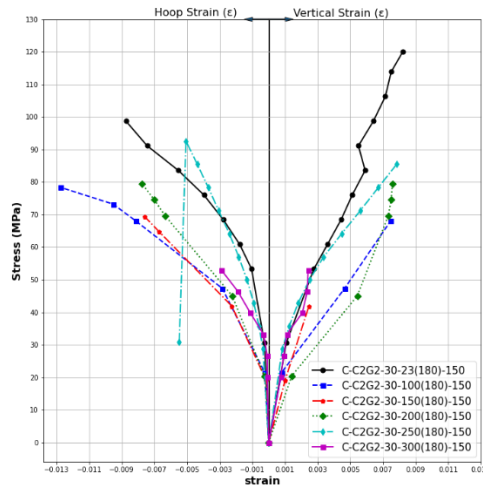
Figure 5-19: Stress-Strain diagram for C-C2G2-30-T180 specimens after being exposed to different temperatures.
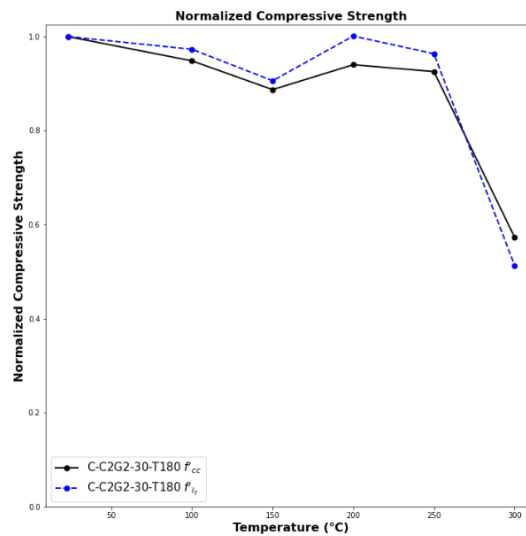
Figure 5-20: Effect of elevated temperature on the mechanical properties of C-C2G2-30-T180 specimens

5.4.4   Comparison and Summary of Small-scale concrete Results

The capacity of the strengthening system, f_{lT}, was obtained by subtracting the compressive strength of the plain concrete, $f_c{}'$, from the strengthened specimen, f_{cc_T}', so that $f_{lT} = f_{cc_T}' - f_{c_T}'$. A comparison chart showing the effect of elevated temperature on f_{lT} for all specimens is presented in **Figure *4-20***. The trend line was drawn using *np.polyfit* function to find a 3rd degree

polynomial fit. What is clear from the chart is that there is a great deal of variance in the results even for individual groups. The variance does decrease for temperatures 100℃ and 150℃ but increases rapidly after that. What is clear from the figure is that most FRP-confined specimens retained more than 75% of their strengthen capacity, f_{lT} up to exposure temperature of 250 ℃ .
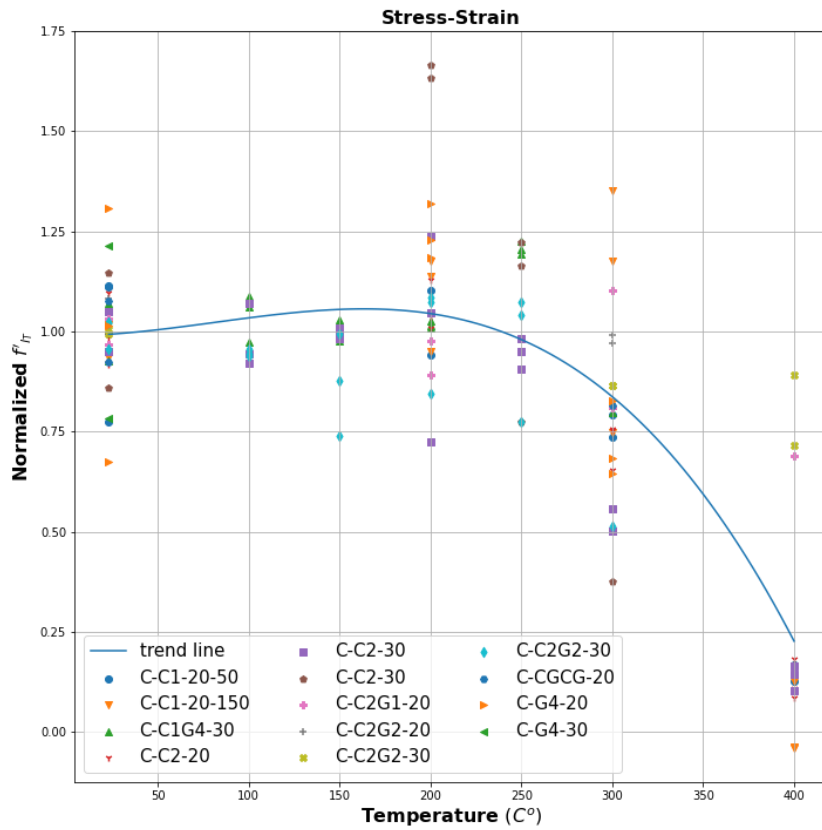
Figure 5-21: Comparison of the effect elevated temperature on f_{lT} of FRP-confiend specimens

5.4.4.1   Strain Energy

One of the advantages of using FRP composites for confinement of concrete is an increase in energy absorption and dissipation. This is especially important in seismic zones where energy dissipation capacity of structural members is vital. The energy absorption capacity can be

quantified in terms of strain energy per unit volume which can be calculated by measuring the

area under stress-strain curve. A summary of findings can be found in **Figure 4-21**.
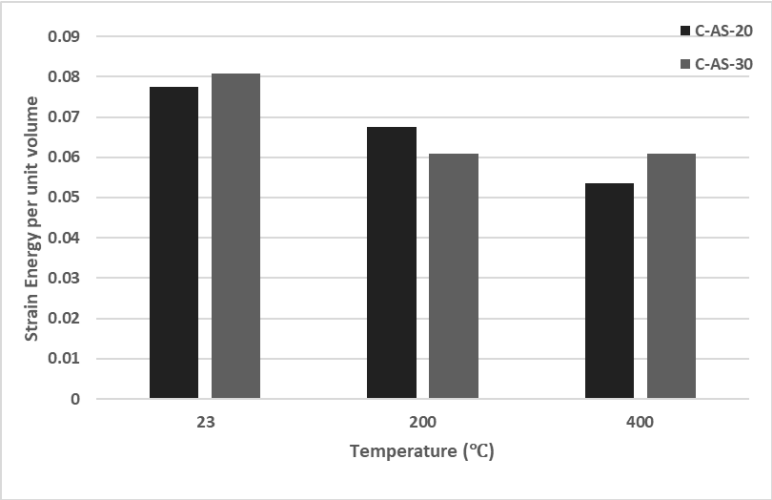
a) As-built concrete specimens
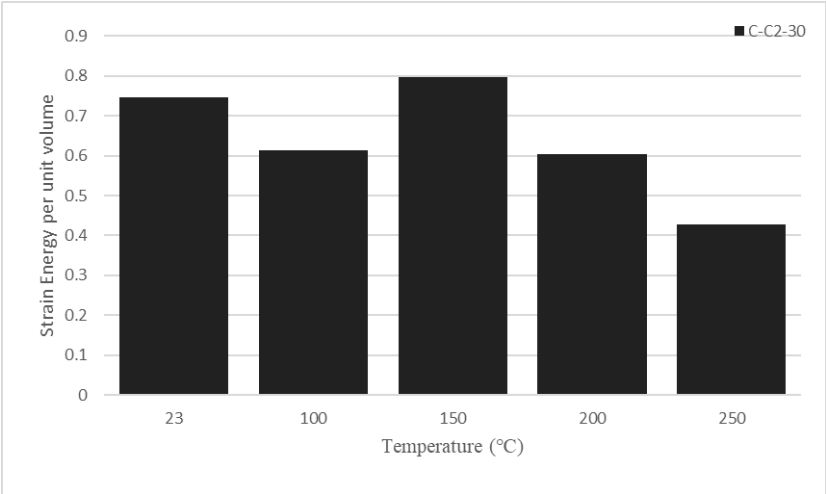
b) CFRP-confined specimens (C-C2-30)
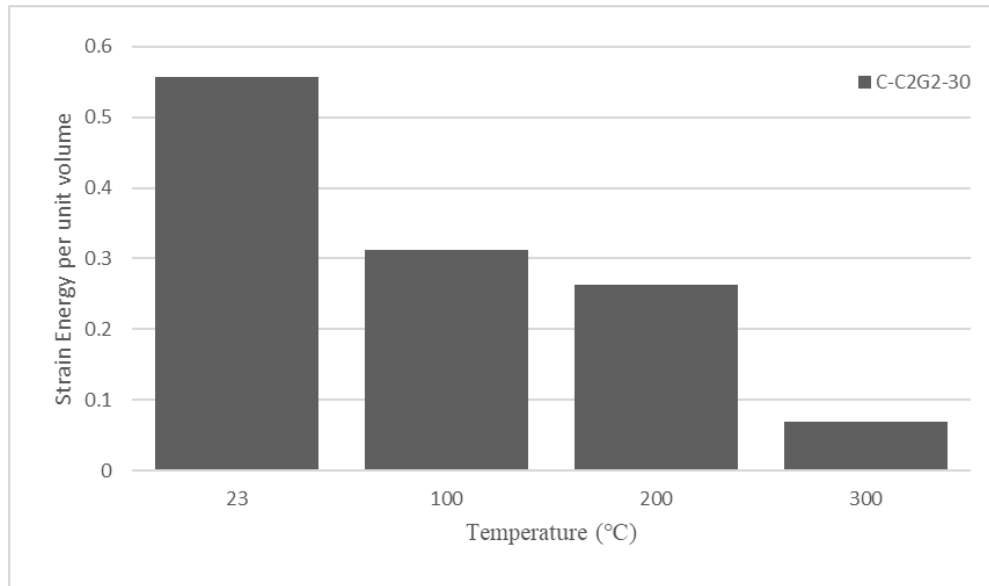
c) CGFRP-Confined Specimens (C-C2G2-30)

b)

Figure 5-22: Strain Energy per Unit Volume before & after Thermal Exposure

5.4.5   Insulated Concrete Specimens

Sikacrete™ 213F is a cement based insulative mortar that is developed by Sika®. A select sample of FRP-confined specimens were protected with either 15mm., denoted 1P, and 30mm., denoted 2P. The mortar was mixed according to the instructions provided by the manufacturer. A view of the heated fire protected specimens can be found in *Figure 5-23*.

a) *View of fire protected specimen after cooling*

b) View of fire protected specimen with the top removed

c) View of FRP surface after thermal exposure

d) Inside view of the furnace post-thermal exposure
700℃

f) View of furnace post-cooling (700 ℃)

g) Fire protected (1 layer) GFRP post-exposure to 700℃

Figure 5-23: Post-thermal exposure view of specimens protected with Sikacrete 213F

Table 5-4: Summary of the compressive strength and strengthening ratios of protected and unprotected FRP-confined specimens

Material	Height (mm.)	Overlap (mm.)	Heating Dur. (min.)	Protection	Temprature (°C)	Max. Stress (Mpa)	f'_{ccT}/f'_c
C1	200	150	90	0	23	83.49	1.88
						86.98	1.96
						88.18	1.99
					200	87.58	1.97
						85.93	1.94
						78.13	1.76
					400	33.9	0.76
						26.94	0.61
						27.06	0.61
				3	400	64.66	1.46
						59.88	1.35
C1G4	300	150	180	0	23	98.28	2.43
						93.93	2.32
						102.24	2.53
					300	73.96	1.83
						75.05	1.85
				1	400	67.99	1.68
						106.62	2.63
C2	200	150	90	0	23	116.82	2.63
						122.26	2.76
						130.87	2.95
					400	42.9	0.97
						37.22	0.84
						35.24	0.79
				3	400	140.62	3.17
						142.98	3.22
				3	400	79.35	3.01
						114	3.00
	300	150	180	0	23	78.11	2.88
						84.07	1.70
						90.81	2.93
					300	44.49	1.11
				1	400	70.28	1.88
						54.28	1.96

					23	121.89	1.99
				0	23	121.5	1.97
C2G2	300	150	180		23	116.37	1.94
					300	68.77	1.76
				2	400	118.69	0.76
					700	48.67	0.61

Figure 5-24: The performance of Sikacrete 213F with CGFRP-confined specimens
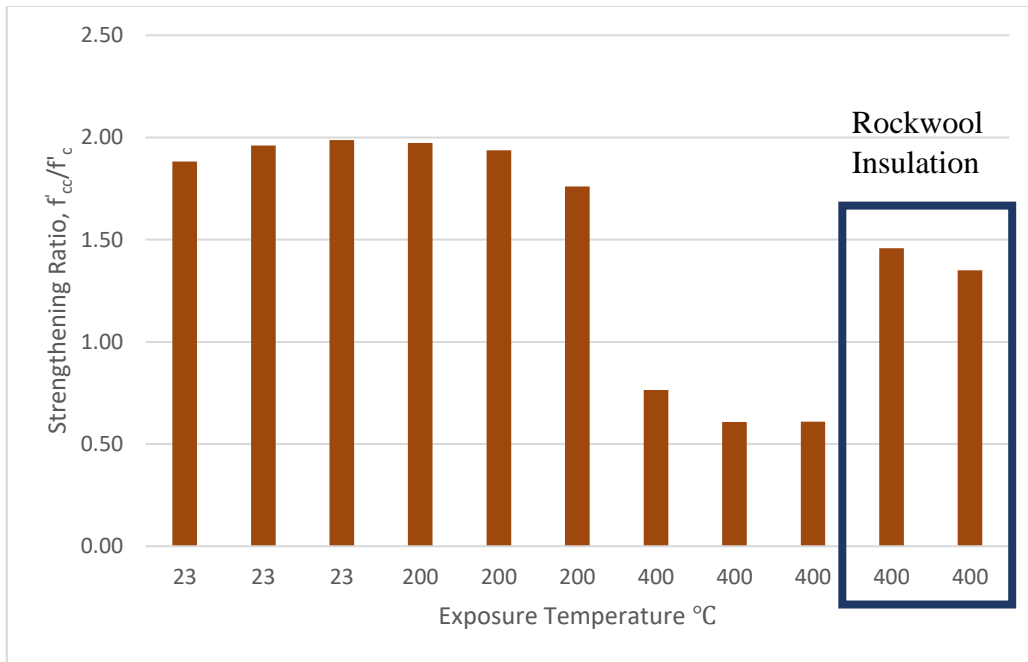
Figure 5-25: The performance of rockwool insulation with CFRP-confined specimens

Chapter 6   FRP COMPOSITE COUPONS EXPERIMENTS

It is important to understand the effect of elevated temperatures on the mechanical and thermal properties of the CFRP materials that will be used in this study for accurate modeling of the structural FRP-confined columns. The mechanical properties of the CFRP were obtained experimentally according to ASTM standards. For tensile mechanical properties, ASTM D3039 [69], was followed. Additionally, mechanical testing was conducted to measure the mechanical behavior of the CFRP after being exposed to an elevated temperature. The FRP laminates were fabricated using Sikawrap™ 530C unidirectional carbon fiber system and Sikadur™ 300 epoxy resin. A summary of the mechanical properties of the CFRP materials can be found in **Table *6-1***.

6.1   Sample Preparation

Two-ply unidirectional CFRP laminates and 4-ply CGFRP hybrid composite laminates were fabricated on February 4, 2021, using a wet layup technique that mimics the typical on-site fabrication process used by the construction industry for column strengthening applications. The temperature at the time of fabrication and curing was 22℃. The relative humidity of the room (RH) was assumed to be similar to outside RH which was 60-65%. The first step of the fabrication was to take a large roll of unidirectional carbon fiber sheet and cut the carbon fiber plies into the appropriate dimensions. Next, the two-part epoxy was thoroughly mixed for five minutes; the pot life (*time until the epoxy starts hardening and the initiation of cross-linking*) was provided by the manufacturer to be 60 minutes at ambient temperature. A primer layer of the epoxy was first applied to the plastic plate. The first carbon fiber unidirectional ply was then

placed on the epoxy and pressed to ensure the fibers facing the fabrication sheet were sufficiently

impregnated (saturated) with the epoxy. The first ply was then taped onto the plate to hold the

fibers in place and to ensure unidirectionality of the fibers. The second layer of epoxy was applied

and pressed down to ensure impregnation of the opposing side of the ply (see Figure *6-1*). The

same steps were repeated for the second ply before placing another plastic plate on top of the

laminate. The laminate was left to cure at room temperature for one week before being demolded.

The hybrid composite was fabricated by laminating two additional E-glass plies on top of the two

carbon plies.

The top plastic plate was removed from the laminate after one week of curing. The CFRP

composite cured specimen (refer to Figure **6-2**) was determined to be representative of a typical

CFRP system fabricated on-site. The final dimensions of the laminate were 68.58 cm $\times$ 24.13 cm.

The taping was kept on the specimen to be removed during the cutting process.

Table 6-1: Properties of: (a) Fiber System and (b) The Epoxy Matrix

(a)

	Carbon	E-glass
f (**MPa**)	4.000	3.000
E (**MPa**)	230,000	84,000
ϵ_u	0.017	0.045
t_{carbon} (**mm**)	0.29	0.

(b)

f_{epoxy} (**MPa**)	45
E_{epoxy} (**GPa**)	3,500
T_g (°C)	53

f_{carbon}: Ultimate tensile strength of carbon fibers
E_{carbon}: Tensile modulus of carbon fibers
ϵ_{carbon}: Ultimate strain of carbon fibers
t_{carbon}: Fabric thickness.

f_{epoxy}: Tensile strength of epoxy
E_{epoxy}: Shear modulus of epoxy.
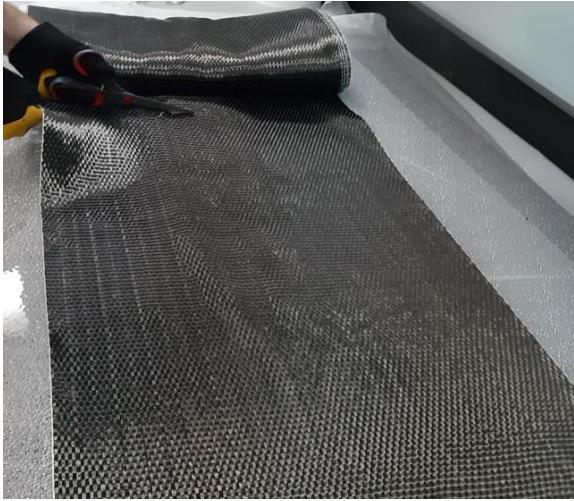
a) Cutting the carbon fiber fabric

b) Mixing of epoxy matrix

c) Rolling first ply of the CFRP laminate

d) Laminating second ply of CFRP laminate

Figure 6-1: Fabrication of the CFRP Composite Laminate

The laminates were machined into coupons and tabs using an angled hand-held rotary grinder (see Figure *6-3*). The dimensions of the machined parts were determined in accordance with ASTM D3039 [69] for tensile testing of FRP composites and ASTM D7616 [70] for single-lap-shear strength testing of FRP composites.
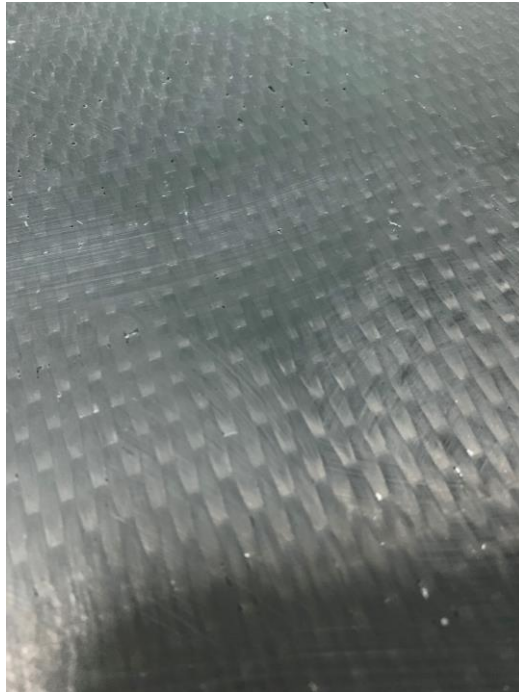
Figure 6-2: Cured CFRP Composite Laminate

Figure 6-3: Cutting of CFRP Composite Laminate

6.2   *FRP Thermal Exposure Protocol*

FRP tension and SLS specimens were placed in a calibrated oven at room temperature. The oven

door was then closed, and oven turned on until the desired temperature was reached. The

specimens were then heated at that temperature for 90 minutes. Once the heating is finished, the

oven doors are left open, and specimens were left until they reach room temperature. CFRP

specimens that were heated at a temperature of 300°C and above experience extreme buckling

during the thermal exposure protol due to a negative value of coeffecient of thermal expansion of

carbon fiber. At a temperature of 500 °C, the epoxy matrix and was completely decomposed and

the carbon fiber had begun decomposing. A view of CFRP specimens after thermal exposure can

be found in **Figure 6-4**.

a) 200°C   b) 300°C

| | c) 400℃ | | d) 500℃ |
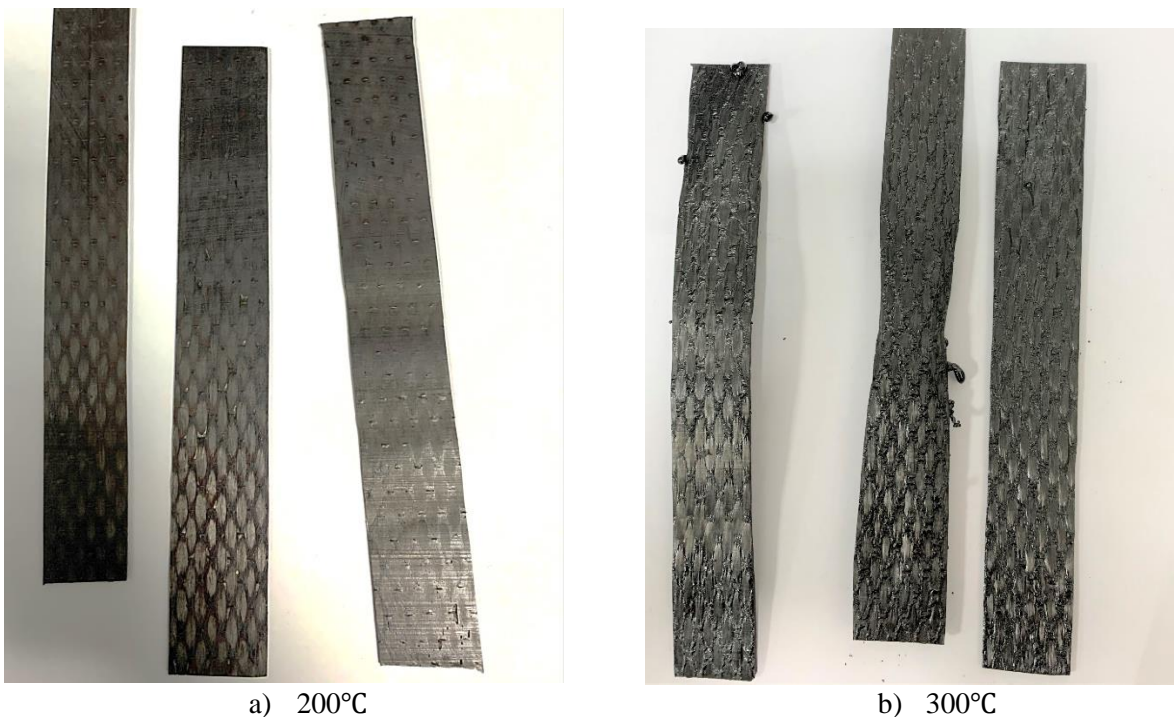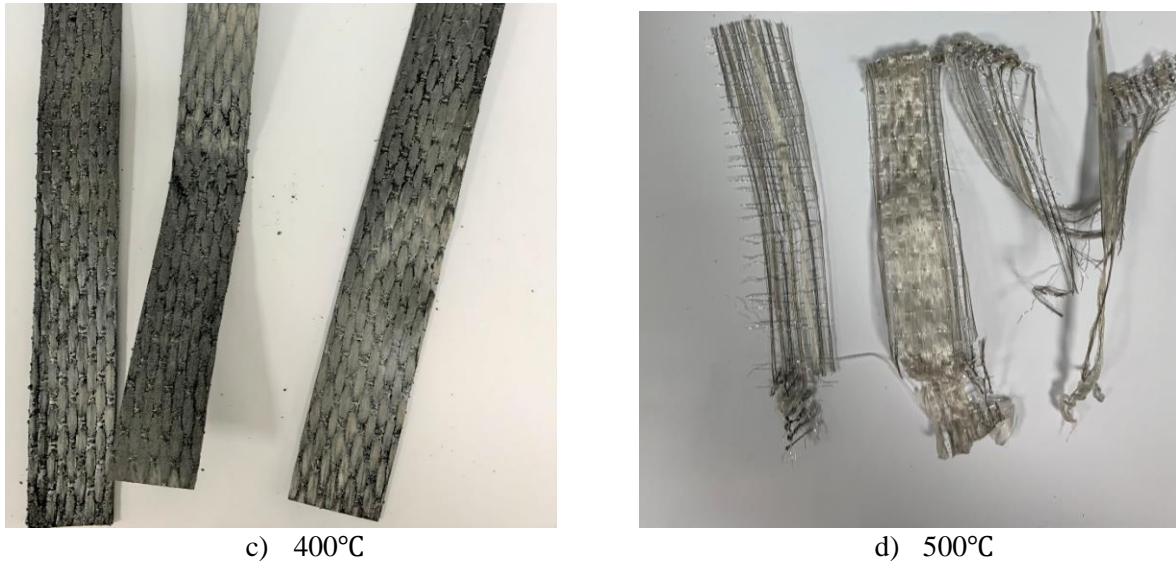
Figure 6-4: The effect of Different Thermal Exposures on the CFRP Laminates

6.3   Post-Thermal Exposure FRP Mechanical Testing

The ultimate tensile strength, the ultimate strain, and the tensile modulus of the CFRP are the most important mechanical properties for the purpose of modeling a confined column. For the purpose of this study, the only axis in which the mechanical properties are relevant is the axis parallel to the direction of the fibers. Testing was conducted in accordance with ASTM D3039 standard [69]. The length of the CFRP coupons, L, is 250 mm, the width, W, is 15 mm and thickness of the CFRP and CGRP, t_f, is 1.58 and 2.88 mm respectively. Tabs were adhered to the coupons along the grip length of the testing machine, L_g, which was determined to be 50.0 mm at each end of the test specimens. The dimensions of CFRP and CGRP specimens and the heating temperatures are summarized in Table 6-2. Strain gauges were installed in the longitudinal direction of the coupons at midspan to obtain strain readings in CFRP. Strain instrumentations were installed on opposite faces to correct errors that might result from bending of the specimens.

The specimens were tested using an Instron$^©$ 8803 machine with a constant crosshead speed of 2.0 mm/min. The Instron machine was equipped with 600 kN capacity hydraulic grip. A mechanical or pneumatic do not supply enough gripping force to avoid slippage of the coupons. The hydraulic grip applies a gripping force that is proportional to applied tensile force.

Figure 6-5: Instron Machine used for Tensile Test

The mechanical properties of the FRP can be calculated using Eq. 6-1 based on the fiber and epoxy material properties given by the manufacturer in **Table 6-1**. The modulus, E_f, the ultimate rupture strength, f_{fu}, and the ultimate rupture strain, ϵ_{fu}, of the CFRP are obtained by knowing the volume fraction of the fibers, V_f. A volume fraction of 0.32 was calculated using $2t_{carbon}/t$. A fiber volume fraction of 0.30 is typical for composite fabricated using wet layup technique.

Table 6-2: Details of the CFRP and CGRP Specimens

Material	Temperature (°C)	Sample #	Width (mm)	thickness (mm.)	Length (mm)	Tab Length (mm)	Tested Length (mm)
CFRP	23	3	14.87	1.27	250	50	150
	100	3	14.97	1.52	200	50	100
	150	3	14.53	1.53	250	50	150
	200	3	15.02	1.68	250	50	150
	250	4	14.43	1.55	250	50	150
	275	3	14.28	1.64	250	50	150
CGFRP	23	3	14.75	2.25	250	50	150
	250	3	15.38	2.74	250	50	150
	300	3	15.10	3.02	250	50	150

$$E_f = E_{carbon}V_{carbon} + E_{epoxy}(1 - V_{carbon})$$

Eq. 6-1

$$f_{fu} = f_{carbon}V_{carbon} + E_{epoxy}(1 - V_{carbon})\epsilon_{carbon}$$

6.4   FRP Tensile Test Results

6.4.1   CFRP Tensile Test Specimens

At temperatures 300 ℃ and above, specimens started to buckle. The extreme extent of the buckling made it impossible to apply tabs to the specimens. Trial specimens were tested without tabs for observation purposes. The specimens were extremely and failed the moment they were placed in the grips. The mode failure was grip failure for all specimens. Specimens heated at a temperature of 400 ℃ ignited and all resin was evaporated. All what remained was a glassy substance. Foster and Bisby [53] have also noted that the tensile elastic modulus of their CFRP specimens increased slightly by elevated temperature exposure up to 200 ℃. They also noted that one of the epoxies they tested increased in tensile strength up to exposure of 200 ℃ but experience rapid degredation at a temperature of 250 ℃. A database of the FRP coupon tension test results is presented in **Table 6-3** and **Table 6-4**

Table 6-3: CFRP coupon tension test result database

Material	Temp. (°C)	ID	Specimen ID	Max. Stress (MPa)	Max. Strain	E (MPa)	Max. Load (N)	Max. Disp. (mm.)
C	23	1	T-C-23_1	954.3	0.0130	65481	18472	1.95
		2	T-C-23_2	987.4	0.0133	53755	19324	1.99
		3	T-C-23_3	1075.6	0.0136	54614	17639	2.04
		4	T-C-23_4	868.4	0.0141	53399	20008	2.12
	100	1	T-C-100_1	768.7	0.0139	55960	18844	2.09
		2	T-C-100_2	704.1	0.0135	55890	18899	2.03
		3	T-C-100_3	680.8	0.0118	54892	15314	1.78
	150	1	T-C-150_1	801.9	0.0106	67129	13725	1.58
		2	T-C-150_2	631.1	0.0122	58537	16744	1.84
		3	T-C-150_3	611.6	0.0117	45579	16142	1.76
	200	1	T-C-200_1	673.2	0.0112	52258	14972	1.68
		2	T-C-200_2	820	0.0126	47579	17715	1.89
		3	T-C-200_3	627.1	0.0147	65481	20392	2.2
	250	1	T-C-250_1	565.8	0.0112	53755	14658	1.68
		2	T-C-250_2	777	0.0103	54614	12517	1.55
		3	T-C-250_3	653.2	0.0116	53399	16160	1.74
		4	T-C-250_4	466.8	0.0112	55960	15178	1.67
	275	1	T-C-275_1	500.7	0.0102	55890	10791	1.54
		2	T-C-275_2	471.8	0.0096	54892	11153	1.44
		3	T-C-275_3	954.3	0.0099	67129	11740	1.49

Table 6-4: **CGFRP coupon tension test result database**

Material	Temp.	ID	Specimen ID	Max. Stress (MPa)	Max. Strain	E (MPa)	Max. Load (N)	Max. Disp. (mm.)
CGCG	23	1	T-CGCG-23_1	932.6	0.0211	44204	31475	3.16
		2	T-CGCG-23_2	838.2	0.0207	40532	28502	3.10
		3	T-CGCG-23_3	998.9	0.0217	46096	31443	3.25
	250	1	T-CGCG-250_1	672	0.0197	34054	31925	2.96
		2	T-CGCG-250_2	436.1	0.0100	43561	15609	1.50
		3	T-CGCG-250_3	713.5	0.0203	35106	30924	3.05
	300	1	T-CGCG-300_1	453.5	0.0161	28241	22016	2.41
		2	T-CGCG-300_2	766.4	0.0170	45134	25177	2.55
		3	T-CGCG-300_3	559.3	0.0200	27947	31457	3.00

6.4.2   Comparison and Discussion of Tension Test Results

The summary of the FRP coupon tension test results is presented in **Table 6-5**. The average of

different mechanical properties for each temperature exposure is summarized.

Table 6-5: Summary of FRP coupon tension test results

Material	Temp. (℃)	No. of Specimen	Max. Stress (MPa)	Norm. Strength	Ave. Ult Strain	Norm. Ult. Strain	E (MPa)	Norm. E	Strength CV	Strain CV	E CV
C	23	4	1005.77	1.000	0.0135	1.00	73458	1.000	5.5	3.5	3
	100	3	780.4	0.776	0.0131	0.97	59543	0.811	11.6	8.5	1
	150	3	704.6	0.701	0.0115	0.85	61231	0.834	10.3	7.1	2.8
	200	4	701.6	0.698	0.0127	0.94	54658	0.744	13.5	11.5	3.9
	250	4	655.78	0.652	0.0111	0.82	59112	0.805	10.5	5	10.4
	275	3	479.77	0.477	0.0099	0.73	48472	0.66	4.3	3	6.3
CGCG	23	3	923.23	1	0.0212	1.00	39685	1.00	5.6	2.4	2.7
	250	3	607.2	0.658	0.0167	0.79	42261	1.07	35	34.7	6.6
	300	3	593.07	0.642	0.0177	0.84	38632	0.97	18.3	11.5	4.9

As can be seen in **Table 6-5**, the general trend is that the strength of the FRP coupons is reduced

after being exposed to an elevated temperature. However, the residual strength is recovered from

a temperature of 150℃ to 200 ℃. This is a phenomonon that is also present in FRP-confined

specimens as will be discussed in the relevant sections. It is also interesting to note that the

coefficient of variance for the average ultimate strength increase with an increasing temperature

before decreasing again at temperatures above 250 ℃. That is also when we see the largest

reduction in strength for the CFRP specimens. One thing that can be seen is that the hybrid

CGFRP composite coupons maintained their strength even after an exposure temperature of

300℃. This shows that the carbon and glass hybrid composite can have promise in the future.

6.5 FRP Single-Lap Shear (SLS) Test Results

A summary of the SLS test results is presented in **Table 6-8**. It appears that an increase in overlap length leads a smaller reduction in shear strength. This can be seen strength vs. temperature charts for CFRP-40 and CFRP-70 specimens in **Figure *6-4***. It is important to note that the CFRP-40 shear strength increased after being exposed to a temperature of 100 ℃ more than CFRP-70. This could be due the high variance for the room temperature cured specimens which led to an unreliable benchmark reading. Another possible reason could be due to the overlap length being insufficient and that exposure to elevated temperature had some post-curing effect that made a large difference in the shear strength.

Table 6-6: CFRP coupon single-lap-shear test result database

Material	Overlap (mm.)	Temp. (℃)	ID	Specimen ID	Shear Strength (N/mm)	Max. Strain	Max. Load (N)	Max. Deformation (mm.)
C	40	23	1	SLS-C-40-23_1	1017.3	0.0093	30518	1.95
			2	SLS-C-40-23_2	1045.6	0.0090	31368	1.88
			3	SLS-C-40-23_3	684.4	0.0064	20531	1.35
		100	1	SLS-C-40-100_1	1109.1	0.0108	33273	2.26
			2	SLS-C-40-100_2	1234.8	0.0105	37044	2.22
			3	SLS-C-40-100_3	1172.2	0.0108	35166	2.27
		200	1	SLS-C-40-200_1	1136.8	0.0106	34103	2.23
			2	SLS-C-40-200_2	1034.7	0.0091	31040	1.91
			3	SLS-C-40-200_3	1076.1	0.0100	32283	2.09
		250	1	SLS-C-40-250_1	653.1	0.0055	19594	1.15
			2	SLS-C-40-250_2	918.0	0.0077	27541	1.62
			3	SLS-C-40-250_3	803.8	0.0070	24113	1.47
	70	23	1	SLS-C-70-23_1	1327.3	0.0117	39819	2.46

|		2	SLS-C-70-23_2	880.4	0.0082	26411	1.72
		3	SLS-C-70-23_3	1068.2	0.0099	32047	2.07
	200	1	SLS-C-70-200_1	1191.8	0.0121	35753	2.54
		2	SLS-C-70-200_2	1286.0	0.0115	38579	2.42
		3	SLS-C-70-200_3	1220.0	0.0115	36600	2.41
	250	1	SLS-C-70-250_1	1164.3	0.0102	34930	2.14
		2	SLS-C-70-250_2	1091.1	0.0102	32734	2.14
		3	SLS-C-70-250_3	1159.8	0.0105	34794	2.21

Table 6-7: CGFRP coupon single-lap-shear test result database

Material	Overlap (mm.)	Temp. (°C)	ID	Specimen ID	Shear Strength (N/mm)	Max. Strain	Max. Load (N)	Max. Deformation (mm.)
CGCG	70	23	1	SLS-CGCG-70-23_1	1281.5	0.0112	38446	2.35
			2	SLS-CGCG-70-23_2	1403.4	0.0137	42103	2.88
			3	SLS-CGCG-70-23_3	1500.2	0.0135	45005	2.84
		250	1	SLS-CGCG-70-250_1	1442.6	0.0135	43277	2.83
			2	SLS-CGCG-70-250_2	1418.5	0.0135	42556	2.82
			3	SLS-CGCG-70-250_3	1234.3	0.0115	37028	2.42
		300	1	SLS-CGCG-70-300_1	918.9	0.0079	27567	1.66
			2	SLS-CGCG-70-300_2	1156.6	0.0105	34697	2.2
			3	SLS-CGCG-70-300_3	938.9	0.0078	28168	1.63

Table 6-8: Summary of FRP coupon single-lap-shear test results

Material	Overlap (mm.)	Temp	No. of Specimen	Ave. Shear Strength (N/mm)	Norm. Strength	Ave. Ult. Strain	Norm. Ult. Strain	Ave. E (MPa)	Norm. E	Strength CV	Strain CV	E CV
C	40	23	3	915.7	1.00	0.0082	1.00	1747.3	1.00	21.9	19.4	6.4
		100	3	1172.0	1.28	0.0107	1.31	1771.8	1.01	5.4	1.6	5.1
		200	3	1082.5	1.18	0.0099	1.21	1790.0	1.02	4.7	7.6	1.5
		250	3	791.7	0.86	0.0067	0.82	1725.4	0.99	16.8	16.7	1.8
	70	23	3	1092.0	1.00	0.0099	1.00	1598.2	1.00	20.6	17.6	4.8
		200	3	1232.6	1.13	0.0117	1.18	1653.4	1.04	3.9	3	2.2
		250	3	1138.4	1.04	0.0103	1.04	1685.9	1.06	3.6	1.7	4.2
CGCG	70	23	3	1395.1	1.00	0.0128	1.00	1834.2	1.00	7.9	10.9	6.2
		250	3	1365.1	0.98	0.0128	1.00	1764.4	0.96	8.3	9	1.8
		300	3	1004.8	0.72	0.0087	0.68	1804.2	0.98	13.1	17.5	4.8
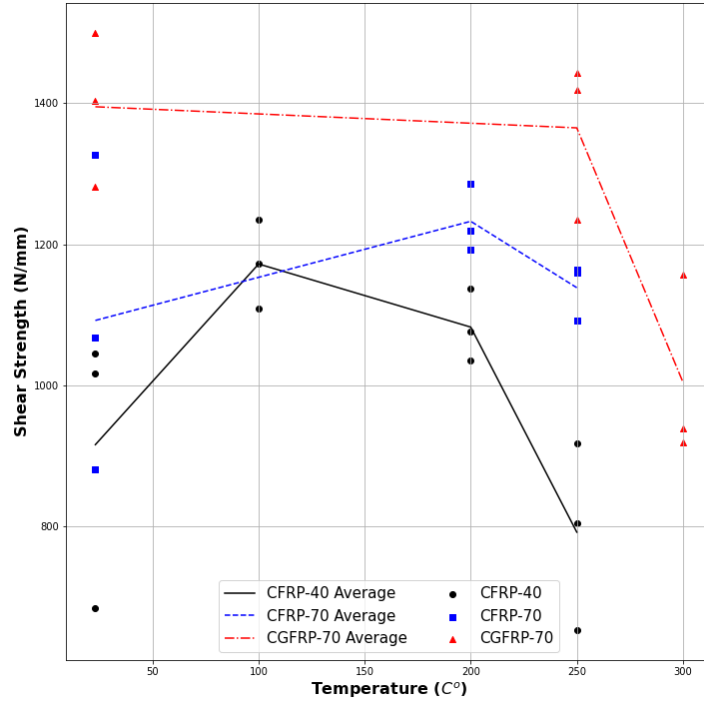
Figure 6-6: Effect of Elevated Temperature Exposure on the SLS Strength of FRP coupons.

Chapter 7   FRP-CONFINED RC COLUMNS EXPERIMENTS

7.1   Overview

Design and analytical procedures for predicting the behavior of concrete at elevated temperatures are well established [15,37,39,71]. For this reason, extensive fire testing on unconfined concrete is not needed.

In the system-based phase of the experimental study, a total of 9 medium-size circular columns specimens were as tested described in **Table *7-1***. The columns were subjected to elevated temperatures for a specified period, after which, the exposed column specimens were allowed to cool down to lab temperature. Axial monotonic testing was then be performed on the fire-damaged column using a universal testing machine to determine the mechanical behavior. The data that was gathered from the experimental program was used to develop models that can assist in predicting the post-fire behavior of FRP-confined columns.

Table 7-1: Column Test Matrix

Material	Specimens	Temp.
AS	1	23
AS	1	300
AS	1	400
C2G2	1	23
C2G2	1	300
CGCG	1	300
C2	1	23
C2	1	300
C2	1	400

As stated earlier, the focus will be on the behavior of circular reinforced concrete columns with CFRP composite and CGFRP hybrid composite jackets. The columns were exposed to the temperatures mentioned in **Table *7-1***.

7.2   Column Fabrication

The reinforced concrete circular columns were fabricated on 06/15/2021. The dimensions and reinforcement details of the columns are presented in **Table 7-2**.

Table 7-2: Specimen details of reinforced concrete columns

Height	1000 mm.
Diameter	180 mm.
Vertical Reinforcement	$8_\varphi 12$
reinforcement ratio, φ	3.55%
Ties	10mm. @150mm.

a) Thermocouple location in the center of the column

b) Casting of RC Columns

c) Applying a primer epoxy coating on the concrete specimens

c) Impregnating the carbon fiber sheet with the epoxy matrix

d) Rolling the carbon fiber fabric on the column specimen (top half)

d) Rolling the carbon fiber fabric on the column specimen (bottom half)

Figure 7-1: Fabrication of Column Specimens and FRP application method

7.3 Column Thermal Exposure Protocol

The heated columns were placed in the oven at room temperature and the was then turned on and left to heat up to the testing temperature. Once the temperature is then maintained for 90 minutes before shutting off the oven and opening the oven door. The columns were left to cool down to room temperature before being removed.

Thermal couples were installed in different locations within the columns to record temperatures within the column cross-section during the standard fire. The temperature within the FRP is of most importance in this experiment. Therefore, the most important thermal couple locations are in the insulation-FRP interface and the FRP/concrete Interface.

## 7.4 Post-Thermal Exposure Axial Column Compressive Test Procedure

The columns were tested under axial compression in a universal testing machine at a displacement-controlled rate of 0.5 mm/sec. Two LVDTs was used to measure vertical deflection over 1/3 of the column height which is 300mm. The LVDTs were mounted at midspan 180 degrees apart from each other. Additionally, each column was instrumented with 7 lateral strain gauges to measure hoop strains. 2 strain gauges were placed 150 mm from the top 180 degree apart. 3 strain gauges were placed at mid higher approximately 120-degrees apart from each other. The last two strain gauges we're located 150 mm from the bottom and placed 180-degrees apart from each other. The top and bottom strain gauges were placed there to measure if there is a difference in column dilation across the height of column.

7.5 Column Test Results

9 columns were tested under monotonic axial compression. The C2G2 hybrid composite column exhibited superior strength, stiffness, and energy absorption compared to the plain carbon composite columns after being exposed to an elevated temperature. Columns Col-C2-23, Col-C2-400, and Col-C2G2-23 all failed prematurely due to stress concentrations near the point of load application. Therefore, only the stiffness of the columns can be calculated.
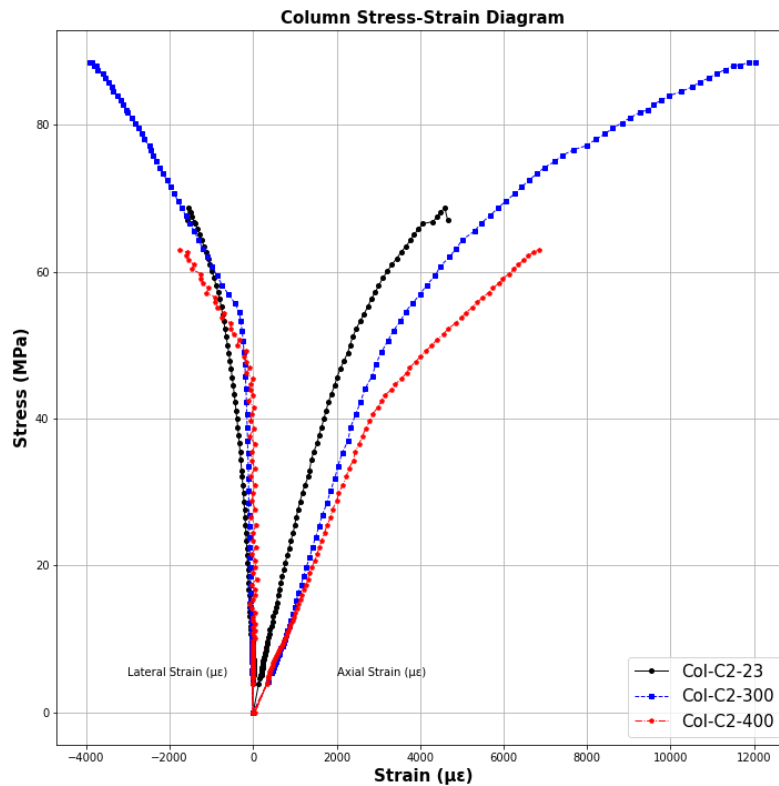
7.5.1 As-built concrete columns

The stress-strain diagram for the as-built columns is presented in **Figure *7-1***. All readings except for the last 100 readings were filter down to 100 readings. The last 100 readings at a rate 10 Hz were plotted without filtering.
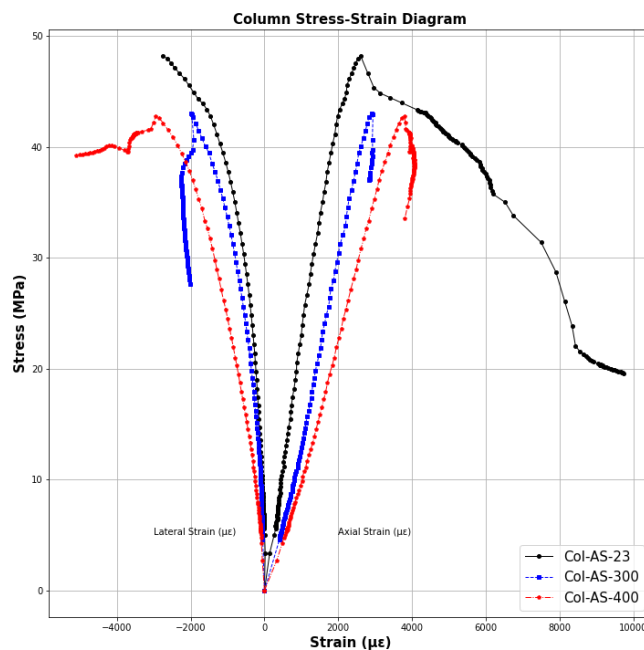
Figure 7-2: Stress-strain diagram for as-built columns after being exposed to different temperatures.

### 7.5.2   CFRP-confined concrete columns

The stress-strain diagram for the control and heated CFRP-confined columns is presented in **Figure 7-2**. All readings were filtered down to 100 readings. There were no sudden changes in the behavior of the columns before failure.

Figure 7-3: Stress-strain diagram for CFRP-confined columns after being exposed to different temperatures.

7.5.3   CGFRP-confined concrete columns

The stress-strain diagram for the control and heated CGFRP-confined columns is presented in **Figure 7-3**. All the readings except for the last 500 were filtered down to 100 readings. The last 500 readings at a rate 10 Hz were plotted without filtering.
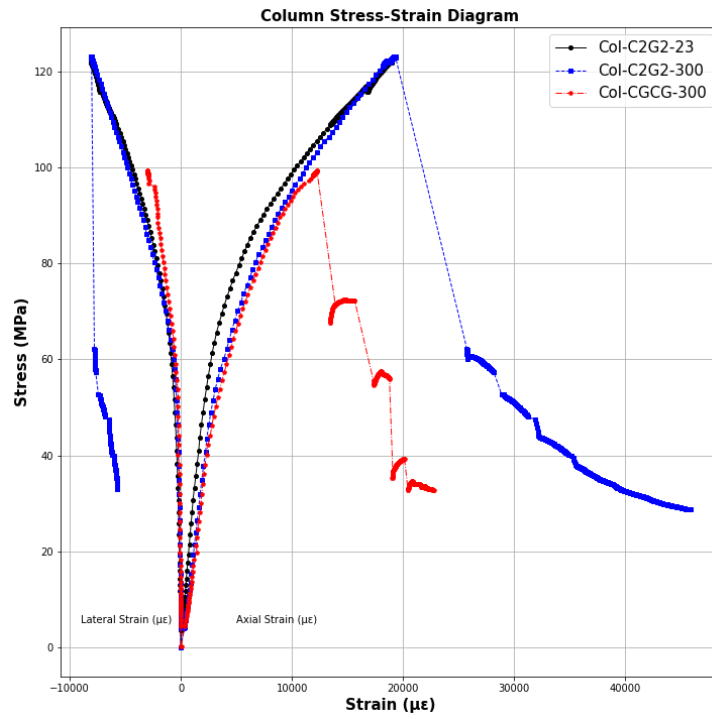
Figure 7-4: Stress-strain diagram for CGFRP-confined columns after being exposed to different temperatures.

Chapter 8   DESIGN PROCEDURE

The post-thermal exposure behavior of the FRP-confined column varies depending on the type of

fiber and polymer used. Even within the epoxy polymer subclass, there is a great deal of variation

in the residual behavior. This is especially true in the temperature region 23-200℃. No significant

variations occur in both compressive strength and ultimate strain when different sizes of FRP-

confined concrete specimens were used [72].

8.1   Prediction of Tensile Strength of FRP Composites Post-Thermal Exposure

The prediction models for longitudinal tensile strength and elastic modulus are presented in **Table

8-1**. The fit of the tensile strength model and elastic modulus model are on the experimental

results are presented in **Figure 8-1** and **Figure 8-2** respectively.

Table 8-1: *Residual On-Axis Mechanical Properties of CFRP laminates*

Ultimate Strength	$1.175 - 0.0086T + 0.00055T^2 - 1.211T^3 \times 10^{-7}$ for $23 \leq T \leq 300$
Elastic Modulus	$1.12 - 0.0063T + 4.356T^2 \times 10^{-5} - 8.426T^3 \times 10^{-8}$ for $23 \leq T \leq 300$
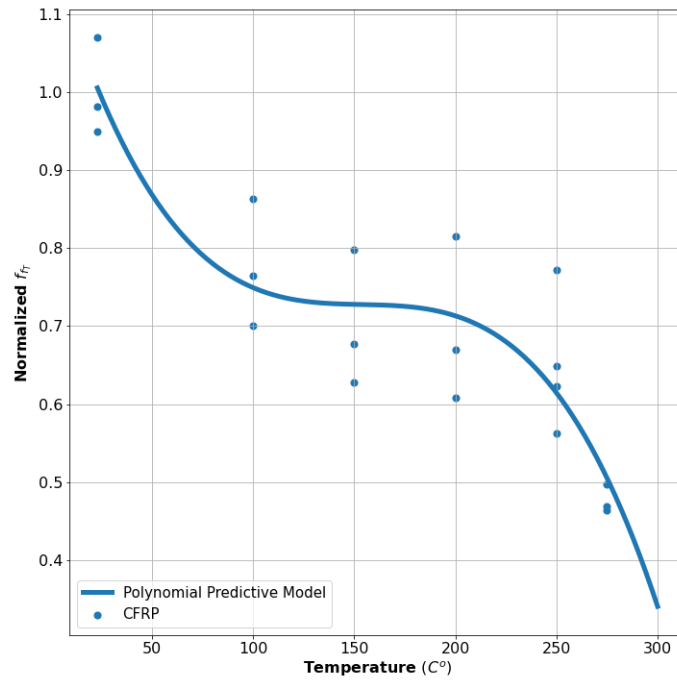
Figure 8-1: *CFRP Composite Residual On-Axis Tensile Strength*
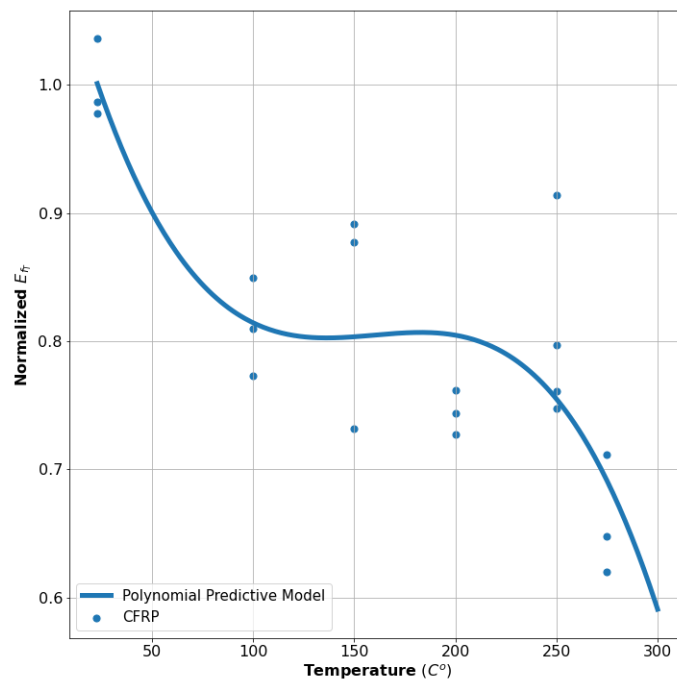
***Figure 8-2:*** *CFRP Composite Residual On-Axis Elastic Modulus*

8.2 Prediction of Compressive Strength of FRP-Confined Concrete Post-Thermal Exposure

The experimental results presented in Chapter 4 were used to develop modification of the Youssef et al. model [34]. A reduction factor, ψ_T, for the confined compressive strength of FRP-confined concrete was determined based on the formulation in Eq. 8-1 and Eq. 8-2. Two different formulations were considered for the reduction factor. The first one is trilinear model where the strength of the specimens is considered constant up to a specific temperature, T_0, after which there is a linear degradation of the material until it reached zero at temperature T_1. This formulation is presented in Eq. 8-3. A predictive model was via a for loop using the statistics library in Python to obtain the T_0 and T_1 that provide the highest R^2 value. Additionally, a conservative design model was developed. The values to T_0 and T_1 were chosen based on observations of the post-heated behavior of different FRP strengthening schemes. The parameters for both the predictive and the design model are presented in **Table 8-2**. Additionally, the tanh model proposed by Bisby and Nguyen was also modified. The formulation of the tanh model is presented in Eq. 8-4 and the parameters are presented in **Table 8-3**

$$\frac{f'_{cc_T}}{f'_{c_T}} = 1 + \beta\psi_T \left(\frac{f'_l}{f'_{c_T}}\right)^\lambda \qquad \textit{Eq. 8-1}$$

$$\frac{f'_{cu}}{f'_{c_T}} = 1 + 2.25\psi_T \left(\frac{f'_{lu}}{f'_{c_T}}\right)^{1.25} \qquad \textit{Eq. 8-2}$$

$$\psi_T = \begin{cases} 1 & ; for\ T < T_0 \\ 1 - \dfrac{T - T_0}{T_1 - T_0} & ; for\ T_0 \leq T \leq T_1 \\ 0 & ; for\ T > T_1 \end{cases} \qquad \textit{Eq. 8-3}$$
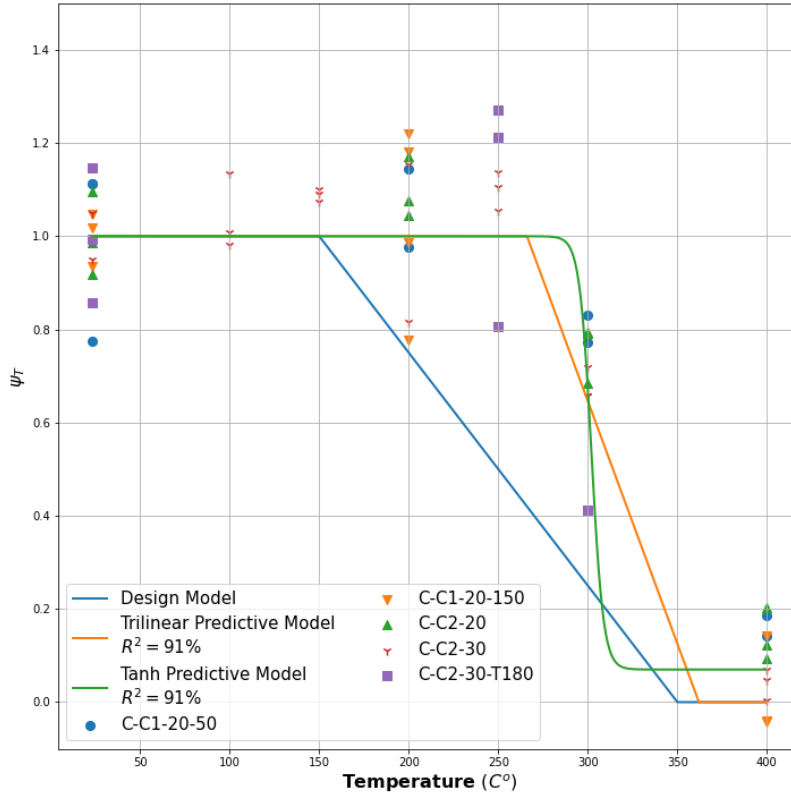
Figure 8-3: *Summary of Reduction Factors for CFRP-Confined Specimens*

Table 8-2: *Parameters for Predictive and Design Models*

Confining Material	Model Type	T_o	T_1
CFRP	Predictive Model	266	362
	Design Model	150	350

$$\psi_T = \left(\frac{1-a}{2}\right)\tanh[-b(T-c)] + \left(\frac{1+a}{2}\right) \qquad \text{Eq. 8-4}$$

Table 8-3: Input Parameters for tanh Predictive Model

	a	b	c	R^2
ψ_T	0.07	0.015	302	91%

Chapter 9   HEAT TRASNFER FE SIMULATION

9.1   Objectives

The goal of the heat transfer simulation is two-fold. One goal to demonstrate the difference in the exposure temperature of FRP with varying insulation thicknesses. This is done to validate the thermocouple readings presented in earlier chapters. The second goal is retrieving the maximum temperature at different points in the column section. This information will be used to adjust the mechanical properties of the column in the Opensees® model in Chapter 10.

9.2   Column Parameters

The dimensions of the simulated columns are identical to the large-scale columns presented in Chapter 7. The columns have a height of 1000mm. and a diameter 190mm with a cover of 20mm. measure to the centerline of the steel stirrups. The steel reinforcement was found to have no effect on the heat transfer and were therefore omitted from the simulation to decrease simulation time.

The columns were simulated with and without FRP confinement (Models TM-1 and TM-2 respectively).

Thermal Model ID	FRP Thickness, t_f (mm.)	Insulation Thickness, t_{in} (mm.)
TM-1	3	0
TM-2	3	30
TM-3	3	45
TM-4	3	60

9.3   Thermal Properties and Meshing of Materials

The thermal properties used in this simulation are the same that were presented in Section 2.2. The insulation used in the simulation was Sikacrete™ 213F. Masoud (2013) provided the temperature dependent properties of insulative material [73].

*Figure 9-1:* Nonlinear Thermal Properties of Sikacrete 213F

Temp	K (W/m-°C)	C (J/Kg-°C)	Density kg/m3
23	0.32	1585.02	700
50	0.31	1556.54	700
75	0.31	1532.12	700
100	0.30	1509.56	700
200	0.30	1438.04	700
300	0.30	1396.44	700
400	0.31	1384.76	700
500	0.33	1403.00	700
600	0.36	1451.16	700
700	0.40	1529.24	700
800	0.45	1637.24	700
900	0.50	1775.16	700
1,000	0.57	1943.00	700
1,100	0.65	2140.76	700

Different mesh sizes were used depending on the geometry of the material. For example, the FRP confinement sizing was set to 3.0 mm. compared to the concrete which was set to 20.0 mm.

9.4   Thermal Exposure Protocol

Two different thermal exposure protocols were established and are denoted as A and B. Each thermal exposure protocol was implemented by subject the outermost face of the structural

element to radiation. The initial condition was made to be 23℃ ambient conditions. The Thermal

Exposure
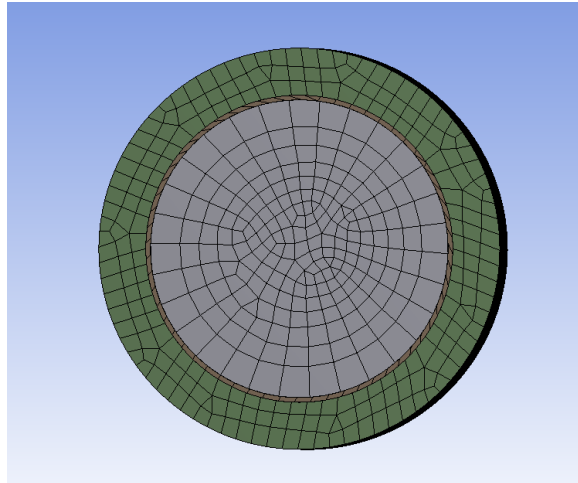
Figure 9-2: Finite Element Mesh on the Insulated Column t_{in}=30mm

Protocol A corresponds to ASTM E119 standard fire with a maximum temperature of above

1052 ℃. The protocol was divided into 7 steps with each step having a unique rate of temperature

rise. The slope of the inverse slope of the temperature-time chart was used determine the initial

time step for the simulation for this particular step so that each time step corresponds to a rise of

1℃. A summary of the time, temperature, and initial time step at each step is presented in **Table**

9-1.

Table 9-1: Temperature variation during Thermal Exposure Protocol A

Step	Time, sec.	Temperature, ℃	Initial Time Step, sec.
1	300	538	0.5
2	600	704	2
3	900	760	5
4	3600	927	15
5	6000	991	30
6	7200	1010	60
7	10800	1052	90

Thermal Exposure Protocol (***B***) has a maximum temperature of 300℃. This temperature was established as the maximum allowable temperature that can be experienced by the FRP for it to retain any considerable mechanical properties.

9.5 Model Validation

A fire test conducted by Chowdhury et al. [64] was used as a reference to validate the model. The uninsulated circular CFRP-confined RC column was subjected to an ASTM E119 standard fire for a duration of 180 minutes. The column had a height of 3,734 mm. and a cross-sectional diameter of 400 mm. The column was reinforced with 8 Ø19.5 mm longitudinal rebars and was fabricated with siliceous aggregate. Temperature readings were recorded using thermocouples at a distance of 0.0 mm., 50.0 mm., 100.0 mm., and 150.0 mm. away from the face of the concrete. The meshing utilized in the heat transfer model is presented in ***Figure 9-3***. Results from the fire test experiments [64] are compared to the heat transfer model predictions in Figure **9-4**. The temperature profile obtained from the simulation is presented in **Figure** *9-4*.
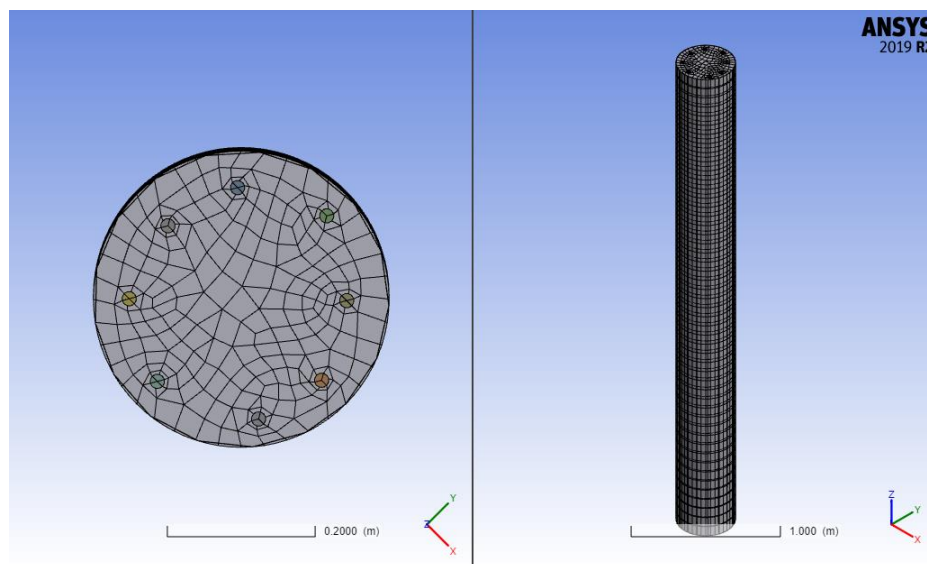
Figure 9-3: Mesh Used in the Heat Transfer Model
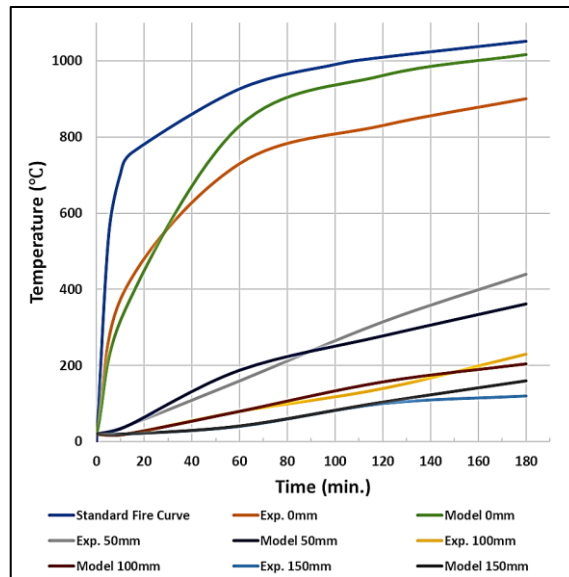
Figure 9-4: Heat Transfer Model Comparison to Results of Fire Experiment

There appears to be a slight differences between the model prediction and measured temperatures in the column though the time-temperatures plots follow the same trend. Chowdhury et al. [64] faced similar issues with their numerical heat transfer model predictions for the uninsulated column. They attributed the discrepancy to the ignition of the FRP wrapping and due to the spalling of the concrete. Their numerical model did agree well with the insulated column that they tested which did not face the same issues. Another explanation is that the furnace temperature did not follow the standard fire curve exactly. This is due to thermal energy absorption by the column dropping the temperature of the furnace in each time incriment.

9.6   Results of Heat Transfer Simulation

Comparison of the temperature variation along the cross section of models was measured at the final time-step to assess the effect to the thermal insulation. The readings start at outer face of the concrete (0 mm.) and end at the center of the concrete cross section (0.95 mm.). The comparison

is presented in **Figure 9-5**. Additionally, the temperature versus time curve was obtained for all the simulated models. The location of the measure temperatures is the FRP surface, concrete surface (0 mm.), location of stirrups (20 mm.), half way between the stirrups and the center of point of the cross-section (57.5), and at the center point off the cross-section (95.0 mm.). The results for the time-temperature curves are presented in *Figure 9-6.*
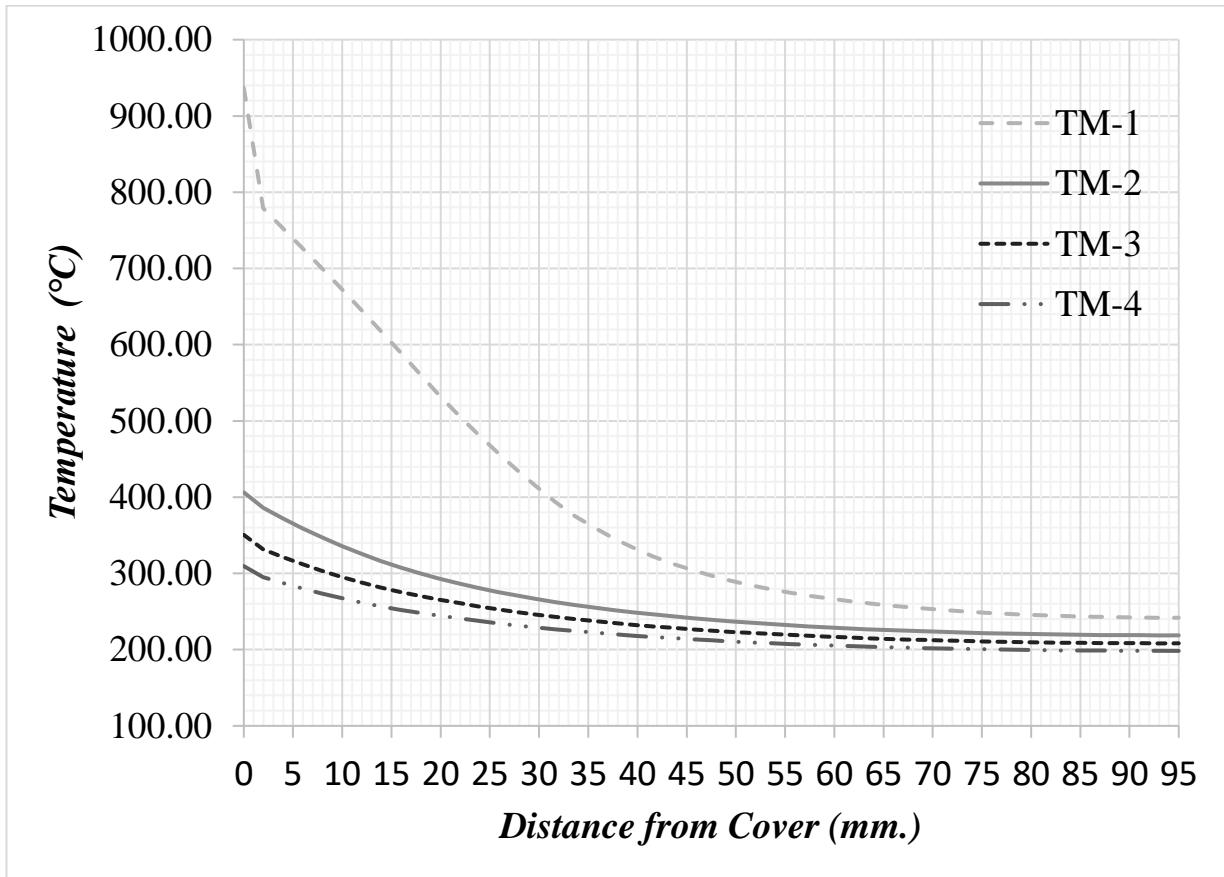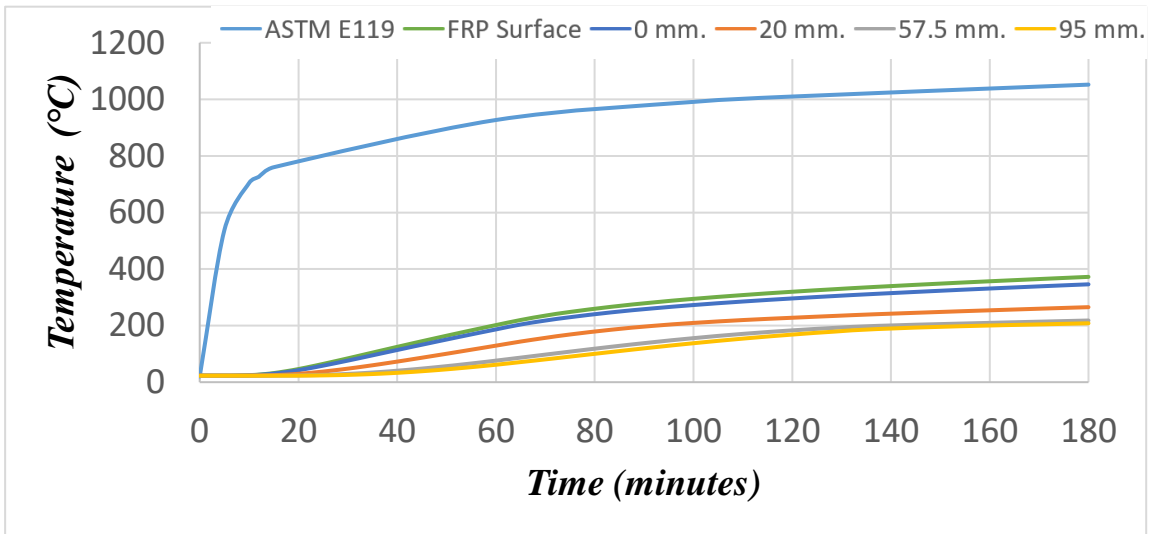

Figure 9-5: Temperature Variation Across the Concrete Column for the Models with Varying Thicknesses of Fire Protection
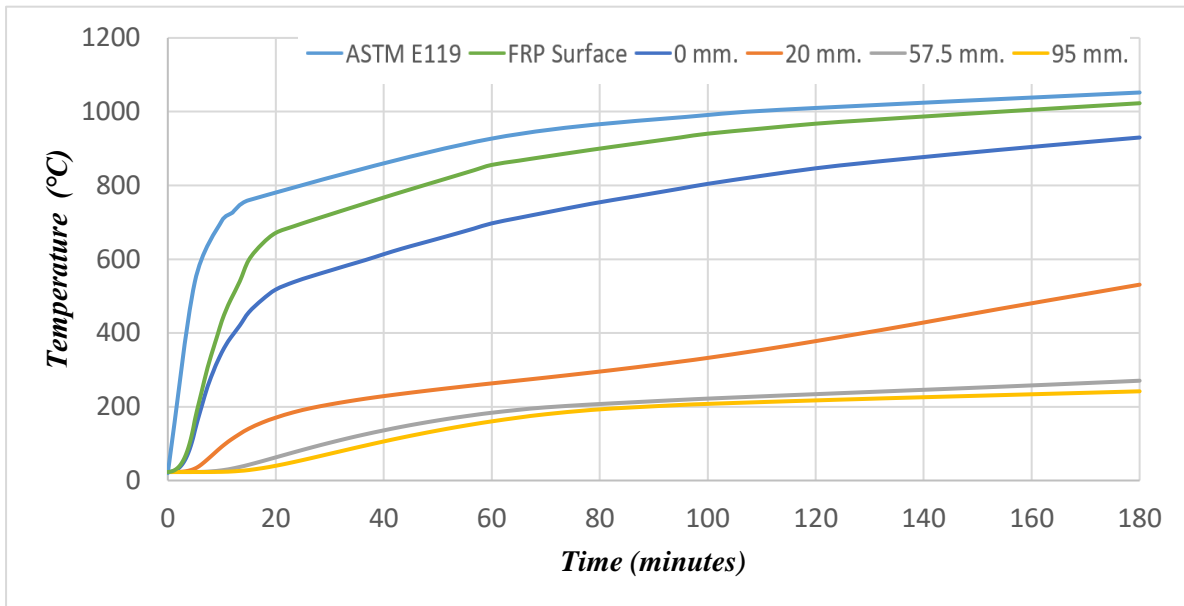
a) TM-1
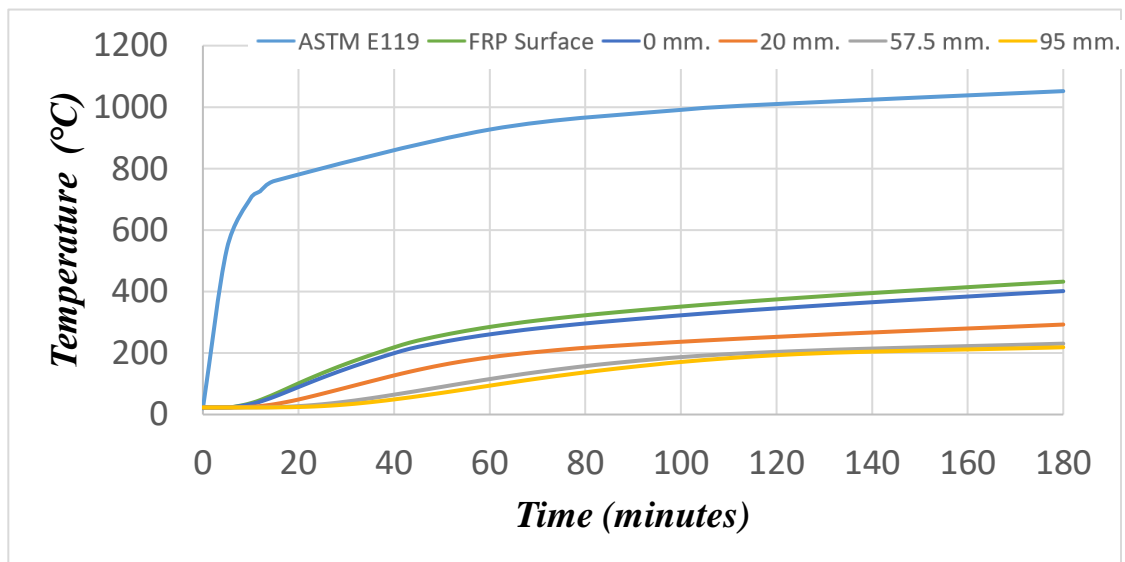
b) TM-2

c) TM-3
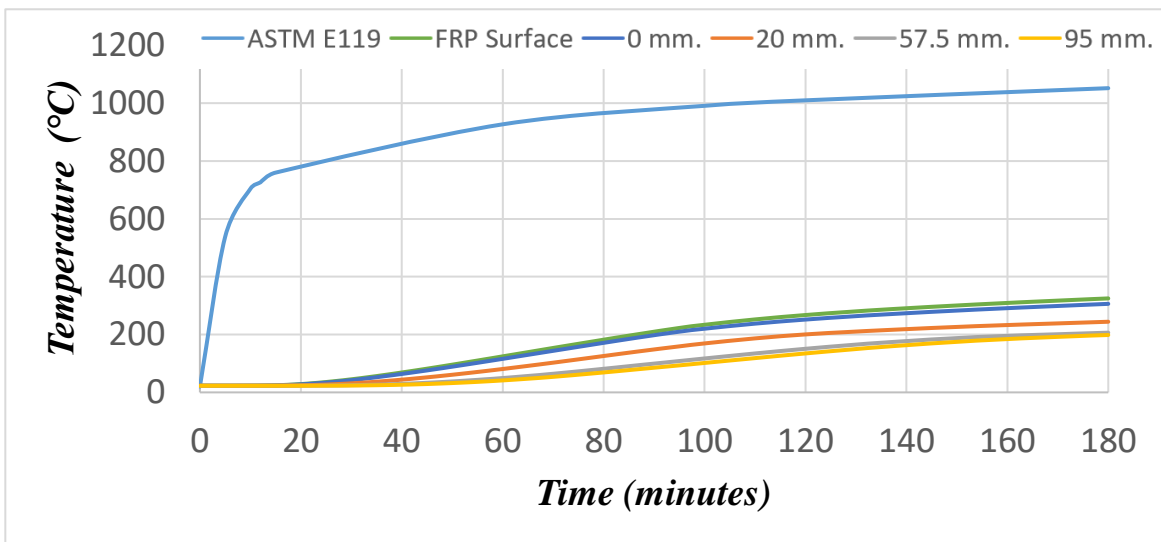
d) TM-4

Figure 9-6: Time-Temperature Curves for the Simulated Models: at different location across the cross section
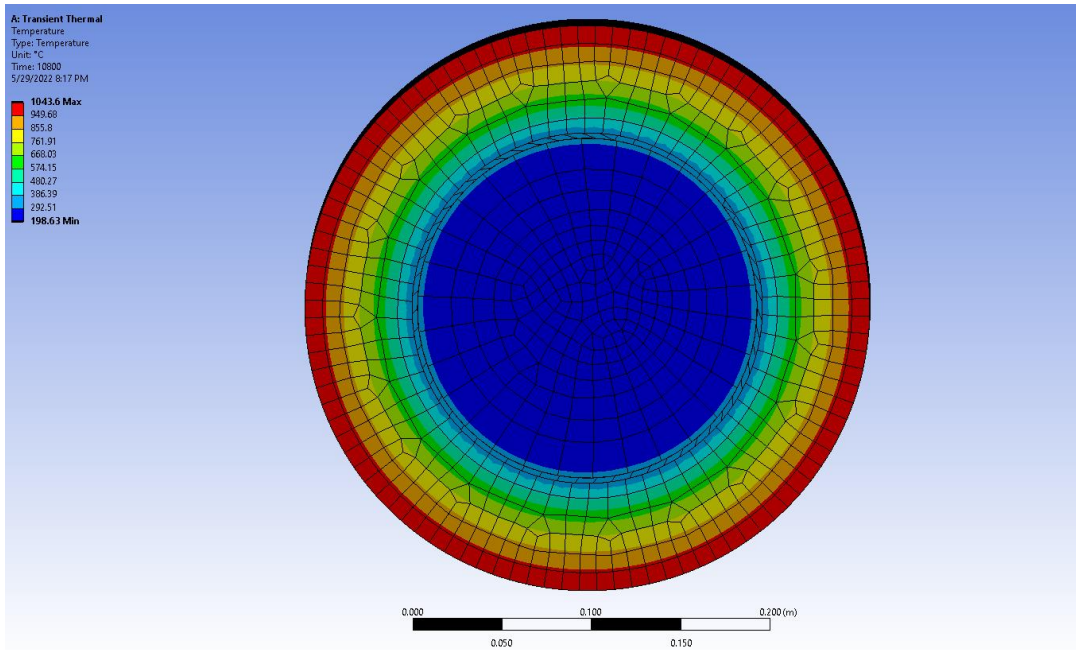
Figure 9-7: Temperature Variation of the Simulated Member with 60 mm. Insulation Thickness (TM-4)

Chapter 10 FRP-CONFIEND RC COLUMN SIMULATION

Opensees® was used to simulate the behavior of the heat damaged reinforced concreted columns. The simulation was conducted on as-built and FRP-confined columns. Two different schemes of the FRP reinforcement were utilized. The effect of thermal exposure on the behavior was simulated and the results were compared.

10.1 Opensees Model Formulation

A 2-node 2-D model was used to simulate the columns. The bottom of the column (node 1) was fixed in 3 degrees of freedom. Both the axial loads and lateral loads were applied to node 2. A fiber section was used to model the cross-sectional stress-strain behavior of the columns. The *dispBeamColumn* element was chosen for both the monotonic and cyclic lateral analysis methods. The material model used to simulate the column was Concrete02 for ss-built concrete columns and FRPConfiendConcrete02 for the FRP-confined columns.

10.2 RC Column Monotonic Axial Simulation

Elsanadedy et al. [72] found that there are no significant size effects with FRP-confined concrete while Jamatia and Deb [74] found that size effects occurs due to inclined cracking near the end restraints. Numerous Studies have found that the envelope of the compression cyclic response of FRP-confined reinforced concrete columns is the same as compression stress-strain response of FRP-confined columns under monotonic axial loading. [74, 75, 76]. Therefore, the axial response of the experimental specimens was used to calibrate the Opensees model that will be used in lateral cyclic loading. First, the experimental results of small-scale FRP-confined specimens were

compared to Opensees simulated results and the modified Youssef et al. model that was introduced in Chapter 8. FRP-confined concrete specimens are presented in **Error! Reference source not found.**. Then, the monotonic axial simulation of reinforced concrete column that are presented in **Error! Reference source not found.**. The results of the column simulation are conservative when it comes to maximum load level but overestimate the maximum displacement. However, the overestimation is very small and can be attributed to modeling of the steel reinfrocement since the error also occurs in the as-built columns.
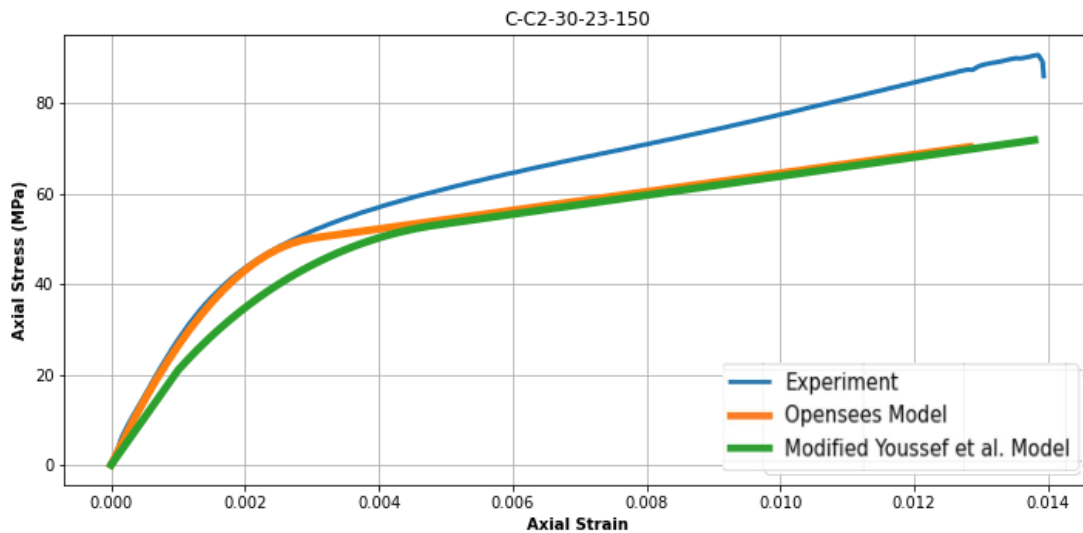
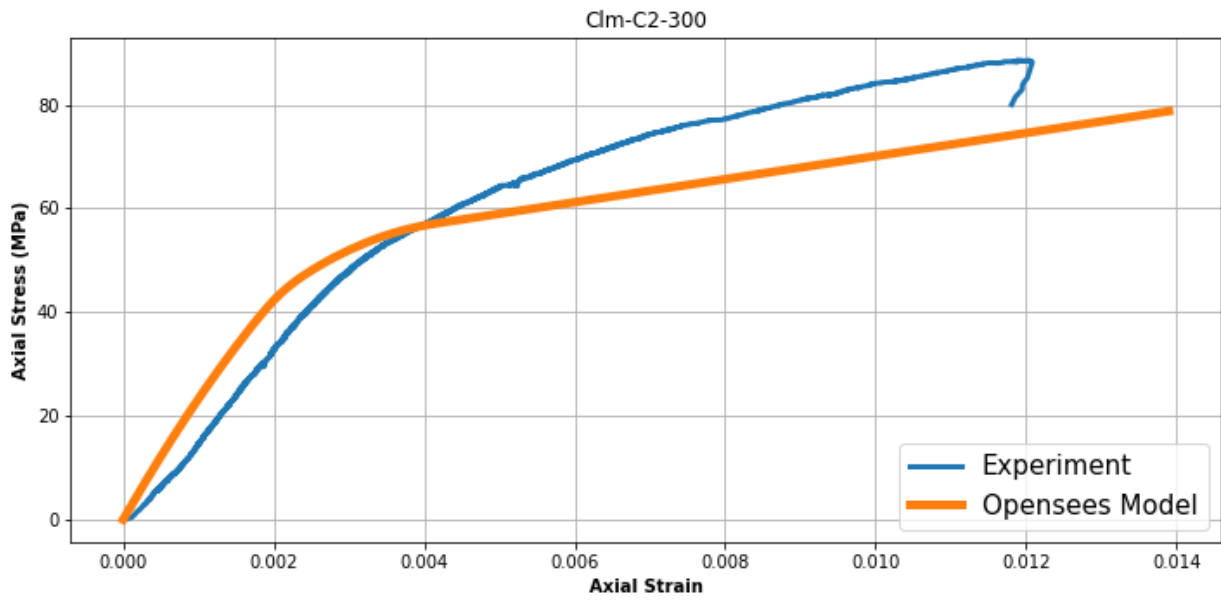a) CFRP-confined specimen (room temeprature)
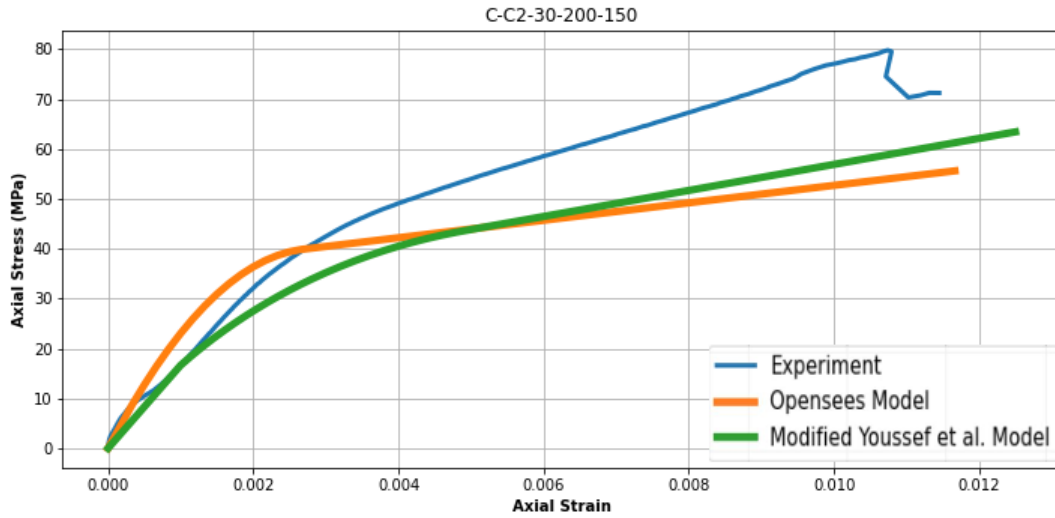
b) CFRP-confined specimen (200 ℃)

Figure 10-1*:* Axial loading simulation of FRP-confined concrete and validation of the modified Youssef et al. model [5].
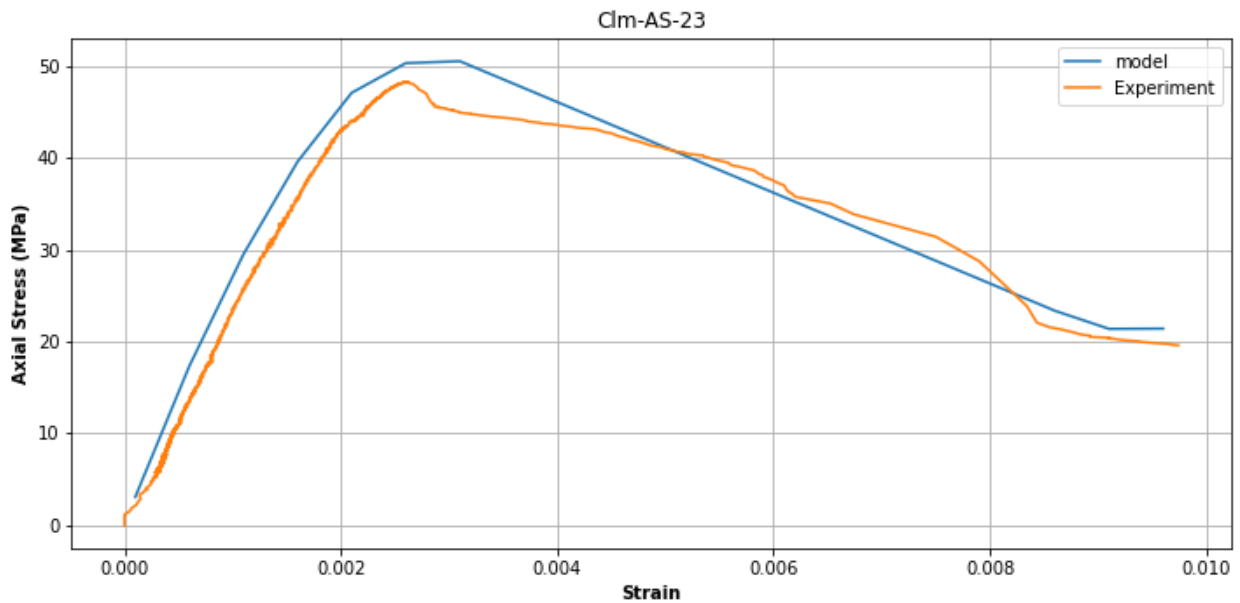
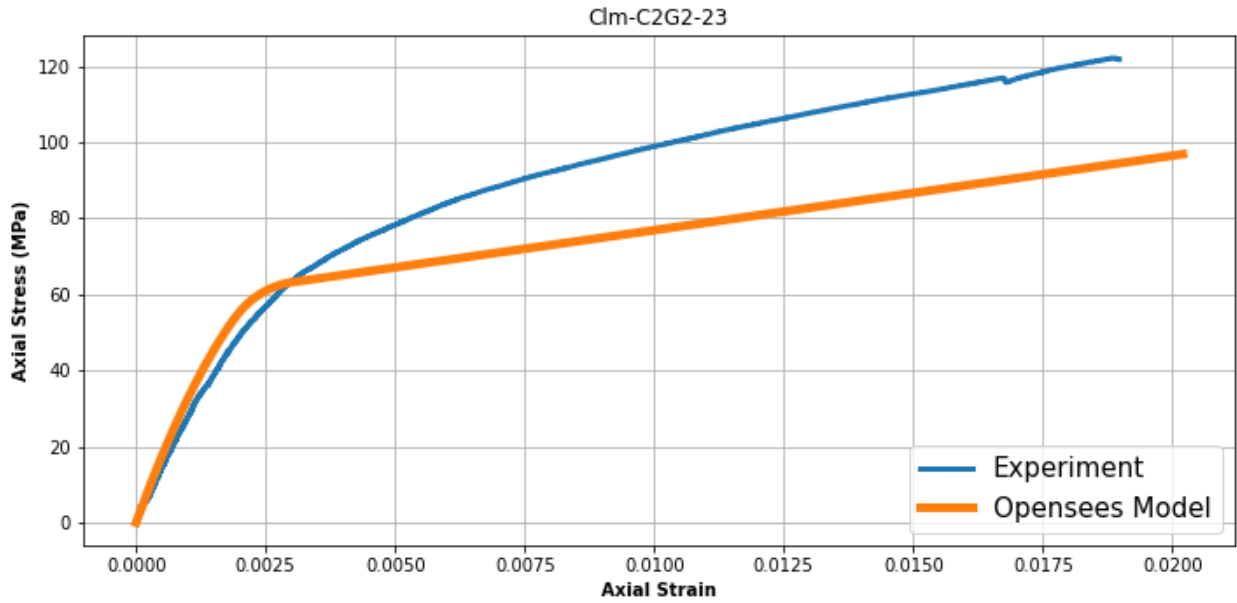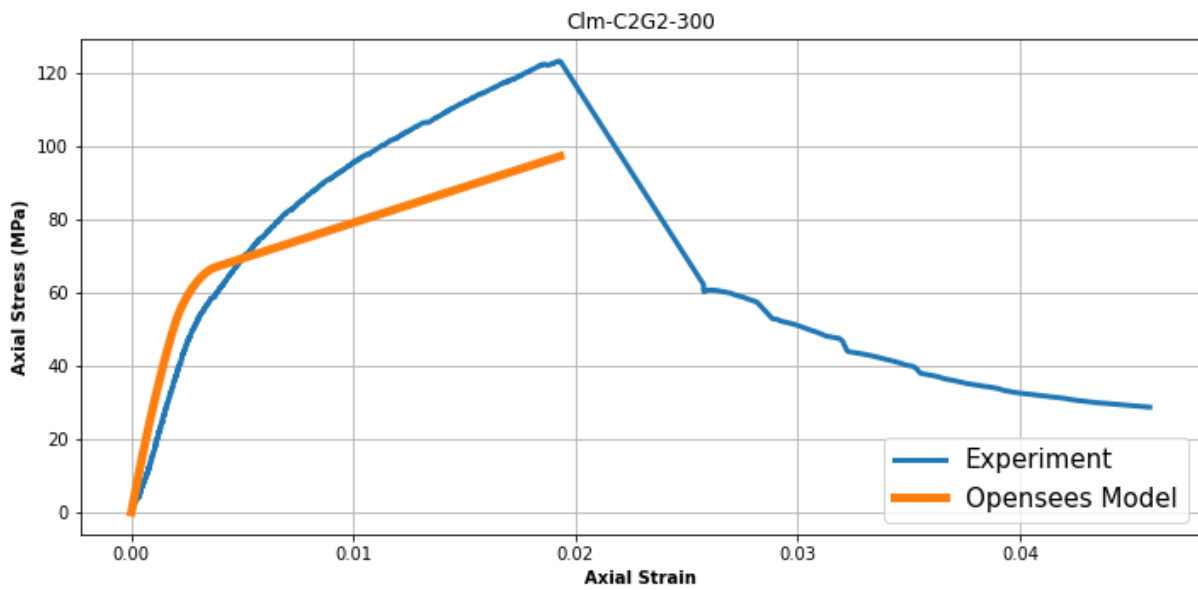

a) As-built concrete columns (room temperature)
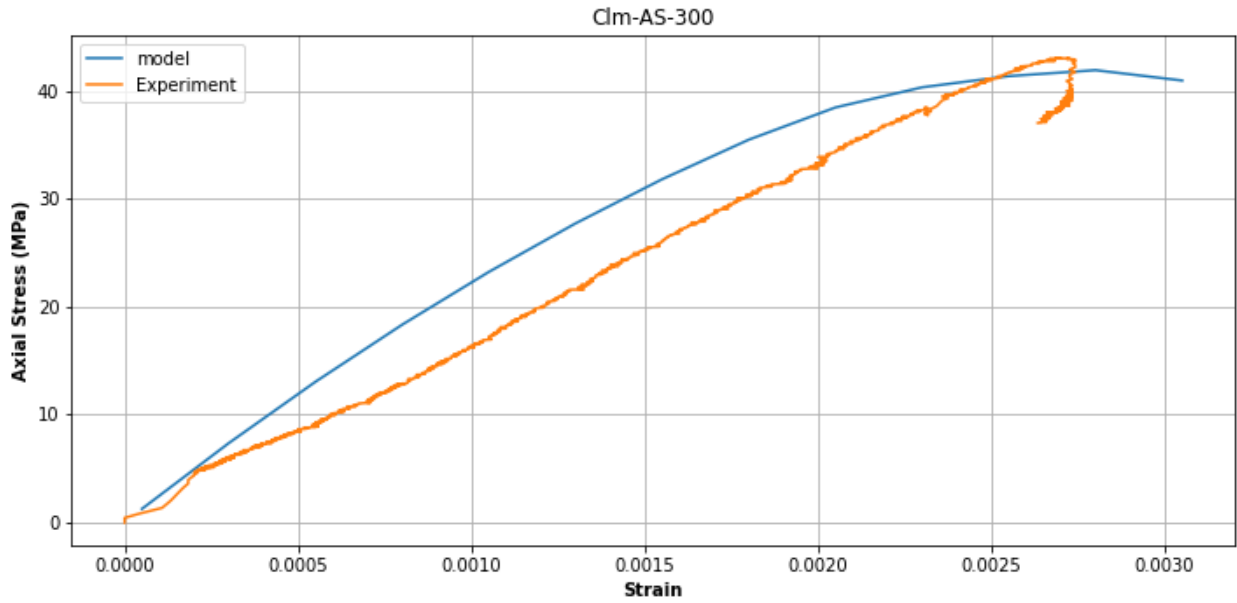
b) As-built concrete columns (300 ℃)

c) CFRP-confined columns (300 ℃)

c) CGFRP-confined columns (23 ℃)

c) CGFRP-confined columns (300 ℃)

Figure 10-2*: Axial loading simulation of tested reinforced concrete columns*

10.3 RC Column Lateral Cyclic Simulation

10.3.1 Loading Protocol and Analysis Parameters

An axial load was first applied to the column with different axial load ratio. The axial load ratio is determined by P/P_o, where P is the applied axial load and P_o the axial design capacity of the unstrengthen and unheated column (Clm-AS-23). The selected load ratios 0.8, 1, and 1.2. The axial load is applied in ten steps and is then held constant during a lateral simulation.

The loading protocol was determined based on drift ratio. The columns were subjected to three cycles at each drift level with displacement-controlled increments of 1.0 mm per step. The selected drift ratio levels are 0.25%, 0.5%, 1%, 1.5%, 2%, 2.5%, 3%, 4%, and finally 10%.
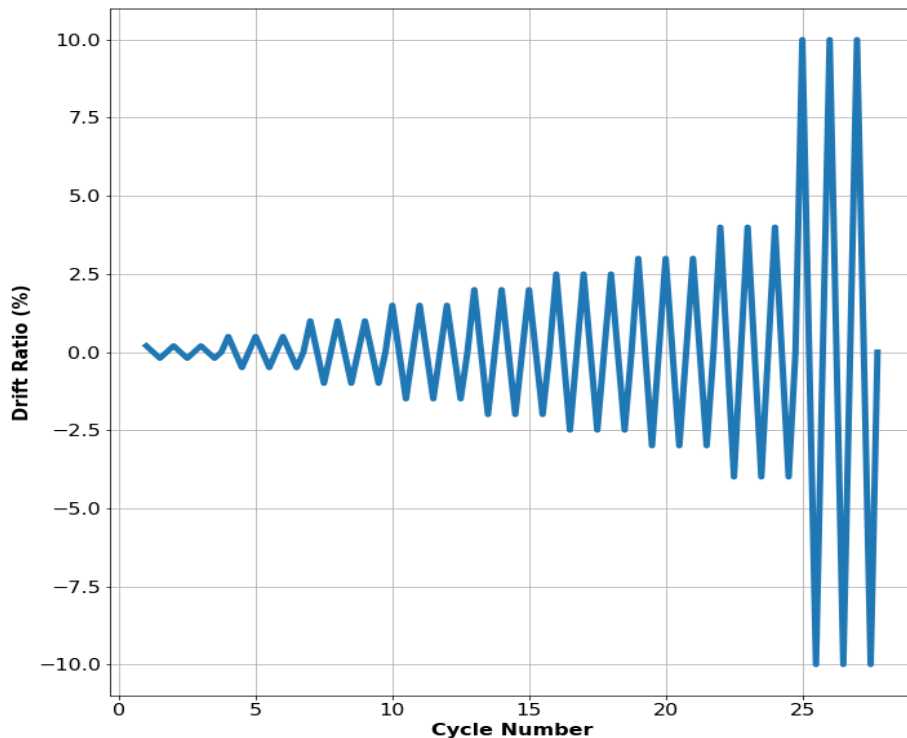

Figure 10-3: Lateral Cyclic Displacement Input (3 cycles at each level)

10.3.2 Results

A summary of the results of lateral cyclic simulation is presented in **Table 10-1**. The hysteresis curves of the simulated column are shown in **Figure 10-4**, **Figure 10-5**, **Figure 10-6**, and **Figure 10-7**. The hysteresis behavior is presented in terms of base shear and top displacement of the column.

Table 10-1: Summary of Lateral Cyclic Simulation

| Model lD	Exposure Temperature, °C	Load Ratio, P/P_{ou}	Base Shear (kN)		Displacement (mm.)	
			Yield	Maximum	Yielding	Ultimate
Clm-AS-23	23	0.25	32.95	45.49	5.33	30
		0.5	35.68	41.68	5.35	10
		0.65	23.4	35.37	4.8	5
		0.75	18.65	28.90	4.44	5
Clm-AS-300	300	0.25	28.50	39.05	5.65	25
		0.5	29.09	31.84	5.25	10
		0.65	13.39	22.74	4.06	5
		0.75	12.80	12.80	2	2
Clm-C2-23	23	0.25	38.69	62.25	9.24	40
		0.5	47.3	66.35	10.7	40
		0.65	48.87	69.33	10.6	40
		0.75	49.18	69.2	10.48	40
Clm-C2-300	300	0.25	30.46	52.3	8.68	40
		0.5	36.3	54.2	9.45	30
		0.65	28.54	51.75	8.73	20
		0.75	24.8	46.43	8.2	15
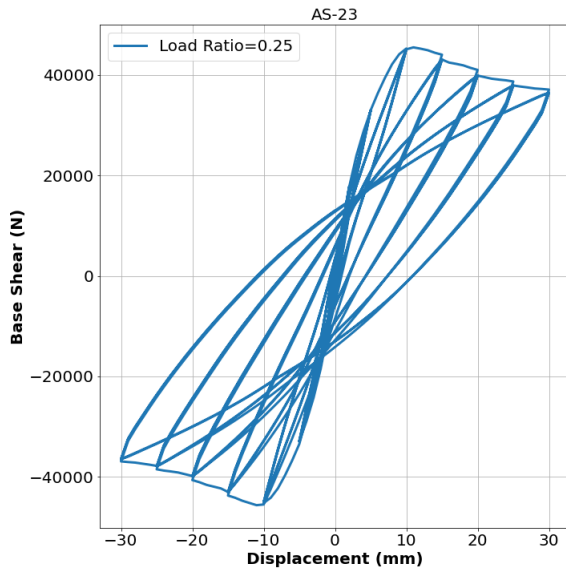
a) Axial Load Ratio = 0.25
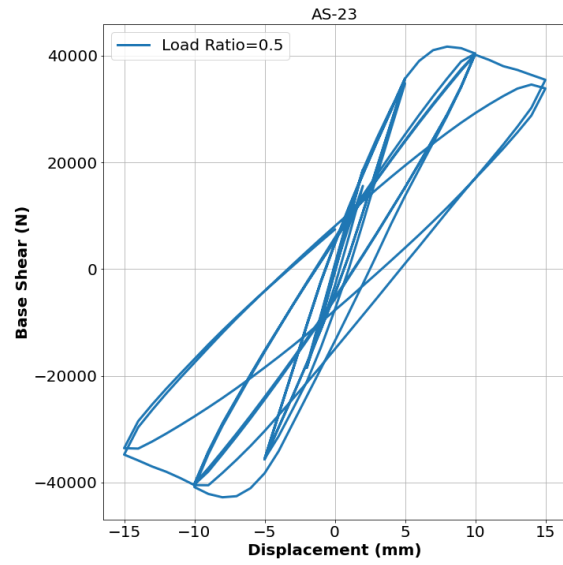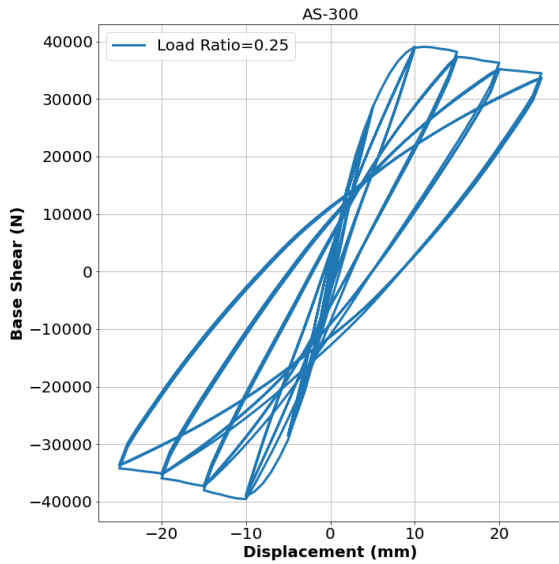
b) Axial Load Ratio = 0.5
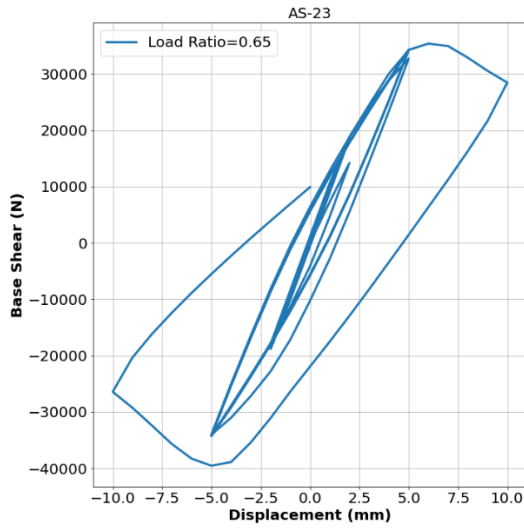
c) Axial Load Ratio = 0.65
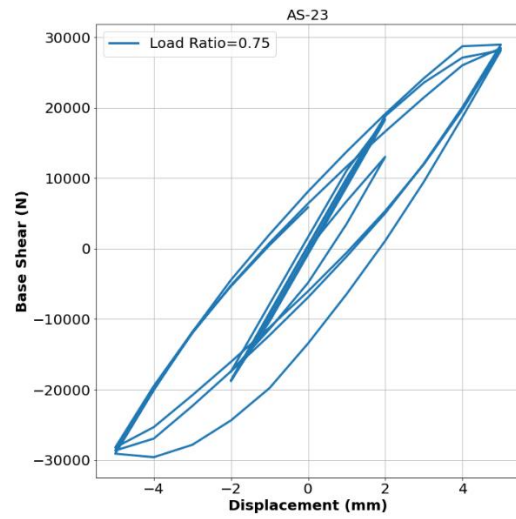
e) Axial Load Ratio = 0.75

Figure 10-4: Force Displacement Hysteresis Curve for AS-23 Specimens

a) Axial Load Ratio = 0.25

b) Axial Load Ratio = 0.5

c) Axial Load Ratio = 0.65
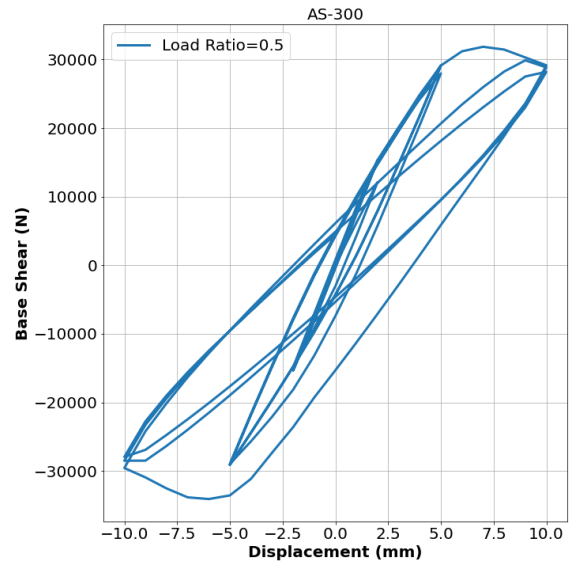
e) Axial Load Ratio = 0.75

Figure 10-5: Force Displacement Hysteresis Curve for AS-300 Specimens

a) Axial Load Ratio = 0.25

b) Axial Load Ratio = 0.5

c) Axial Load Ratio = 0.65

e) Axial Load Ratio = 0.75

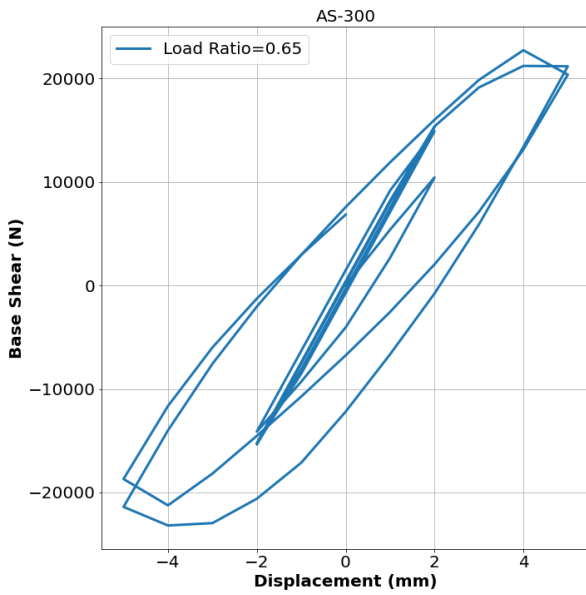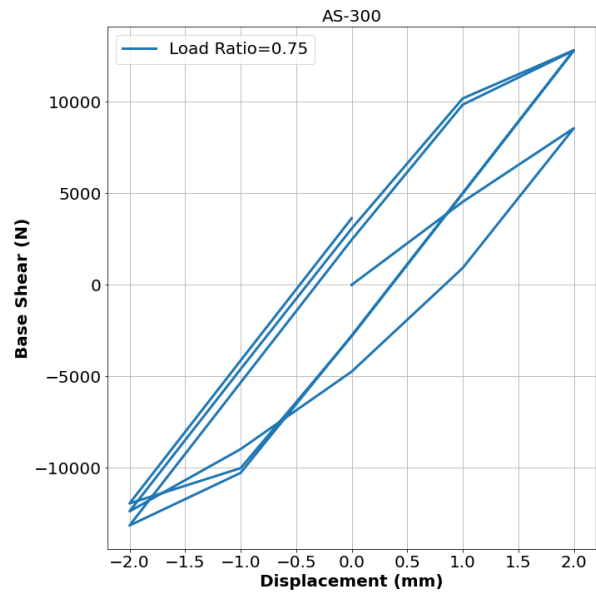***Figure 10-6:*** Force Displacement Hysteresis Curve for C2-23 Specimens
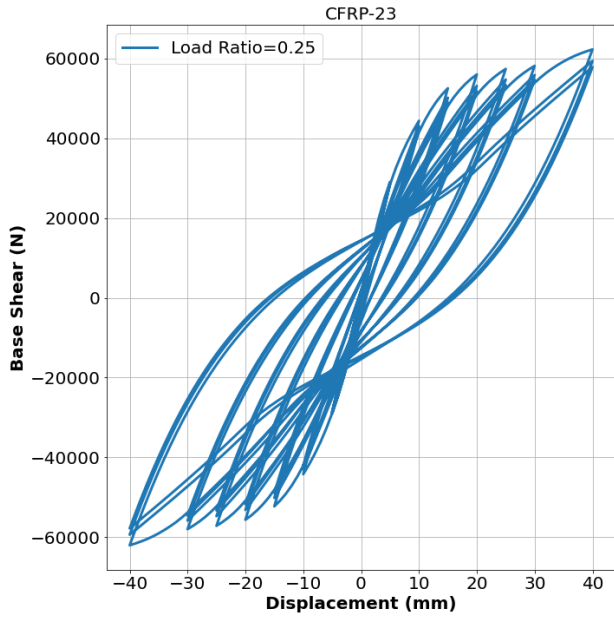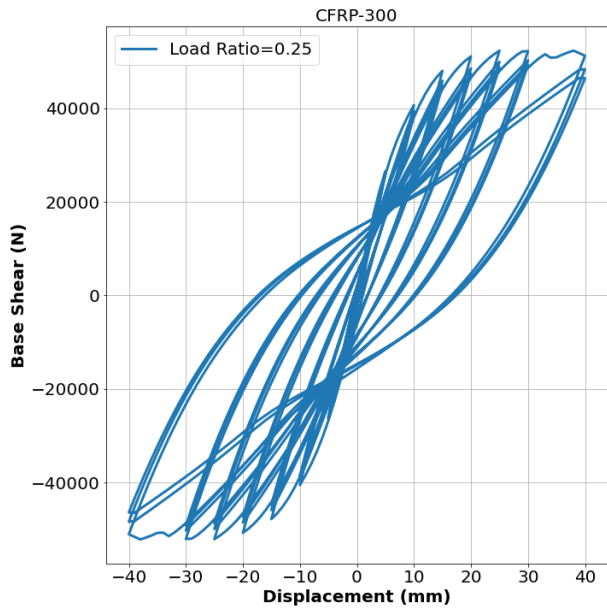
a) Axial Load Ratio = 0.25

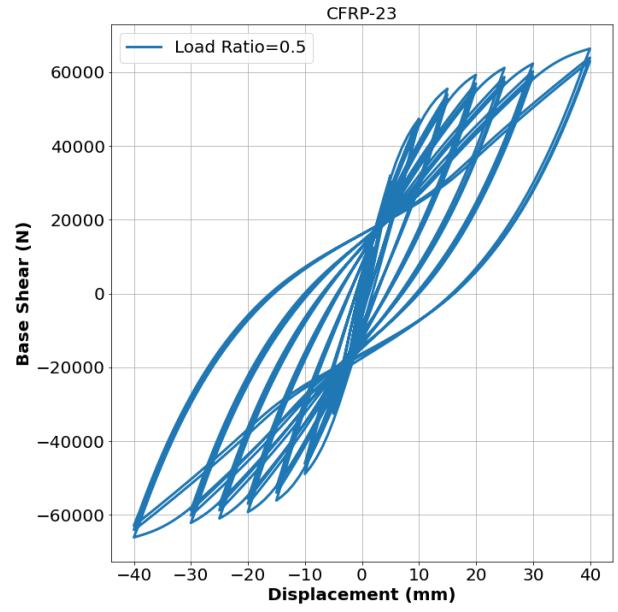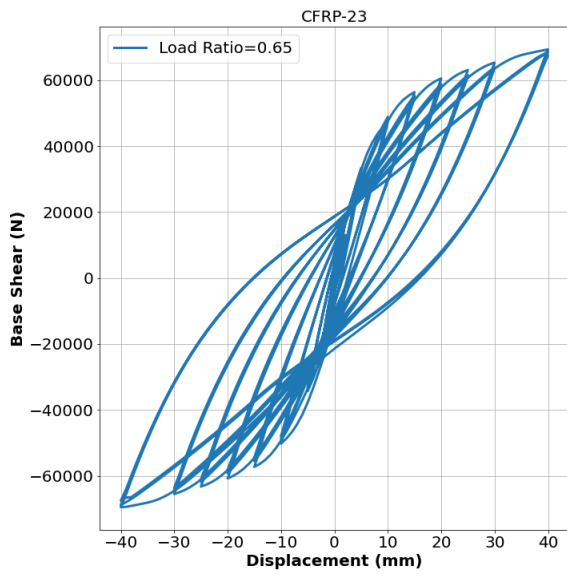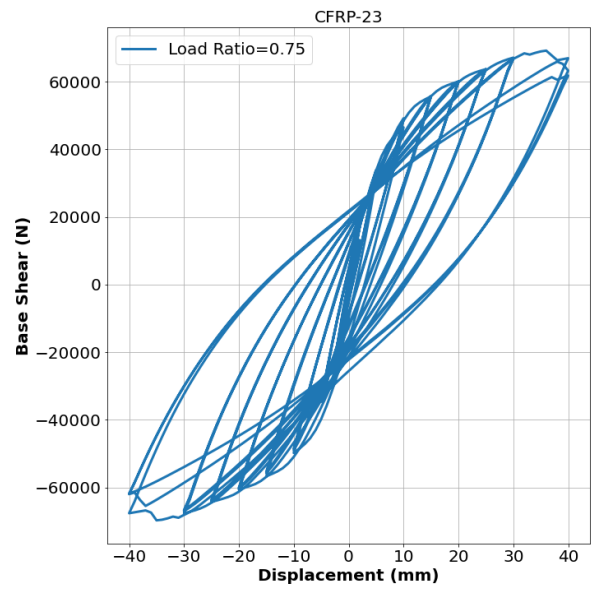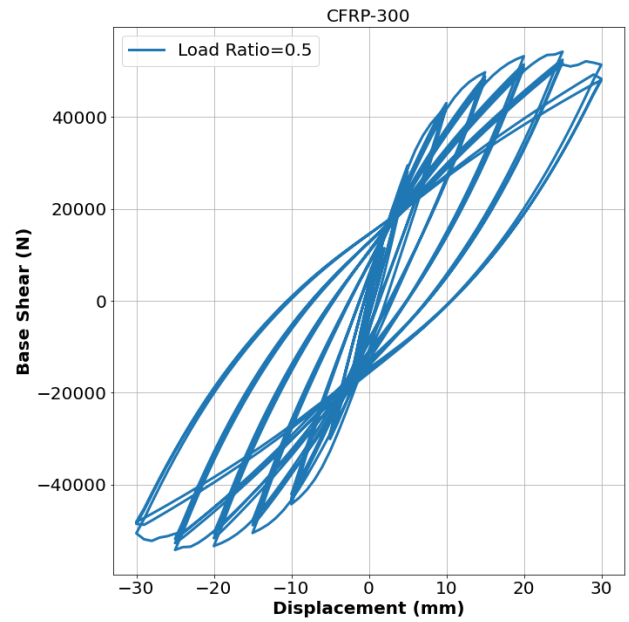b) Axial Load Ratio = 0.5
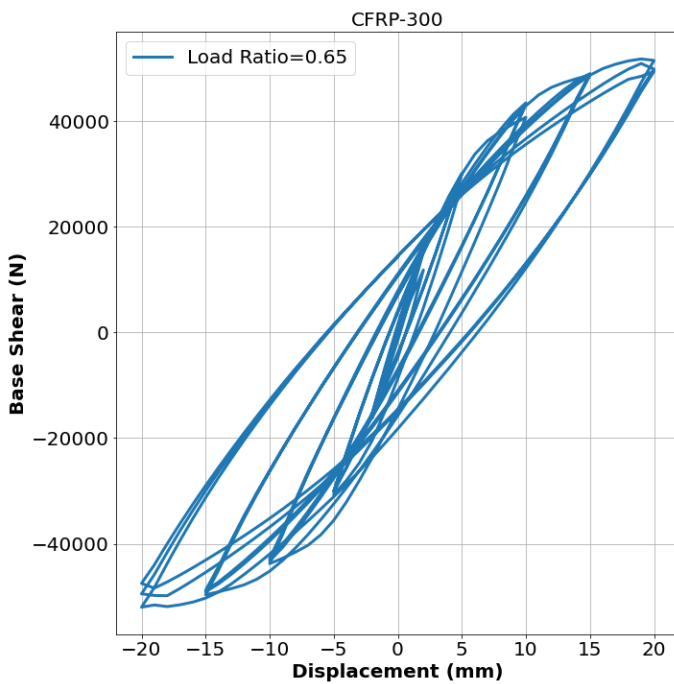
c) Axial Load Ratio = 0.65
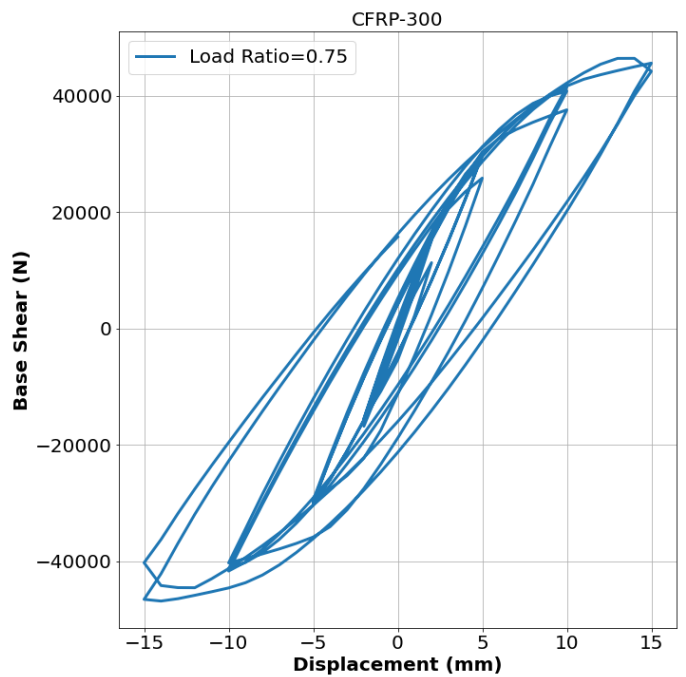
e) Axial Load Ratio = 0.75

Figure 10-7: Force Displacement Hysteresis Curve for C2-300 Specimens

The envelope curve was estimate from the hysteresis curve by finding the maximum base shear (positive) and minimum (negative) and corresponding displacement at each load cycle. **Figure 10-8** shows the envelope curve of two selected model superimposed on the force displacement curve. The envelope curves of simulated columns are presented in **Figure 10-9**.

Only drift ratios where the column experienced three full cycles were considered for energy dissipation calculations. This was done to allow for a better comparison between the columns.
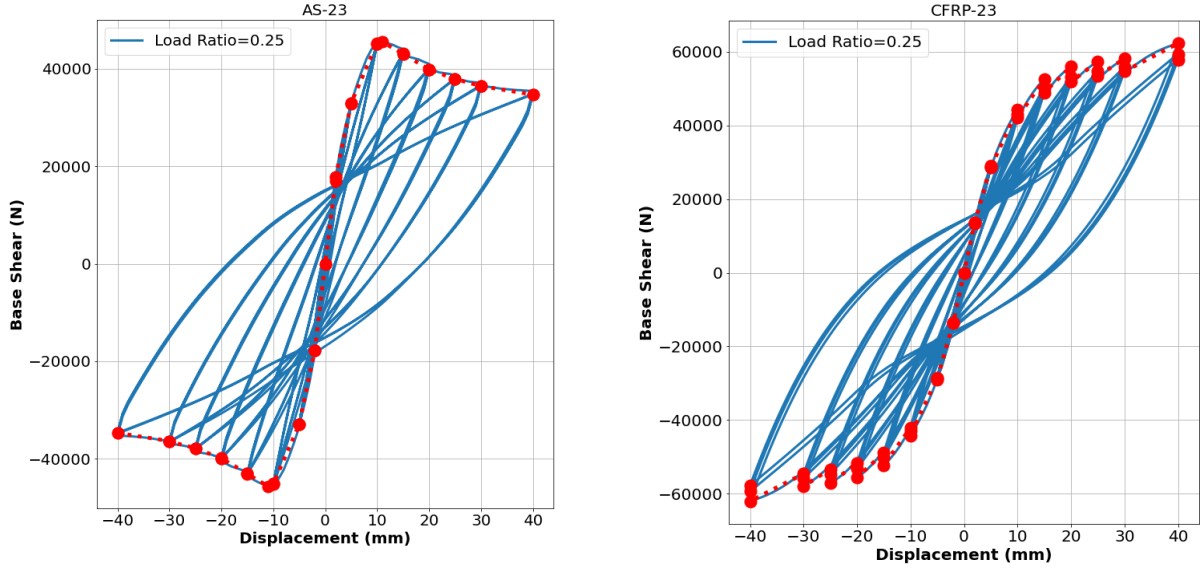
Figure 10-8: Envelope Curve Superimposed on Force Displacement Curve for Columns a) Clm-AS-23, and b) Clm-C2-23
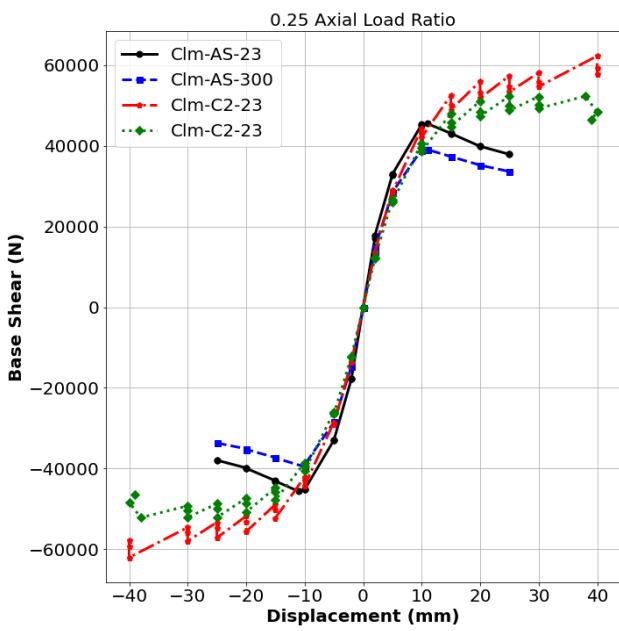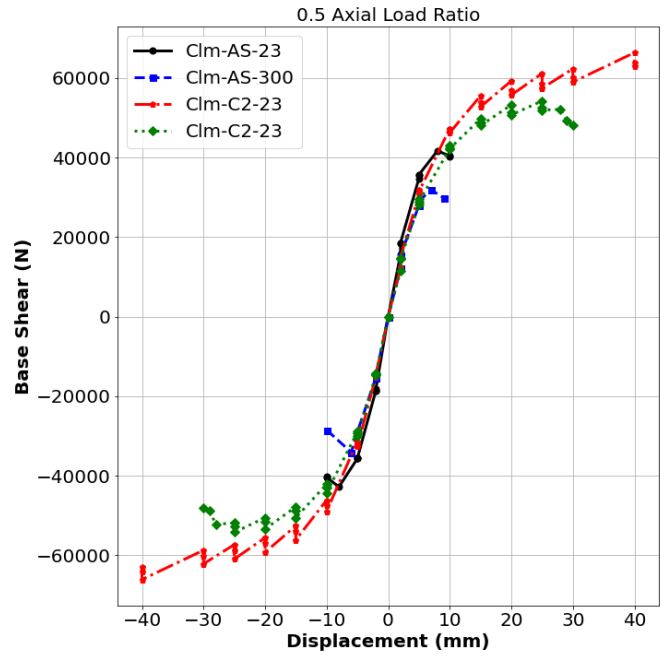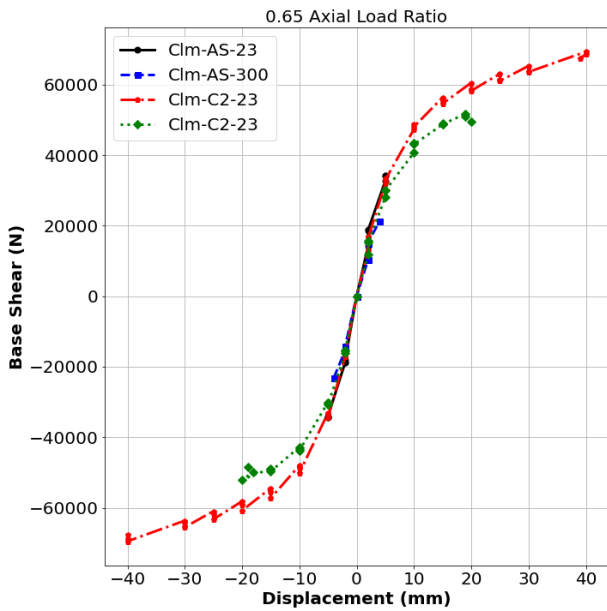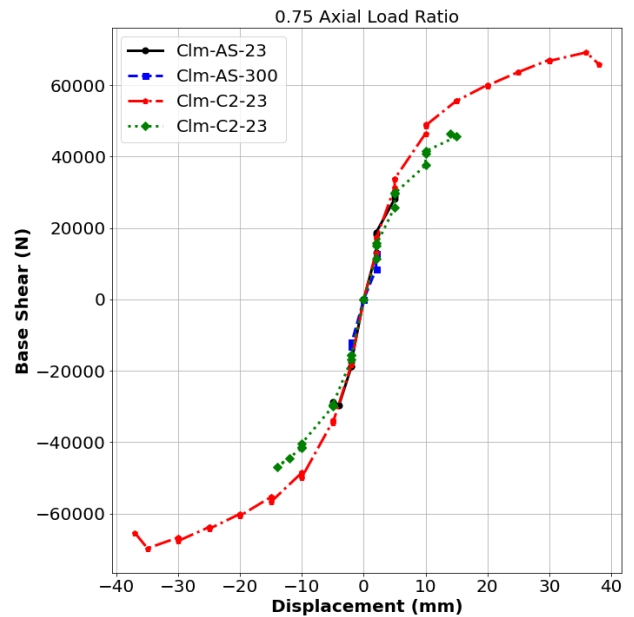
Figure 10-9: Envelope Base Shear vs. Displacement Curve of the Simulated Columns

The three main design parameters that are tabulated by ASCE-7 are the following:

(a) *Response modification factor, R*

(b) *Deflection amplification factor, C_d*

(c) *Overstrength factor, Ω_o*

The R value represents the energy dissipation capabilities of the structural system or element. A system or an element with a high R value can absorb the energy induced by seismic ground motion through plastic deformation in the form strain energy. The R factor is used to reduce the design base shear of the structure. The deflection amplification factor represents the ductility of the system. C_d is used to estimate the inelastic deformation of the structure from deflection calculated through elastic analysis.

The base shear corresponding to the first yield point, V_y can be estimated from the envelope curve of the cyclic force-displacement curve. First, the elastic modulus needs to be calculated by getting the tangent of the linear elastic portion of the envelope curve. From there, the yield point can be calculated by finding the intersection tangent modulus and a theoretical V_m line. This procedure is demonstrated in Figure **10-8**. The ductility of the specimens, μ, can then be calculated by Δ_u/Δ_y. A comparison of the ductility of the columns is presented in **Figure 10-9**.
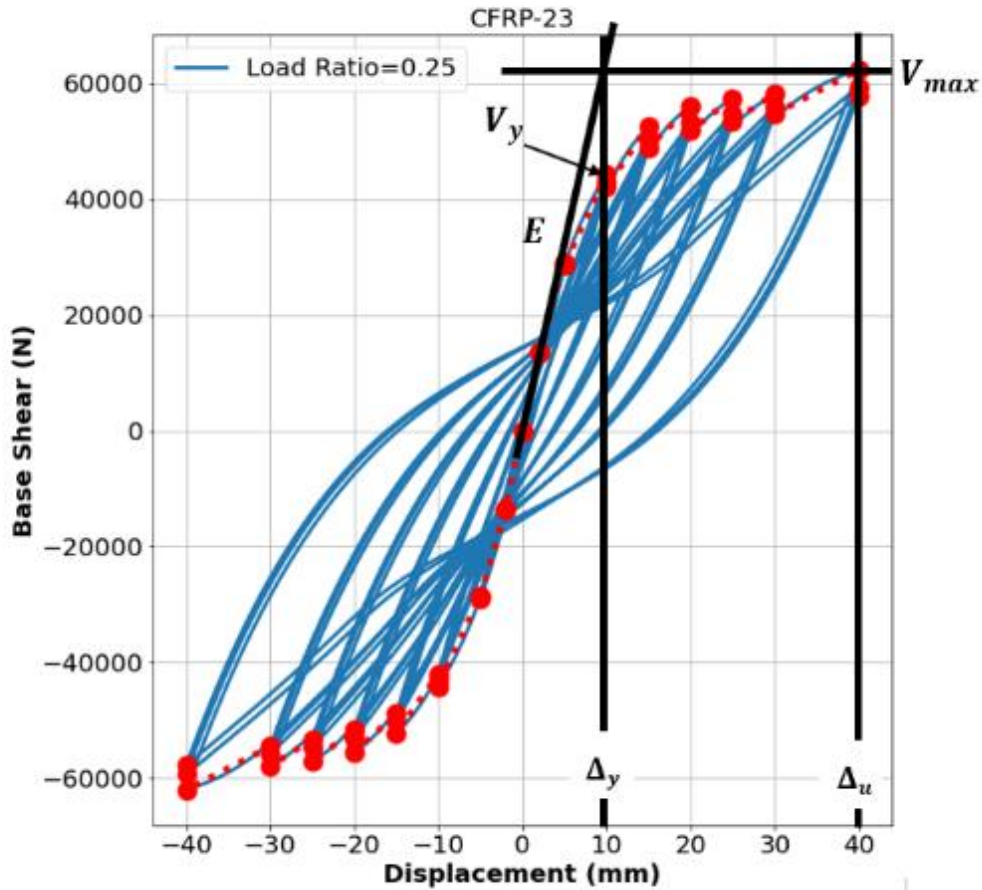
Figure 10-10: Procedure for Obtaining Yield and Ultimate Parameters of the Simulated Columns

The ductility of the columns decreases with increasing axial load ratios. This finding is consistent with what is found in the literature [21,32,34]. The heat damaged columns, Clm-AS-300 and Clm-C2-300 experienced a higher reduction in ductility compared to their unheated counterparts, Clm-AS-23 and Clm-C2-300 respectively. At a load ratio of 0.25, Clm-C2-300 demonstrated higher ductility compared to the unheated column, Clm-C2-23. However, the ultimate drift ratio

of the unheated columns is consistently the largest at all axial load levels. The CFRP-confined RC column experienced the greatest ductility degradation in all other axial load levels.

The energy dissipation capacity of each column was calculated for each axial load level. The energy dissipation at each cycle was calculated by finding the area inside the hysteresis loop of force-displacement curve. The cumulative energy dissipation of each column was calculated in N-mm. (Joules) and are presented in **Figure 10-10**. The ultimate drift ratios of the columns are presented in **Figure 10-11**.
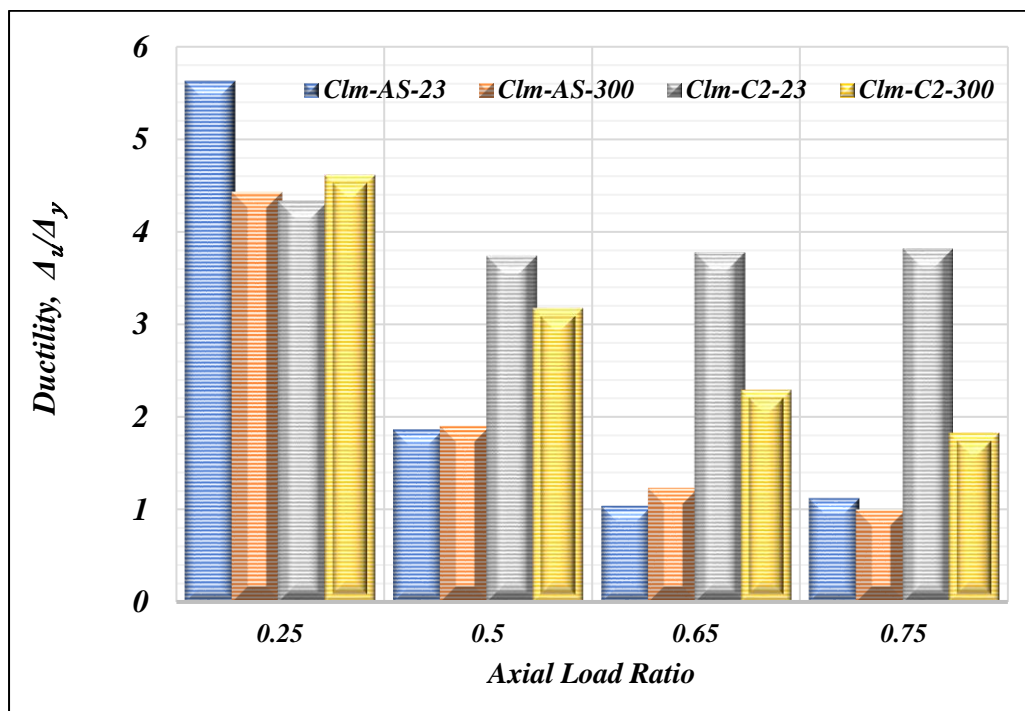
Figure 10-11: A Comparison of the Ductility, μ, of the Simulated Columns at Different Axial Load Ratios
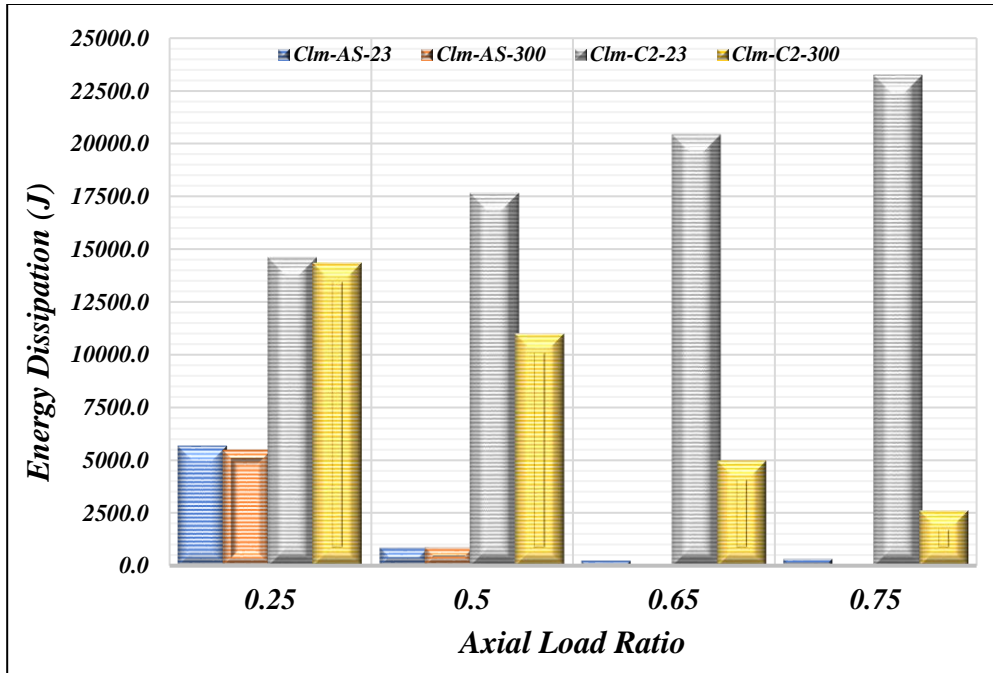
Figure 10-12: Comparison of the Energy Dissipation of the Simulated Columns at Different Axial Load Ratios
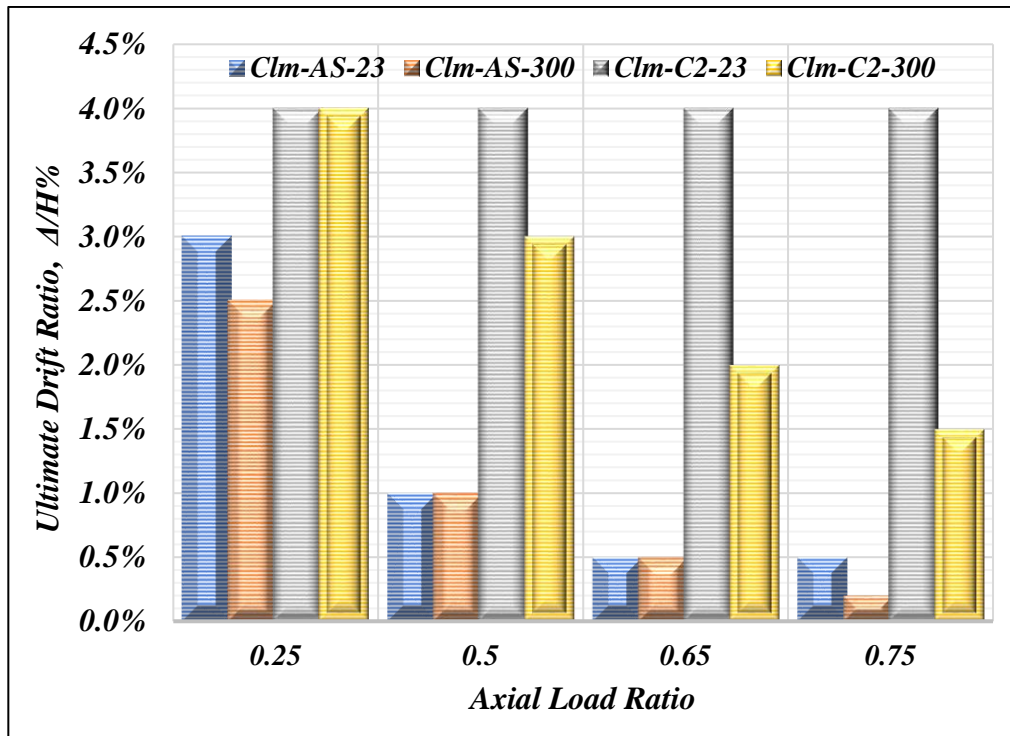
Figure 10-13: Comparison of the Ultimate Drift Ratios, $\Delta/H\%$, of the Simulated Columns at Different Axial Load Ratios

Chapter 11 CONCLUSIONS AND RECOMMENDATIONS FOR FUTURE RESERCH

11.1 Conclusions

The research presented in this dissertation focused on assessing the post-thermal exposure residual behavior of FRP-confined concrete columns. Based on the in-depth comprehensive literature review, there is no accurate method available for predicting post-fire performance of FRP-confined reinforced concrete columns. Considering that seismic retrofitting is one of the main applications of FRP composites in construction, this is a glaring deficiency in the industry. The findings of this study are summarized as follows:

- As exposure temperature increases, there is a substantial reduction in the ultimate strength, ductility, and energy absorption capacity of FRP-confined concrete as demonstrated by the small-scale and large-scale specimens as well as the lateral cyclic simulation results.

- The extent of degradation depends on many factors including, exposure temperature, exposure duration, column diameter, type of FRP composite material constituents, and FRP laminate thickness.

- Increasing the thickness of the fire protection system reduces the maximum exposure temperature of FRP up to a point, after which the effect of increasing the thickness fire protection becomes less influential.

- Opensees$^{®}$ was used to simulate the behavior of the heat damaged reinforced concreted columns with and without FRP composites. Results indicated that the Opensees$^{®}$

FRPConfiendConcrete02 material model is suitable to accurately predict post-fire exposure performance, provided that the residual mechanical properties of the CFRP composite are known that in this research was determined experimentally.

- The protocol used in developing the Opensees® model can be included in this public-domine software to assist structural engineers in assessing the effect of fire and the resulting degraded mechanical properties associated with such events on the overall performance in any reinforced concrete structure.

- Results obtained from the experimental program revealed the necessity of changing the geometry and details of RC members such as columns when tested for fire rating. It was found that the bulk majority of published experimental work utilized specimens with unprotected end surfaces in contrary to the actual case of a typical RC column in a building or a bridge where the roof (or bridge deck) and the floor (or foundation such as pile cap) act as protective and insulative media (see *Figure 10-1*). For this reason, and based on experimental program experience, it is strongly recommended to ad thick portions of concrete at the column ends to realistically simulate the fire damage and delay the premature local failure of specimen ends (refer to *Figure 10-2*).
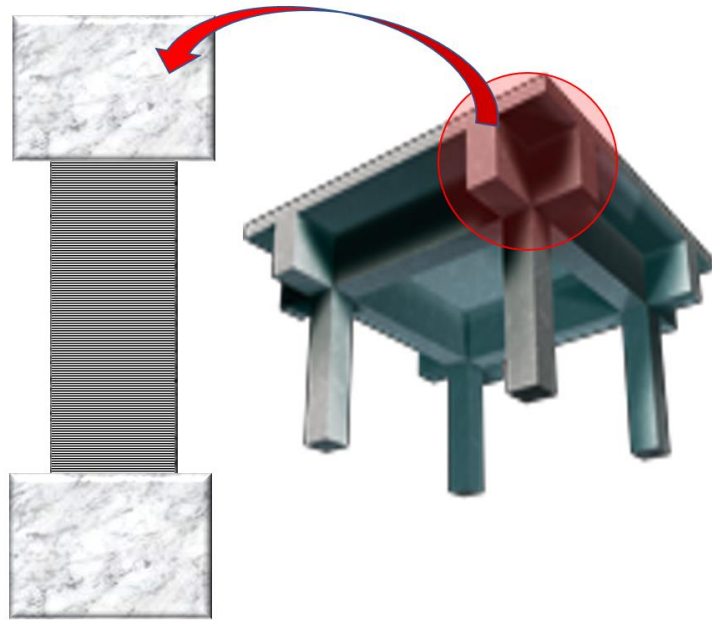
Figure 11-1: Resemblance of Capped Column to Real Structures

Thick concrete end cap

Heavily damaged
unprotected surface

Thick concrete end cap

Exposure to excessive heat waves from the
oven to the unprotected end surfaces of
the concrete specimens
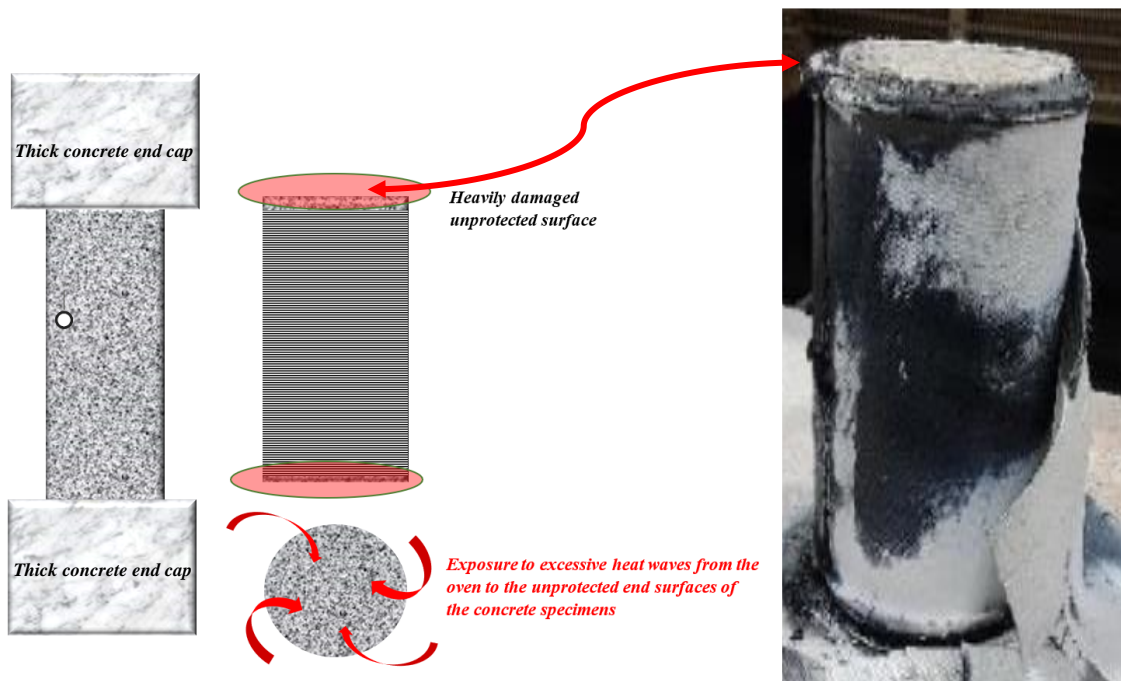
Figure 11-2: Demonstration of Recommended Fire Test Procedure

- Available models for the residual strength of concrete were found to be accurate and in agreement with the experimental results.

- During thermal exposure, the FRP coupon specimens reached steady-state conditions in a shorter time as compared to FRP-confined specimens tested in the same environment. This is due to the higher thermal mass (thermal absorption capacity) of concrete specimens as compared to FRP composite laminates.

- During the wet layup fabrication of the composite laminates, it was noticed that the epoxy resin consumption (saturation) of E-glass fabrics is higher than that absorbed by the carbon fiber fabrics.

- The flammability of the epoxy matrix was observed only for specimens strengthened with hybrid carbon/E-glass jackets. The onset temperature of the flames was determined to be 300℃.

- The outcome of this study will increase the confidence level structural engineer via provided a wealth of information that will assist in predict residual strength of RC columns confined with FRP composites. Results also provides a confirmation on the necessity of using proper fire protection systems to increase reliability of composites in repair and strengthening applications.

11.2 RECOMMENDATIONS FOR FUTURE WORK

There were many lessons learned while conducting the experimental program and during the analysis and simulation phase. Based on the findings of this study, the following recommendations can be made:

- Work needs to be done to convince the industry and the research community to dedicate resources and efforts towards studying the post-thermal behavior of FRP composites used in structural applications.

- Two carbon/epoxy FRP composites can exhibit different thermal degradation behaviors. Therefore, additional unique composite materials need to be evaluated to develop a universal prediction model.

- It is important to assess thermo-mechanical properties of FRP-composites used in civil applications. The behavior of the material at elevated temperatures is not the same as the post-cooling behavior. It is, therefore, important for researchers and practitioners to differentiate. A much larger database is needed to develop a more comprehensive model.

- Special fire protection systems need to be developed and tested for FRP composites applications. Most of the widely available fire protection systems were developed for structural materials that are less susceptible to thermal degradation either due to the properties of the material itself or due to thickness of the material that is used (e.g., concrete and steel).

- In this study, preliminary assessment of the use of hybrid composite jackets made of interior thick CFRP laminates with a thin laminate of E-glass acting as a protective layer

due to the superior thermal properties of E-glass. However, and as stated earlier, the heat-sensitive constituent of FRP composites is the polymer matrix. However, initial results is promising and therefore more detailed work in this area is recommended.

- Many concrete specimens exploded during the thermal exposure protocol. This behavior is cause by expansion of the concrete that is induced by the pressure from moisture vapor which induces internal tensile stresses in the concrete. This phenomenon is responsible for spalling of the concrete cover during fire events which exposes the heat sensitive steel reinforcement to the fire. Therefore, it is recommended to test performance of concrete specimens that are reinforced with chopped strands to assess the impact of tensile strength on concrete survivability during and after thermal exposure.

- Finally, special considerations need to be made for the thermal mass of the fire tested specimens in order to make accurate comparisons between fire tested specimens.

REFERENCES

[1]   American Concrete Institute., ACI Committee 440., Guide for the design and construction of externally bonded FRP systems for strengthening concrete structures, American Concrete Institute, 2017.

[2]   A.S. Mosallam, A. Bayraktar, M. Elmikawi, S. Pul, S. Adanur, Polymer Composites in Construction: An Overview Permalink, SOJ Mater. Sci. Eng. (2014). https://escholarship.org/uc/item/5xf7s8nj.

[3]   S. Sheikh, G. Yau, Seismic behavior of concrete columns confined with steel and fiber-reinforced polymers Glass Fibre Reinforced Polymer C, ACI Struct. J. 99 (2002). https://www.researchgate.net/publication/279594399.

[4]   M.A. Haroun, A.S. Mosallam, M.Q. Feng, H.M. Elsanadedy, Experimental Investigation of Seismic Repair and Retrofit of Bridge Columns by Composite Jackets, J. Reinf. Plast. Compos. 22 (2003). https://doi.org/10.1177/0731684403035573.

[5]   M.N. Youssef, M.Q. Feng, A.S. Mosallam, Stress-strain model for concrete confined by FRP composites, Compos. Part B Eng. 38 (2007) 614–628. https://doi.org/10.1016/j.compositesb.2006.07.020.

[6]   J. Liu, S.A. Sheikh, Fiber-Reinforced Polymer-Confined Circular Columns under Simulated Seismic Loads, 2013.

[7]   L. Xing, G. Lin, J.F. Chen, Behavior of FRP-Confined Circular RC Columns under Eccentric Compression, J. Compos. Constr. 24 (2020).

https://doi.org/10.1061/(ASCE)CC.1943-5614.0001036.

[8] A.S. Mosallam, Structural Performance of Pultruded Composites under Elevated Temperatures, Adv. Mater. Res. 79–82 (2009). https://doi.org/10.4028/www.scientific.net/AMR.79-82.2223.

[9] A. Mosallam, F. Abdi, Z. Qian, Fire resistance simulation of loaded deck sandwich panel and deck-bulkhead assembly structures, Compos. Part B Eng. 39 (2008). https://doi.org/10.1016/j.compositesb.2007.02.022.

[10] Joint ACI/TMS Committee 216., Masonry Society (U.S.), Code requirements for determining fire resistance of concrete and masonry construction assemblies (ACI 216.1-07, TMS-216-07) : an ACI/TMS Standard, American Concrete Institute, 2007.

[11] J.P. Firmo, J.R. Correia, P. França, Fire behaviour of reinforced concrete beams strengthened with CFRP laminates: Protection systems with insulation of the anchorage zones, Compos. Part B Eng. 43 (2012) 1545–1556. https://doi.org/10.1016/j.compositesb.2011.09.002.

[12] J.P. Firmo, J.R. Correia, L.A. Bisby, Fire behaviour of FRP-strengthened reinforced concrete structural elements: A state-of-the-art review, Compos. Part B Eng. 80 (2015) 198–216. https://doi.org/10.1016/j.compositesb.2015.05.045.

[13] L.A. Bisby, Fire behaviour of fibre-reinforced polymer (FRP) reinforced or confined concrete, Queen's University, 2003. https://www.researchgate.net/publication/36189430.

[14] V.K.R. Kodur, L.A. Bisby, M.F. Green, Experimental evaluation of the fire behaviour of

insulated fibre-reinforced-polymer-strengthened reinforced concrete columns, Fire Saf. J. 41 (2006) 547–557. https://doi.org/10.1016/j.firesaf.2006.05.004.

[15]   J.G. Dai, W.Y. Gao, J.G. Teng, Finite element modeling of insulated FRP-strengthened RC beams exposed to fire, J. Compos. Constr. 19 (2015). https://doi.org/10.1061/(ASCE)CC.1943-5614.0000509.

[16]   L.A. Bisby, M. Green, E.U. Chowdhury, Fire Performance of FRP Systems for Infrastructure: A State-of-the-Art Report, (2005). https://doi.org/10.4224/20377587.

[17]   E. Chowdhury, L. Bisby, M. Green, N. Bénichou, V. Kodur, Heat transfer and structural response modelling of FRP confined rectangular concrete columns in fire, Constr. Build. Mater. 32 (2012) 77–89. https://doi.org/10.1016/j.conbuildmat.2010.12.064.

[18]   K. Himoto, Comparative Analysis of Post-Earthquake Fires in Japan from 1995 to 2017, Fire Technol. 55 (2019) 935–961. https://doi.org/10.1007/s10694-018-00813-5.

[19]   C. Scawthorn, J. Eidinger, A. Schiff, Fire following earthquake, technical council on lifeline earthquake engineering, Monograph No. 26., American Society of Civil Engineers, 2005.

[20]   R.A. Campbell, B.M. Pickett, V. La Saponara, D. Dierdorf, Thermal characterization and flammability of structural epoxy adhesive and carbon/epoxy composite with environmental and chemical degradation, J. Adhes. Sci. Technol. 26 (2012) 889–910. https://doi.org/10.1163/156856111X593621.

[21]   D.-S. Gu, ; Gang Wu, Z.-S. Wu, Y.-F. Wu, Confinement Effectiveness of FRP in

Retrofitting Circular Concrete Columns under Simulated Seismic Load, J. Compos. Constr. 14(5) (2010) 531–540. https://doi.org/10.1061/ASCECC.1943-5614.0000105.

[22] Y. Bin Park, M.G. Song, J.J. Kim, J.H. Kweon, J.H. Choi, Strength of carbon/epoxy composite single-lap bonded joints in various environmental conditions, Compos. Struct. 92 (2010) 2173–2180. https://doi.org/10.1016/j.compstruct.2009.09.009.

[23] L.A. Bisby, M.F. Green, V.K.R. Kodur, Response to fire of concrete structures that incorporate FRP, Prog. Struct. Eng. Mater. 7 (2005) 136–149. https://doi.org/10.1002/pse.198.

[24] N. Bénichou, H. Mostafaei, M.F. Green, K. Hollingshead, The impact of fire on seismic resistance of fibre reinforced polymer strengthened concrete structural systems, Can. J. Civ. Eng. 40 (2013) 1044–1049. https://doi.org/10.1139/cjce-2012-0521.

[25] M. Yaqub, C.G. Bailey, Seismic performance of shear critical post-heated reinforced concrete square columns wrapped with FRP composites, Constr. Build. Mater. 34 (2012). https://doi.org/10.1016/j.conbuildmat.2012.02.076.

[26] B. Behnam, H.R. Ronagh, P.J. Lim, Numerical evaluation of the post-earthquake fire resistance of CFRP-strengthened reinforced concrete joints based on experimental observations, Eur. J. Environ. Civ. Eng. 20 (2016). https://doi.org/10.1080/19648189.2015.1018448.

[27] International Code Council-Evaluation Service (ICC-ES), Acceptance Criteria for concrete and reinforced and unreinforced masonry strengthening using externally bonded fiber

reinforced polymer FRP composite systems (AC125), Brea, CA, USA, 2010. www.icc-es.org.

[28]   L. Lam, J.G. Teng, Design-oriented stress-strain model for FRP-confined concrete, in: Constr. Build. Mater., 2003: pp. 471–489. https://doi.org/10.1016/S0950-0618(03)00045-X.

[29]   ACI 318-19 Building Code Requirements for Structural Concrete and Commentary, American Concrete Institute, 2019. https://doi.org/10.14359/51716937.

[30]   A. Mosallam, K. Mosalam, ACI 440F: Task force on design of externally bonded FRP systems for seismic strengthening concrete structures, 2004.

[31]   Y. Idris, T. Ozbakkaloglu, Seismic behavior of high-strength concrete-filled FRP tube columns, J. Compos. Constr. 17 (2013). https://doi.org/10.1061/(ASCE)CC.1943-5614.0000388.

[32]   T. Ozbakkaloglu, M. Saatcioglu, Displacement-based model to predict lateral drift capacities of concrete-filled FRP tube columns, Eng. Struct. 147 (2017) 345–355. https://doi.org/10.1016/j.engstruct.2017.05.045.

[33]   T. Paulay, M.J.N. Priestly, Seismic design of reinforced concrete and masonry buildings, John Wiley and Sons, New York, 1992. https://doi.org/10.1002/9780470172841.

[34]   O. Youssf, M.A. ElGawady, J.E. Mills, Displacement and plastic hinge length of FRP-confined circular reinforced concrete columns, Eng. Struct. 101 (2015) 465–476. https://doi.org/10.1016/j.engstruct.2015.07.026.

[35] D.S. Gu, Y.F. Wu, G. Wu, Z.S. Wu, Plastic hinge analysis of FRP confined circular concrete columns, Constr. Build. Mater. 27 (2012) 223–233. https://doi.org/10.1016/j.conbuildmat.2011.07.056.

[36] ASTM E119, Standard Test Methods for Fire Tests of Building Construction and Materials, ASTM International, West Conshohocken, PA, ASTM Int. West Conshohocken, PA. 552 (2016) 1–36. https://doi.org/10.1520/E0119-20.These.

[37] T.T. Lie, Structural Fire Protection : Manual of Practice., American Society of Civil Engineers, 1992.

[38] EN 1994-1-2: Eurocode 4: Design of composite steel and concrete structures – Part 1-2: General rules - Structural fire design, 1994.

[39] Q. Ma, R. Guo, Z. Zhao, Z. Lin, K. He, Mechanical properties of concrete at high temperature-A review, Constr. Build. Mater. 93 (2015) 371–383. https://doi.org/10.1016/j.conbuildmat.2015.05.131.

[40] S. Lim, Effects of elevated temperature exposure on cement-based composite materials, University of Illinois at Urbana-Champaign, 2015.

[41] T.T. Lie, T.J. Roe, T.D. Lin, Residual strength of fire-exposed reinforced concrete columns, Spec. Publ. 92. (1986) 153–174. https://doi.org/10.4224/40001373.

[42] R.J.A. Hamad, M.A. Megat Johari, R.H. Haddad, Mechanical properties and bond characteristics of different fiber reinforced polymer rebars at elevated temperatures, Constr. Build. Mater. 142 (2017) 521–535. https://doi.org/10.1016/j.conbuildmat.2017.03.113.

[43] Y.F. Chang, Y.H. Chen, M.S. Sheu, G.C. Yao, Residual stress-strain relationship for concrete after exposure to high temperatures, Cem. Concr. Res. 36 (2006) 1999–2005. https://doi.org/10.1016/j.cemconres.2006.05.029.

[44] R.A. Hawileh, A. Abu-Obeidah, J.A. Abdalla, A. Al-Tamimi, Temperature effect on the mechanical properties of carbon, glass and carbon-glass FRP laminates, Constr. Build. Mater. 75 (2015) 342–348. https://doi.org/10.1016/j.conbuildmat.2014.11.020.

[45] M.D. Banea, L.F.M. Da Silva, R.D.S.G. Campilho, Effect of temperature on tensile strength and mode i fracture toughness of a high temperature epoxy adhesive, J. Adhes. Sci. Technol. 26 (2012) 939–953. https://doi.org/10.1163/156856111X593649.

[46] S.J. John, A.J.K. Och, F.L.M. Tthews, Measuring and predicting the durability of bonded carbon fibre/epoxy composite joints, 1991.

[47] E.U. Chowdhury, R. Eedson, L.A. Bisby, M.F. Green, N. Benichou, Mechanical Characterization of Fibre Reinforced Polymers Materials at High Temperature, Fire Technol. 47 (2011) 1063–1080. https://doi.org/10.1007/s10694-009-0116-6.

[48] X. Gabrion, V. Placet, F. Trivaudey, L. Boubakar, About the thermomechanical behaviour of a carbon fibre reinforced high-temperature thermoplastic composite, n.d. https://hal.archives-ouvertes.fr/hal-01446381.

[49] S. Feih, A.P. Mouritz, Tensile properties of carbon fibres and carbon fibre-polymer composites in fire, Compos. Part A Appl. Sci. Manuf. 43 (2012) 765–772. https://doi.org/10.1016/j.compositesa.2011.06.016.

[50]   S. Budhe, M.D. Banea, S. de Barros, L.F.M. da Silva, An updated review of adhesively bonded joints in composite materials, Int. J. Adhes. Adhes. 72 (2017) 30–42. https://doi.org/10.1016/j.ijadhadh.2016.10.010.

[51]   M. Detassis, A. Pegoretti, C. Migliaresi, Effect of temperature and strain rate on interfacial shear stress transfer in carbon/epoxy model composites, Compos. Sci. Technol. 53 (1995). https://doi.org/10.1016/0266-3538(94)00069-7.

[52]   A.P. Kulcarni, R.F. Gibson, Non-destructive characterisation of effects of temperature and moisture on elastic moduli of vinyl ester resin and E-glass/vinyl ester resin composite, in: Proc. Am. Soc. Compos. 18th Annu. Tech. Conf., Florida, 2003.

[53]   A.G. Gibson, Y.S. Wu, J.T. Evans, A.P. Mouritz, Laminate theory analysis of composites under load in fire, J. Compos. Mater. 40 (2006) 639–658. https://doi.org/10.1177/0021998305055543.

[54]   S.K. Foster, L. Bisby, Fire Survivability of Externally Bonded FRP Strengthening Systems, J. Compos. Constr. 12 (2008) 553–561. https://doi.org/10.1061/ASCE1090-0268200812:5553.

[55]   P.L. Nguyen, X.H. Vu, E. Ferrier, Characterization of pultruded carbon fibre reinforced polymer (P-CFRP) under two elevated temperature-mechanical load cases: Residual and thermo-mechanical regimes, Constr. Build. Mater. 165 (2018) 395–412. https://doi.org/10.1016/j.conbuildmat.2017.12.244.

[56]   Y.J. Kim, T. Siriwardanage, A. Hmidan, J. Seo, Material characteristics and residual bond

properties of organic and inorganic resins for CFRP composites in thermal exposure, Constr. Build. Mater. 50 (2014) 631–641. https://doi.org/10.1016/j.conbuildmat.2013.10.009.

[57] Y.A. Al-Salloum, H.M. Elsanadedy, A.A. Abadel, Behavior of FRP-confined concrete after high temperature exposure, Constr. Build. Mater. 25 (2011) 838–850. https://doi.org/10.1016/j.conbuildmat.2010.06.103.

[58] M.Z. Naser, V.A. Uppala, Properties and material models for construction materials post exposure to elevated temperatures, Mech. Mater. 142 (2020). https://doi.org/10.1016/j.mechmat.2019.103293.

[59] A. Mosallam, Design Guide for FRP Composite Connections, American Society of Civil Engineers, Reston, VA, 2011. https://doi.org/10.1061/9780784406120.

[60] D. Cree, E.U. Chowdhury, M.F. Green, L.A. Bisby, N. Bénichou, Performance in fire of FRP-strengthened and insulated reinforced concrete columns, in: Fire Saf. J., 2012: pp. 86–95. https://doi.org/10.1016/j.firesaf.2012.08.006.

[61] M.T. McGurn, P.E. Desjardin, A.B. Dodd, Numerical simulation of expansion and charring of carbon-epoxy laminates in fire environments, Int. J. Heat Mass Transf. 55 (2012) 272–281. https://doi.org/10.1016/j.ijheatmasstransfer.2011.09.013.

[62] L.A. Bisby, M.F. Green, V.K.R. Kodur, Modeling the behavior of fiber reinforced polymer-confined concrete columns exposed to fire, J. Compos. Constr. 9 (2005) 15–24. https://doi.org/10.1061/(ASCE)1090-0268(2005)9:1(15).

[63] A. Palmieri, S. Matthys, L. Taerwe, Fire endurance and residual strength of insulated concrete beams strengthened with near-surface mounted reinforcement, J. Compos. Constr. 17 (2013) 454–462. https://doi.org/10.1061/(ASCE)CC.1943-5614.0000338.

[64] E.U. Chowdhury, L.A. Bisby, M.F. Green, V.K.R. Kodur, Investigation of insulated FRP-wrapped reinforced concrete columns in fire, Fire Saf. J. 42 (2007) 452–460. https://doi.org/10.1016/j.firesaf.2006.10.007.

[65] F.P. Incropera, A.S. Lavine, T.L. Bergman, D.P. DeWitt, Fundamentals of heat and mass transfer., Wiley, 2007.

[66] W.Y. Gao, J.G. Dai, J.G. Teng, Simple Method for Predicting Temperatures in Insulated, FRP-Strengthened RC Members Exposed to a Standard Fire, J. Compos. Constr. 19 (2015). https://doi.org/10.1061/(ASCE)CC.1943-5614.0000566.

[67] C.G. Bailey, M. Yaqub, Seismic strengthening of shear critical post-heated circular concrete columns wrapped with FRP composite jackets, Compos. Struct. 94 (2012) 851–864. https://doi.org/10.1016/j.compstruct.2011.09.004.

[68] B. Shan, Y. Xiao, Y. Guo, Residual Performance of FRP-Retrofitted RC Columns after Being Subjected to Cyclic Loading Damage, J. Compos. Constr. 10 (2006). https://doi.org/10.1061/(ASCE)1090-0268(2006)10:4(304).

[69] ASTM D3039/D3039M-17, Standard Test Method for Tensile Properties of Polymer Matrix Composite Materials, ASTM International, West Conshohocken, PA, USA, 2017. https://doi.org/10.1520/D3039_D3039M-17.

[70] ASTM International, D5868-01 Standard Test Method for Lap Shear Adhesion for Fiber Reinforced Plastic (FRP) Bonding, West Conshohocken, PA, USA, 2014.

[71] B. Williams, L. Bisby, V. Kodur, M. Green, E. Chowdhury, Fire insulation schemes for FRP-strengthened concrete slabs, Compos. Part A Appl. Sci. Manuf. 37 (2006) 1151–1160. https://doi.org/10.1016/j.compositesa.2005.05.028.

[72] H.M. Elsanadedy, Y.A. Al-Salloum, S.H. Alsayed, R.A. Iqbal, Experimental and numerical investigation of size effects in FRP-wrapped concrete columns, Constr. Build. Mater. 29 (2012) 56–72. https://doi.org/10.1016/J.CONBUILDMAT.2011.10.025.

[73] A. Masoud, Structural and thermal behaviour of insulated FRP-strengthened reinforced concrete beams and slabs in fire, Queen's University (Canada), 2013.

[74] J. Rimen, D. Arghya, Size Effect in FRP-Confined Concrete under Axial Compression, J. Compos. Constr. 21 (2017) 4017045. https://doi.org/10.1061/(ASCE)CC.1943-5614.0000825.

[75] M. Gao, C. Xiaohuang, Y. Libo, H. Hyeon-Jong, Monotonic and Cyclic Axial Compressive Properties and Modeling of Basalt FRP-Retrofitted Predamaged Short Columns, J. Compos. Constr. 24 (2020) 4020023. https://doi.org/10.1061/(ASCE)CC.1943-5614.0001034.

[76] L. Lam, J.G. Teng, Stress–strain model for FRP-confined concrete under cyclic axial compression, Eng. Struct. 31 (2009) 308–321. https://doi.org/10.1016/J.ENGSTRUCT.2008.08.014.

[77] L. Lam, J.G. Teng, C.H. Cheung, Y. Xiao, FRP-confined concrete under axial cyclic compression, Cem. Concr. Compos. 28 (2006) 949–958. https://doi.org/10.1016/J.CEMCONCOMP.2006.07.007.